Western Graduate&PostdoctoralStudies

Western University
Scholarship@Western

Electronic Thesis and Dissertation Repository

2-15-2018 1:30 PM

Functional Changes Associated with SHROOM3 Deficiency and Mutation: Implications in Renal Pathophysiology and Disease

Doyun Ko, *The University of Western Ontario*

Supervisor: Drysdale, Tom A., *The University of Western Ontario*
Co-Supervisor: Kelly, Gregory M., *The University of Western Ontario*
A thesis submitted in partial fulfillment of the requirements for the Master of Science degree in Biology
© Doyun Ko 2018

Follow this and additional works at: https://ir.lib.uwo.ca/etd

Part of the Cell and Developmental Biology Commons, Diseases Commons, and the Physiology Commons

Recommended Citation

Ko, Doyun, "Functional Changes Associated with SHROOM3 Deficiency and Mutation: Implications in Renal Pathophysiology and Disease" (2018). *Electronic Thesis and Dissertation Repository*. 5245.
https://ir.lib.uwo.ca/etd/5245

This Dissertation/Thesis is brought to you for free and open access by Scholarship@Western. It has been accepted for inclusion in Electronic Thesis and Dissertation Repository by an authorized administrator of Scholarship@Western. For more information, please contact wlswadmin@uwo.ca.

Abstract

Chronic kidney disease (CKD) is a substantial global health burden that has recently been linked to the genetic locus *SHROOM3* by several genome-wide association studies. Shroom3 is an actin-binding protein that is necessary for inducing apical constriction in epithelial cells. Our lab has previously shown that Shroom3 is critical for proper kidney development and loss of Shroom3 produces symptoms associated with CKD. As hypertension is both a leading cause and comorbidity of CKD, I hypothesized that loss of *Shroom3* confers increased susceptibility to hypertension. Using a high-salt induced model of hypertension, I show that *Shroom3* deficient mice do not become hypertensive but exhibit an increased salt-sensitive blood pressure response. Additionally, I show that human *SHROOM3* variants currently identified within our population have attenuated apical constriction activity. Collectively, the findings from our *in vivo* and *in vitro* work implicate the consequences of reduced *Shroom3* function in the pathophysiology of human disease.

Keywords

Shroom3, chronic kidney disease, kidney, hypertension, sodium, salt, blood pressure, apical constriction, epithelium, actin

Acknowledgments

First and foremost, I would like to express my sincerest gratitude to my supervisor, Dr. Thomas Drysdale, for his ongoing mentorship and guidance. No words will suffice to convey how thankful I am for your patience, kindness, and support throughout the entirety of this journey. Through all my struggles and self-doubt, you have time and time again, encouraged me and pushed me to succeed. I will never forget my experience in your lab and the lessons I have learned. Thank you for agreeing to take me under your wing and for this opportunity.

To past and present members of the Drysdale Lab, you have made this experience what it was. To our incredible lab technician, Lucimar Ferreira, I wish I could put into words how appreciative I am of everything you have done for me. Thank you for all the time and energy you have invested into helping me with my project, you have been pivotal to its progress. I would also like to extend my thanks to our previous lab technician, Jean Wang, for showing me my way around the lab when I first started my Master's and for her training with lab techniques. Thank you to my lab mates Victoria Deveau, Alex Szpak, and Jonathan Hu for your constant support and friendship. To Victoria, I would not have survived some of those late lab nights without you, I am going to miss you and all the laughs we shared.

This work would not have been possible without the help, guidance, and support of several people. A very special thank you to Dr. Robert Gros who generously allowed me to use his blood pressure equipment, Dr. Lakshman Gunaratnam who provided invaluable guidance and aid with kidney work, and Dr. Aaron Haig for his assistance with histological analysis. I would also like to acknowledge my co-supervisor Dr. Gregory Kelly as well as my advisory committee members, Dr. Sashko Damjanovski and Dr. Jamie Kramer, for their willingness to provide me with constructive feedback and insightful advice. Special thank you to Dr. Gregory Kelly for taking the time to read and edit my thesis.

Lastly, to my friends and family, I would not be where I am today without your unwavering love and support. To my parents, thank you for your constant words of encouragement and for being my biggest supporters, I am forever in debt for everything you have done for me. To my mom, especially; you never once hesitated to push your own problems aside to listen to mine, you have been my backbone in every sense of the word and I truly could not have done this without you.

Table of Contents

Abstract i

Acknowledgments ii

Table of Contents iii

List of Tables vi

List of Figures vii

List of Appendices ix

List of Abbreviations x

Chapter 1 1

1 Introduction 1

1.1 The Mammalian Kidney 1

1.1.1 Functional Anatomy 1

1.1.2 Renal Physiology 2

1.2 Chronic Kidney Disease 5

1.2.1 Epidemiology 5

1.2.2 Detection and Progression 7

1.2.3 Etiology and Comorbidities 8

1.2.4 Cell Response to Stress 11

1.2.5 Hypertension and CKD 15

1.2.6 Genome-Wide Association Studies (GWAS) 18

1.3 Shroom3 22

1.3.1 Identification 22

1.3.2 Shroom3 Protein Structure 22

1.3.3 Cellular Functions of Shroom3 and Mechanisms of Action 25

1.3.4 Tissue-Specific Activities of Shroom3 28

1.4 Implications of Shroom3 in Disease 35
1.4.1 Human *SHROOM3* Variants 35
1.4.2 Pulmonary Arterial Hypertension 40
1.4.3 HIV-Associated Neurocognitive Disorders (HAND) 41
1.4.4 Chronic Kidney Disease 41
1.5 Hypertension and CKD: Re-visited 44
1.5.1 Hypertension Induced by Renal Dysfunction 44
1.5.2 Developmental Origins for Hypertension: The Brenner Hypothesis 46
1.5.3 Regulation of Blood Pressure by the Kidney 47
1.5.4 Sodium Intake and Hypertension 50
1.6 Rationale, Hypotheses, Objectives 51
1.6.1 Rationale 51
1.6.2 Hypothesis and Objectives 51
Chapter 2 53
2 Materials and Methods 53
2.1 Mice 53
2.2 Genotyping 53
2.3 High-Salt Model 54
2.4 Blood Pressure Measurements (Tail-Cuff) 54
2.5 Tissue Collection 55
2.6 Urinalysis 55
2.7 Generation of *SHROOM3* Variants 56
2.8 Cell Culture and Transfection 56
2.9 Immunofluroescence 58
2.10 Statistical Analysis 59
Chapter 3 60

3 Results 60

3.1 Physiological effects of *Shroom3* loss 60

3.1.1 Body weight and heart rate 61

3.1.2 Blood Pressure 61

3.1.3 High-salt diet increases blood pressure variability in *Shroom3*$^{+/Gt}$ mice.. 69

3.2 A short-term high-salt diet does not promote renal injury in *Shroom3*$^{+/Gt}$ mice .. 72

3.3 Effects of *Shroom3* loss under prolonged exposure to high dietary salt intake.... 74

3.3.1 Blood Pressure 74

3.3.2 Urinalysis 78

3.3.3 Loss of *Shroom3* promotes cardiac hypertrophy on a long-term high-salt diet..... 81

3.3.4 Evaluation of renal injury 81

3.4 Functional assessment of human *SHROOM3* variants 84

Chapter 4 88

4 Discussion 88

4.1 Overview 88

4.2 Loss of *Shroom3* elevates blood pressure variability but not hypertension in the presence of a sodium insult 88

4.3 Potential long-term effects of *Shroom3* loss upon prolonged exposure to a high-salt diet 91

4.4 Altered cellular function of human *SHROOM3* variants 97

4.5 Future Directions and Conclusions 98

References 100

Appendices 125

Curriculum Vitae 131

List of Tables

Table 1.1 CKD stages and prevalence. 9

Table 1.2 Risk factors for CKD. 10

Table 1.3 List of *SHROOM3* variants predicted to be probably damaging by PolyPhen-2 in known domain locations. 37

Table 1.4 Classification of hypertension.. 45

Table 2.1 Primer sequences for PCR used to generate *SHROOM3* variants 57

List of Figures

Figure 1.1 Structure of the mammalian kidney 3

Figure 1.2 Schematic diagram of glomerular filtration 6

Figure 1.3 Podocyte injury induced by hypertension 19

Figure 1.4 Conserved domains of Shroom3 24

Figure 1.5 Schematic illustration of Shroom3's proposed mechanisms for apical constriction and apicobasal elongation 29

Figure 1.6 Progressive cycle of hypertension and CKD. 48

Figure 3.1 Comparison of baseline physiological parameters between WT and *Shroom3+/Gt* mice. 62

Figure 3.2 Effects of high-salt diet and *Shroom3* loss on body weight 63

Figure 3.3 Effects of high-salt diet and *Shroom3* loss on heart rate 64

Figure 3.4 Effects of high-salt diet and Shroom3 loss on diastolic blood pressure. 66

Figure 3.5 Effects of high-salt diet and Shroom3 loss on mean arterial pressure 67

Figure 3.6 Effects of high-salt diet and *Shroom3* loss on systolic blood pressure 68

Figure 3.7 A high-salt diet increases SBP variance in *Shroom3*$^{+/Gt}$ mice 70

Figure 3.8 Absolute change in systolic blood pressure in response to a high-salt diet..... 71

Figure 3.9 Loss of *Shroom3* leads to elevated blood pressure variability on a high-salt diet.. 73

Figure 3.10 Histological assessment of kidneys from WT and *Shroom3*$^{+/Gt}$ mice on a short-term high-salt diet 75

Figure 3.11 Effects of a long-term high-salt diet and *Shroom3* loss on systolic blood pressure 77

Figure 3.12 Loss of *Shroom3* leads to sustained increases in blood pressure variability on a prolonged high-salt diet 79

Figure 3.13 A high-salt diet decreases urinary protein and creatinine 80

Figure 3.14 Loss of *Shroom3* increases heart weight to body weight ratio on a long-term high-salt diet..... 83

Figure 3.15 Histological assessment of kidneys from WT and *Shroom3*$^{+/Gt}$ mice on a long-term high-salt diet. 83

Figure 3.16 Human variants of *SHROOM3* have attenuated ability to drive apical constriction..... 87

List of Appendices

Appendix A: Supplemental information for blood pressure measurements and list of mice omitted from statistical analysis..... 125

Appendix B: Representative variability in SBP response of *Shroom3*$^{+/Gt}$ mice on a high-salt diet..... 126

Appendix C SBP measurements used for BPV analysis.. 127

Appendix D: List of identified human *SHROOM3* variants of interest.. 128

Appendix E: Representative electropherograms of variants confirmed by DNA sequencing 129

Appendix F: Representative analysis of apical constriction determined by ZO-1 staining.. 130

List of Abbreviations

AJC	Apical junctional complex
Ang II	Angiotensin II
ANOVA	Analysis of Variance
ASD	Apx/Shrm Domain
BP	Blood pressure
bp	Base pair
BPV	Blood pressure variability
CAN	Chronic allograft nephropathy
Cdc42	Cell division control protein 42 homolog
CE	Convergent extension
Celsr	Cadherin EGF LAG seven-pass G-type receptors 1–3
CHARGE	Cohorts for Heart and Aging Research in Genomic Epidemiology
CHD	Congenital heart disease
CKD	Chronic kidney disease
CNS	Central nervous system
CVD	Cardiovascular disease
DAPI	4',6-diamidino-2-phenylindole
DBP	Diastolic blood pressure
DMEM	Dulbecco's Modified Eagle's Medium
DNMs	De novo mutations
DOCA	Desoxycorticosterone-trimethylacetate
DS	Dahl salt-sensitive
Dvl	Dishevelled
ECM	Extracellular matrix
eGFR	Estimated glomerular filtration rate
ELISA	Enzyme linked immunosorbent assay
EMT	Epithelial-mesenchymal transition
ENU	N-ethyl-N-nitrosourea
ESP	Exome Sequencing Project
ESRD	End-stage renal disease

EDTA	Ethylenediaminetetraacetic acid
FA	Folic acid
FBS	Fetal bovine serum
FERM	Four-point-one, Ezrin, Radixin, Moesin
FGF	Fibroblast growth factor
FHH	Fawn-Hooded Hypertensive
FP	Foot processes
FPE	Foot process effacement
FSGS	Focal segmental glomerulosclerosis
GBM	Glomerular basement membrane
GEF	Guanine nucleotide exchange factor
GFB	Glomerular filtration barrier
GFP	Green fluorescent protein
GFR	Glomerular filtration rate
Gt	Gene-trap allele
GWAS	Genome-wide association studies
H&E	Hematoxylin & Eosin
HIV	Human immunodeficiency virus
HR	Heart rate
HS	High-salt
HYD	Hydralazine
IL-10	Interleukin 10
KIM-1	Kidney injury molecule 1
LoF	Loss-of-function
LR	Left-right
MAP	Mean arterial pressure
MCP-1	Monocyte chemoattractant protein 1
MDCK	Madin-Darby canine kidney
MEM	Minimum Essential Media
MM	Metanephric mesenchyme
mmHg	Millimeter of mercury
MRLC	Non-muscle myosin II regulatory light chain

MT	Microtubules
MTOCs	Microtubule-organizing centers
NHLBI	National Heart, Lung, and Blood Institute
NS	Normal-salt
NTD	Neural tube defect
PAH	Pulmonary arterial hypertension
PBS	Phosphate Buffer Solution
PCP	Planar cell polarity
PCR	Polymerase Chain Reaction
PDZ	PSD/Dgl/ZO-1
PFA	Paraformaldehyde
PirB	paired immunoglobulin-like receptor B
Pitx1	Paired Like Homeodomain 1
POSH	Plenty of SH3s
PolyPhen-2	Polymorphism phenotyping version 2
QTL	quantitative trait loci
RAS	Renin-angiotensin system
RhoA	Ras homolog family member A
RNAi	RNA interference
ROCK	Rho-associated coiled-coil-containing protein kinase
RT-PCR	Real-time Polymerase Chain Reaction
SAD	Sinoaortic denervation
SBP	Systolic blood pressure
SD	Standard deviation
SDS	Sodium dodecyl sulfate
SNPs	Single-nucleotide polymorphisms
TGF-ß	Transforming growth factor beta
TNF-α	Tumor necrosis factor-alpha
TCF7L2	Transcription factor 7-like-2
UB	Ureteric bud
UMOD	Uromodulin
UNX-DOCA	Uninephrectomy-desoxycorticosterone-trimethylacetate

UPCR	Urinary protein to creatinine ratio
WT	Wild-type
ZO1	Zonula occludens-1

Chapter 1

1 Introduction

Studying the contribution of genetic factors to the pathogenesis of human diseases has been invaluable in advancing our fundamental understanding of disease susceptibility and processes. These studies can begin at the level of genome-wide association studies (GWAS) that specifically aim to identify novel genetic risk factors by detecting associations between genetic variants within the human population and complex disease traits. The work presented in my thesis focuses on one such candidate gene, *SHROOM3* that has been identified by several GWAS as having a strong correlation to chronic kidney disease (CKD). Shroom3 is an actin-binding protein that has been characterized as a regulator of epithelial cell shape change during morphogenesis. Although it is most widely recognized for its role during development, increasing evidence for a role of Shroom3 in a range of human disorders is emerging, many of which have developmental origins. Recently, direct functional support for the GWAS that have strongly associated *SHROOM3* to *CKD* has been provided using several animal models (Khalili et al., 2016; Yeo et al., 2015). These studies have shown that Shroom3 is critical for proper kidney function and loss of Shroom3 produces phenotypes associated with CKD symptoms. However, whether decreased Shroom3 activity directly increases susceptibility to disease remains unknown. The aim of my project is to investigate how altered Shroom3 activity has the potential to predispose individuals to disease by answering two research questions: does Shroom3 deficiency increase susceptibility to hypertension and do potentially damaging *SHROOM3* variants currently identified within the human population have compromised cellular function?

1.1 The Mammalian Kidney

1.1.1 Functional Anatomy

The kidneys are bilateral organs of the renal system that fulfill a number of vital functions, of which the most fundamental is the filtration of blood. Specifically, the kidneys remove excess waste and toxic metabolic compounds then excrete them into

urine, while simultaneously reabsorbing nutrients and water (Davidson, 2008; Takasato & Little, 2015; Tanner, 2009). In addition to overseeing this essential physiological process, the kidneys are also important regulators of homeostasis as they help maintain blood pressure and bone density as well as water, pH, electrolyte, and acid-base balance (Little & McMahon, 2012; Tanner, 2009).

Each kidney can be separated into two distinct regions: a peripheral layer, the cortex, and an inner layer, the medulla (Tanner, 2009). The medulla is further subdivided into an inner medulla and outer medulla, which contains the collecting ducts and short loops of Henle (Davidson, 2008). The cortex comprises all other nephron components including the glomeruli, convoluted tubes, and cortical collecting ducts, and is where primary filtration takes place (Tanner, 2009). This gross anatomical division establishes an osmotic gradient between the cortex and medulla that is critical for the absorption of water from urine (Davidson, 2008).

1.1.2 Renal Physiology

Filtration in the kidney takes place in functionally independent units known as nephrons, that are found throughout the cortex and medulla (Figure 1.1) (Davidson, 2008). Typically, there are around one million nephrons present in a human kidney and around 11 000 in a mouse kidney (Davidson, 2008). Each nephron consists of the glomerulus, Bowman’s capsule, and a double hairpin-shaped tubule that drains into the renal pelvis (Kurts et al., 2013). Three processes occur within the nephron in order to form urine: glomerular filtration, tubular reabsorption, and tubular secretion (Tanner, 2009).

First, blood is supplied to the kidney by the renal artery. The incoming vascular network is then subdivided until a single afferent arteriole enters the glomerulus where it is subdivided into a capillary network and exits via a single efferent arteriole (Schwartz & Furth, 2007; Tryggvason, 2005). The capillaries are surrounded by the foot processes of epithelial podocytes that filter the blood as part of the glomerular filtration barrier (GFB) (Brinkkoetter et al., 2013). The plasma filtrate is pooled into the urinary space of the Bowman’s capsule and travels down the proximal convoluted tubule, where the majority

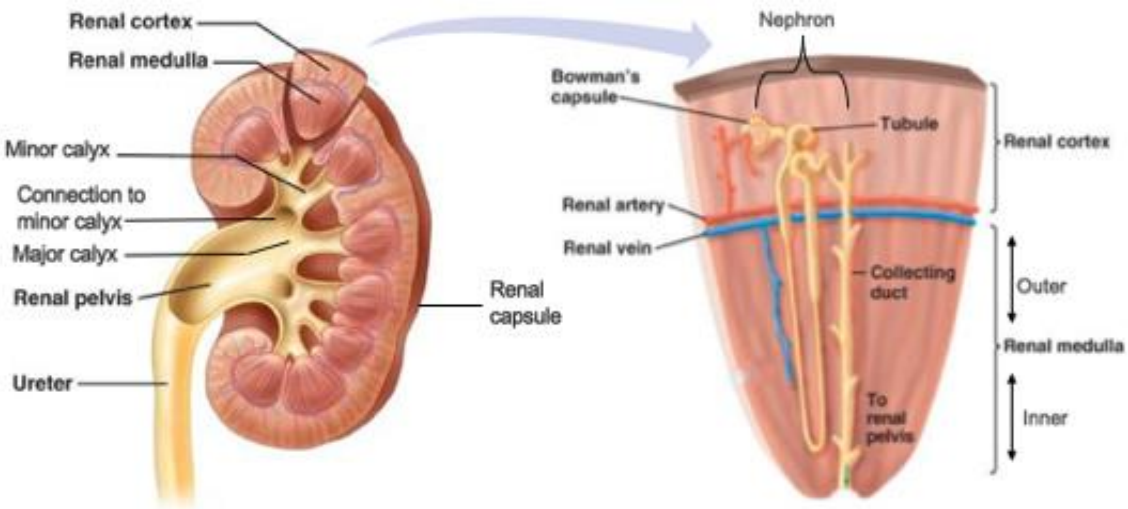

Figure 1.1 Structure of the mammalian kidney. A schematic diagram showing the gross anatomical structure of the kidney sectioned longitudinally (left) and a close-up of the renal lobe showing the orientation of the nephron relative to the kidney (right). Adapted from *Pearson Education* (2009).

of water reabsorption takes place through the peritubular capillaries (Lote, 2013; Tanner, 2009). Simultaneously, organic ions including drugs and toxins from the blood are secreted into the filtrate (Lote, 2013; Tanner, 2009). Further reabsorption of water and some solutes is carried out by the peritubular capillaries as the filtrate travels through the loops of Henle towards the distal convoluted tubule (Lote, 2013; Tanner, 2009). While passing through the distal convoluted tubule, metabolic waste products (i.e. hydrogen and potassium ions) found in the blood are secreted into the filtrate (Lote, 2013; Tanner, 2009). Lastly, the filtrate reaches the collecting duct where the final reabsorption of water takes place, concentrating the urine before it is projected into the ureter for excretion (Lote, 2013; Tanner, 2009).

1.1.2.1 Nephrogenesis

Mammalian nephrogenesis occurs through three morphological stages known as the pronephros, mesonephros, and metanephros. The final and only non-transitory stage, the metanephros, gives rise to the definitive adult kidney (Davidson, 2008). Kidney development is initiated and maintained through the reciprocal interactions between two key embryonic tissues derived from the intermediate mesoderm: the ureteric bud (UB) and the metanephric mesenchyme (MM) (Takasato & Little, 2015). At E10.5-11 in mice, the MM induces the formation of the UB as an outgrowth of the pronephric duct. The UB then invades the MM, marking the initiation of metanephric development (Davidson, 2008). Upon invasion of MM, the UB undergoes a process of branching morphogenesis through sequential rounds of division to elongate into a ureteric tee, which ultimately gives rise to the collecting duct system (Short & Smyth, 2016). Simultaneously, induction of the MM by the UB causes a subpopulation of condensed MM near the UB tips to cluster into pre-tubular aggregates that eventually differentiate into nephrons (Short & Smyth, 2016). Nephron differentiation involves the dynamic process of mesenchymal-to-epithelial transition that facilitates the morphogenesis of the pre-tubular aggregate into a renal vesicle, a comma-shaped body, and an s-shaped body (Dressler, 2006). Once the s-shaped body is formed, the proximal end becomes invaded by blood vessels marking the initiation of glomerulogenesis while the distal end fuses with the collecting duct (Dressler, 2006). This highly conserved process of nephron formation occurs during the

later stages of organogenesis; in mice, nephron formation continues until 14 days after birth, while in humans, it ceases at 36 weeks of gestation (Davidson, 2008; Short & Smyth, 2016).

1.1.2.2 Glomerular Filtration

The glomerulus is a specialized structure comprised of a capillary network underlying the Bowman's capsule that functions to ultrafiltrate plasma (Figure 1.2) (Lote, 2013). The glomerular filter, or glomerular filtration barrier (GFB), serves as a macromolecular sieve restricting the passage of large plasma proteins (i.e. albumin) while simultaneously allowing the passage of plasma water and small solutes (Kasner et al., 2013). Perturbations to the GFB and its constituent layers have been shown to result in the leakage of protein into urine, a marker of CKD (Menon et al., 2015). There are three layers comprising the GFB: the fenestrated endothelial cells, the glomerular basement membrane (GBM), and the epithelial podocyte cells (Haraldsson et al., 2008). Importantly, the critical role of podocytes in maintaining the structural integrity of the GFB has been evidenced by multiple studies, one of which found that all single gene mutations causing nephrotic disorders reside in podocyte-specific genes (Wiggins, 2007).

1.2 Chronic Kidney Disease

1.2.1 Epidemiology

Chronic kidney disease (CKD) is a major public health concern, currently affecting 11-13% of the global population and increasing in prevalence (Hill et al., 2016). CKD is a condition defined by a progressive decline in renal function as indicated by the presence of structural or functional abnormalities in the kidney sustained for longer than 3 months (Moe et al., 2017; National Kidney Foundation, 2002; Webster et al., 2017). Ranked as the 14th leading cause of death worldwide, CKD is a significant cause of morbidity and mortality, imposing a substantial global economic and health burden (Webster et al., 2017). In Canada, national trends in the prevalence of CKD have mirrored global ones (Arora et al., 2013). CKD currently affects 12.5% of Canadians, with treatments for end-stage renal disease accounting for $1.9 billion in health care costs in 2000 (Arora et al., 2013; Zelmer, 2007). The rising prevalence of CKD in Canada is attributed to the

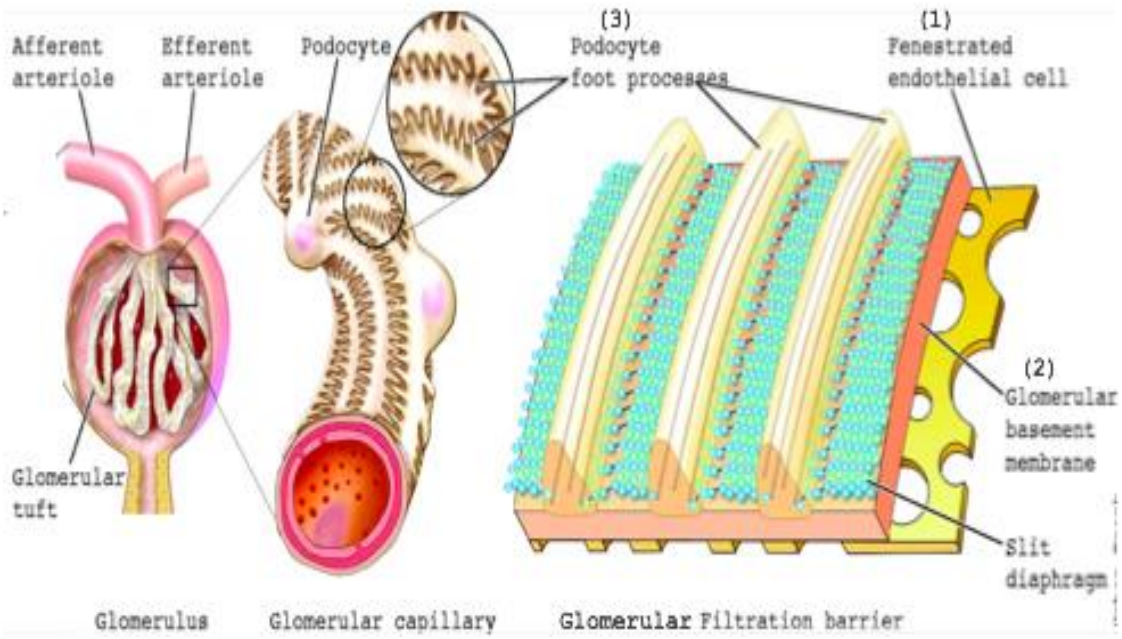

Figure 1.2 Schematic diagram of glomerular filtration. Diagram of the glomerulus (left), glomerular capillary (middle), and GFB (right). The afferent arteriole delivers blood to the glomerulus and branches within it to form a capillary network (glomerular tuft). Each glomerular capillary wall is lined with a GFB. First, blood passes travels through the fenestrations between endothelial cells (1), then an extracellular glomerular basement membrane (2), and finally a podocyte epithelial layer (3). The plasma filtrate is pooled in the Bowman's capsule and led through the remaining components of the nephron, while the ultrafiltrated blood is returned to circulation by the efferent arteriole. Image modified from (Tryggvason and Wartiovaara, 2005).

increasing level of the aged and overweight in our population; age and weight are both inversely correlated to kidney function (Arora et al., 2013; National Kidney Foundation, 2002).

1.2.2 Detection and Progression

1.2.2.1 Diagnosis

There are several assessments that can be used as a proxy for kidney function and health, but diagnosis of CKD usually occurs on the basis of one of two screenings. The first diagnostic tool is a urinalysis to detect the degree of proteinuria, which is defined by the presence of more than 300 mg of protein in urine with more than 3.5 g of protein per day being excreted in nephrotic syndrome. Urinary excretion of protein is a hallmark of abnormal kidney filtration; albumin is the most commonly used biomarker for proteinuria assessments and the presenting symptom is accordingly known as albuminuria (Haraldsson et al., 2008). The standard method for proteinuria detection is a urine dipstick test which utilizes a reagent strip device that changes colour if protein is present at a level that is above the normal range (Lamb et al., 2009). To further quantify the amount of protein present in the urine, a protein to creatinine ratio (UPCR) is used on a spot urine sample; a ratio is necessary as it corrects for variations in urinary protein concentration due to hydration (Levey et al., 2003). Previously, 24 hour timed urine collection were used to measure proteinuria, but the UPCR of a spot urine sample has since become the preferred assay (Lamb et al., 2009; Levey et al., 2003).

The second diagnostic parameter is a measure of the estimated glomerular filtration rate (eGFR), which indirectly provides the flow-rate of blood being filtered by the kidney and is considered the gold-standard method for diagnosis of CKD (Levey & Coresh, 2012; Levey & Inker, 2016). GFR is most commonly determined using an estimation based on the 24-hour urinary clearance or serum level of an endogenous filtration biomarker in combination with prediction equations that take into account variables such as body size, age, and sex (Levey & Inker, 2016; National Kidney Foundation, 2002). The most commonly used biomarker for eGFR is creatinine ($eGFR_{cr}$) (Levey & Inker, 2016). An individual's GFR is determined by two factors: the number of functioning nephrons

present and the rate of filtration in each nephron, with the latter being largely dependent on the integrity of the GFB (Brinkkoetter et al., 2013; Schwartz & Furth, 2007). A GFR of less than 60 mL/minute/1.73m^2 over a period of 3 months or longer is sufficient for CKD diagnosis (National Kidney Foundation, 2002).

1.2.2.2 CKD Stages and Treatment

CKD is classified into five different stages on the basis of GFR, with each successive stage corresponding to an increasingly diminished GFR (Table 1.1). Proper evaluation and course of action for CKD patients begins with recognizing and identifying the correct disease stage and further requires a fundamental understanding of the separate but related concepts of diagnosis, disease complications and severity, and risks and comorbidities associated with loss of kidney function (National Kidney Foundation, 2002). Treatment at stages 1 and 2 is centered around slowing disease progression through the controlled management of comorbidities including hypertension and diabetes. At stage 3, other complications of decreased GFR, such as anemia, and bone disease, in addition to hypertension and diabetes, are targeted for amelioration. By stage 4, once the eGFR drops below 30 ml/min/1.73m^2, patients should be prepared for kidney replacement therapy which is necessary for survival upon progression to stage 5. The final stage of CKD or end-stage renal disease (ESRD) is kidney failure that is defined by an eGFR of less than 15ml/min/1.73m^2, and can only be treated by means of dialysis or kidney transplantation (National Kidney Foundation, 2002).

1.2.3 Etiology and Comorbidities

1.2.3.1 Risk Factors

The difficulty in the treatment and management of CKD is attributed to its diverse range of aetiologies, including genetic, autoimmune, metabolic and toxic, mechanical, environmental, and dietary factors (Nogueira et al., 2017). Risk factors for CKD are defined by their contribution to the susceptibility, onset, progression, and/or end-stage of the disease, with the majority of research being focused on identifying earlier stage risk factors (Table 1.2). Susceptibility factors include sociodemographic and genetic factors

Table 1.1 CKD stages and prevalence. The five stages of CKD and corresponding global and national prevalence rates with the description, GFR threshold, and course of action for each stage (below); N/A prevalence estimate not available. Adapted from the National Kidney Foundation (2002) with data from (Hill et al. 2016; Arora et al. 2013).

STAGE	***Pre***	***Stage 1***	***Stage 2***	***Stage 3***	***Stage 4***	***Stage 5***
Description	At increased risk	Kidney damage with normal or ↑ GFR	Kidney damage with mild ↓ GFR	Moderate ↓ GFR	Severe ↓ GFR	Kidney failure
GFR (mL/min/1.73 m^2)	≥ 60 (with CKD risk factors)	≥ 90	60-89	30-59	15-29	< 15
Course of Action	Screening; control of risk factors	Diagnosis and treatment of comorbid conditions, slowing progression, CVD risk reduction	Estimating progression	Evaluating and treating complications (i.e. comorbidities)	Preparation for renal replacement therapy	Renal replacement therapy in the form of dialysis or kidney transplant
Global prevalence (above) Prevalence in Canada (*italicized*, below)	N/A	3.5% *6.9%*	3.9% *2.5%*	7.6% *2.9%*	0.4% N/A	0.1% N/A

Table 1.2 Risk factors for CKD. Adapted from National Kidney Foundation (2002) with data from (Nahas and Bello, 2005).

Risk Factor	***Definition***	***Examples***
Susceptibility	Increases susceptibility to kidney damage	Family history or genetic predisposition, older age, males, low birthweight and infant malnutrition (reduced nephron endowment), low income or education, ethnic minority status in developed countries, low income or education
Initiation	Directly initiates kidney damage	Diabetes, high blood pressure, autoimmune diseases, systemic infections, urinary stones, drug toxicity (consumption of analgesics), smoking, obesity
Progression	Causes worsening kidney damage and faster decline in kidney function after initiation of kidney damage	Non-modifiable: genetics, race, age, sex (see initiation factors above) Modifiable: increased hypertension, poor glycemic control in diabetes, smoking, obesity
End-stage	Increases morbidity and mortality in kidney failure	Anemia, low serum albumin level, late referral, smoking, drug toxicity

that predispose individuals to CKD. Initiation risk factors include the two main causes of CKD, diabetes and hypertension. If any initiation factors are left untreated or symptoms worsen, they transition into progression factors, thereby increasing the rate of progression of already established CKD. Other factors such as obesity and smoking have also been implicated (National Kidney Foundation 2002; Nahas and Bello 2010).

1.2.3.2 Comorbidities

Hypertension and diabetes are widely accepted as the two main causes of CKD in all developed and most developing countries (Levey & Coresh, 2012; Webster et al., 2017). They are also considered to be significant comorbidities of CKD, with each disease exacerbating the progression and outcomes of the other. Section *1.2.5* will examine hypertension in the pathophysiology of CKD more closely. Importantly, all three collectively increase the risk of cardiovascular disease (CVD) (Wright & Hutchison, 2009). CVD is a significant outcome to consider in CKD treatment and management, as patients with CKD are more likely to die of CVD complications than they are to develop kidney failure (National Kidney Foundation, 2002; Sarnak et al., 2003). In fact, in all stages of CKD, death is a more likely outcome than progression to ESRD (Jha et al., 2013). Thus, the amelioration of hypertension and diabetes in the early stages of CKD is critical in attenuating both renal and CVD progression (Nahas & Bello, 2010).

1.2.4 Cell Response to Stress

1.2.4.1 Renal Fibrosis

Despite the complex etiology of CKD, the progression of CKD eventually converges into common histolopathological and functional manifestations, generally characterized by the appearance of a fibrotic phenotype in the tubular, vascular, and glomerular compartments of the kidney, termed tubulointerstitial fibrosis, vasclular sclerosis, and glomerulosclerosis respectively (Hewitson, 2012). Renal fibrosis is hallmarked by the replacement of damaged renal tissues by a scar-like formation as a result of excess extracellular matrix (ECM) accumulation and deposition (López-Novoa et al., 2011). The cellular response to stress in the kidney is similar to wound-healing processes in other tissues, whereby an initial insult leads to the activation of an inflammatory pro-

proliferative response that involves circulating and migratory immune system cells (López-Novoa et al., 2011; Nogueira et al., 2017). However, for reasons that remain elusive, this initially restorative inflammatory response becomes deregulated and induces uncontrollable and aberrant matrix synthesis and cell proliferation, resulting in tissue scarring (Hewitson, 2012; López-Novoa et al., 2011; Nogueira et al., 2017). Depending on the location of the fibrotic phenotype, kidney disease can be broadly grouped into tubulointerstitial, renovascular, and glomerular diseases (López-Novoa et al., 2011).

Glomerular diseases, or glomerulopathies, are renal disorders that alter glomerular structure and function. They can arise independently or secondary to tubulointerestitial and renovascular diseases, but progress significantly faster than tubulointerstitial ones (López-Novoa et al., 2011). Glomerulopathies can be defined as either inflammatory, caused by systemic and renal infections, or non-inflammatory, caused by chemical or mechanical damage such as in the case of diabetes and hypertension (López-Novoa et al., 2011). The histopathology of glomerulopathies is diverse, but common aberrant morphologies include podocyte injury, crescent formations caused by ECM accumulation, and focal and segmental glomerulosclerosis (López-Novoa et al., 2011). Focal segmental glomerulosclerosis (FSGS) is a glomerulopathy characterized by a histologic pattern of glomerular scarring (Rosenberg & Kopp, 2017). At the beginning stages of the disease, the glomerulosclerosis is both focal, only limited to a small portion of the glomeruli, and segmental, only affecting one section of the glomerulus (D'Agati et al., 2014). As the disease progresses, glomerulosclerosis becomes widespread and global (D'Agati, 2008). The pathogenesis of FSGS involves two main mechanisms relating to podocytes: loss of the filtration barrier and podocyte depletion (D'Agati et al., 2014).

1.2.4.2 Podocyte Injury

Podocytes are terminally differentiated epithelial cells that sit on the urinary aspect of the GBM facing the Bowman's capsule, and act as the final barrier of the GFB (Menon et al., 2012). They have three structural components consisting of the cell body, primary processes, and foot processes (Brinkkoetter et al., 2013). The cell body protrudes into the urinary space of the Bowman's capsule and gives rise to primary processes that extend down to the capillaries of the glomerulus (Pavenstadt et al., 2003). At the outer surface of

the capillaries, the primary processes split into secondary foot processes (FP) that anchor and wrap themselves around the capillaries, adhering to the GBM while the cell body remains afloat (Brinkkoetter et al., 2013; Kriz et al., 2013). The FP are highly specialized contractile structures that interdigitate to form filtration slits between adjacent processes (Pavenstadt et al., 2003). A membranous cell-to-cell junction called a slit diaphragm bridges the space between filtration slits (Brinkkoetter et al., 2013). Podocytes first emerge as a separate cell population in the S-shaped body of the developing nephron where cells facing the Bowman's space are seen to express podocyte-specific markers (Brunskill et al., 2011). Importantly for our work, *Shroom3* is expressed in the podocyte at all stages of life including development and adulthood.

Podocytes represent the sites of initial injury in nearly all human glomerulopathies and animal models of proteinuric glomerular disease, with only a few exceptions (D'Agati, 2008). Of importance, progressive loss of podocytes is the most frequent cause of end-stage renal failure (Kriz et al., 2013). Several pathogenic mechanisms underlying podocyte injury manifest as ultrastructural changes (Brinkkoetter et al., 2013). Specifically, these changes involve the loss of the interdigitating pattern of FP, referred to as foot process effacement (FPE) (Kriz et al., 2013). FPE is distinguished by two stages. The first stage is marked by the shortening of FP and displacement or loss of the slit diaphragms (Kriz et al., 2013). In the second, more progressive stage, complete flattening and retraction of the FP into primary processes is observed, eventually merging with the cell bodies (Kriz et al., 2013). Because the podocytes are floating cell bodies that only attach to the GBM by their foot processes, FPE often results in podocyte detachment in conjunction with apoptosis, leaving behind naked areas of the GBM (Kriz et al., 2013). These exposed areas then allow for leakage of proteins across the GFB, resulting in proteinuria (Kriz et al., 2013).

A tightly regulated actin cytoskeleton accounts for the core structure of podocytes and the assembly and maintenance of their FP (Pavenstadt et al., 2003). The cytoskeletal network within FP consists of a dense bundle of actin filaments that extends along the length of the foot processes and a shorter, branched cortical network that is found at the cell periphery and anchors elements of the slight diaphragm (Reiser & Altintas, 2016). The

function of podocytes critically depends on their structural integrity and several studies have revealed that injury to podocytes results in a common final pathway of cytoskeletal reorganization followed by FPE (Tian & Ishibe, 2016). Thus, proteins that regulate the plasticity of the podocyte actin cytoskeleton are essential for the sustained function of the GFB (Faul et al., 2007). One such protein is the GTPase family member Ras homolog family member A (RhoA) which activates the serine/threonine kinases ROCK1 and 2 (Amano et al., 2010; Kistler et al., 2012). ROCKs phosphorylate the regulatory light chain (RLC) of non-muscle myosin II, which can then form dynamic actomyosin contractile networks with actin filaments (Amano et al., 2010). Importantly, ROCKs are downstream effectors of Shroom3 that are necessary for its apical constriction function, as will be extensively discussed in *1.3*. The function of RhoA with respect to podocytes appears to be stabilization of FP structure and protection from FPE, and this function is dependent on basal RhoA expression. *In vitro*, overexpression (Zhu et al., 2011) and disruption of RhoA (Huang et al., 2016) leads to FPE and podocyte apoptosis in cultured podocytes (Kistler et al., 2012).

Other regulators of the podocyte actin cytoskeleton that have been shown to be crucial to proper kidney function include synaptopodin (Asanuma et al., 2005, Asanuma et al., 2006) and podocalyxin (Schmieder et al., 2004), which are podocyte-specific regulators of RhoA. Additionally, Rho guaninine dissociation inhibitor (GDI)-α (Togawa et al., 1999), as well as Nck1 and Nck2 (Jones et al., 2006; Verma et al., 2006) have been found to be essential for maintaining proper podocyte structure. Lastly, α-actinin-4, a mutation in which causes familial FSGS in humans (Kaplan et al., 2000) has been shown to induce glomerulopathies *in vivo* upon knockout in mice (Dandapani et al., 2007; Kos et al., 2003).

It is therefore not surprising that Shroom3, an established regulator of the actin cytoskeleton specifically expressed in podocytes, has been found to be necessary for maintenance of podocyte structure. Specifically, loss of *Shroom3* and targeted podocyte-specific disruption of *Shroom3* directly results in FPE in mice and zebrafish, respectively (Khalili et al., 2016; Yeo et al., 2015).

1.2.5 Hypertension and CKD

Hypertension is the second leading cause of CKD, accounting for 28.4% of all CKD cases in the USA (Townsend and Taler 2015). The prevalence of hypertension increases with worsening kidney function and has made blood pressure reduction an important course of action for slowing CKD progression (Townsend & Taler, 2015). This inverse relationship between kidney function and blood pressure (BP) is evidenced by a direct correlation between relative risk of developing ESRD and BP severity (Judd & Calhoun, 2015). In fact, a health screening registry revealed that individuals with a baseline BP of 180/100 mm Hg were 15 times more likely to progress to ESRD than individuals with a baseline BP of 110/70 mm Hg (Tozawa et al., 2003). To fully understand how CKD progresses, it is crucial to investigate how hypertension contributes to renal injury.

1.2.5.1 Pathophysiology

Hypertensive nephrosclerosis is sclerosis of the kidney caused specifically by hypertension and is pathogenically independent of other renal diseases such as diabetic nephropathy (Luft, 2000). The extent of renal damage caused by hypertension-related mechanisms is determined by the systemic BP load, the degree to which the load is transmitted to renal microvasculature, and local tissue susceptibility factors to injury resulting from increased pressure including genetic factors, pre-existing glomerular hypertrophy and structural integrity of the podocyte layer (Ravera, 2006).

Under normal conditions, increases in systemic BP are controlled by autoregulatory mechanisms such that renal blood flow and glomerular capillary pressure are maintained relatively constant, thereby preventing the transmission of the BP load to renal microvasculature (Bidani & Griffin, 2004; Ravera, 2006). However, under chronic hypertensive conditions, the autoregulatory mechanism exceeds its threshold and increases in systemic BP directly induce an increase in renal blood flow and capillary pressure, allowing the BP load to reach the renal microvasculature (Bidani & Griffin, 2004). The increase in glomerular capillary pressure as a result of increased systemic blood pressure is termed glomerular hypertension (Endlich & Endlich, 2012). Glomerular

hypertension causes mechanical distension of the capillary tuft causing it to expand, resulting in glomerular hypertrophy (Endlich & Endlich, 2012).

Glomerular hypertrophy is necessarily accompanied by a stretch in the overlying foot processes, initially functioning as an adaptive response (Kretzler et al., 1994). This causes reorganization of the actin cytoskeleton, ultimately resulting in FPE and detachment of the podocyte from the GBM, an inevitable result of the mechanical and shear forces imposed by the increased pressure load reaching the glomerulus (Nogueira et al., 2017; Pavenstadt et al., 2003). Damage to podocytes, in turn, leads to increased leakage of proteins across the GFB. This explains why proteinuria is almost always observed in concert with hypertension in CKD patients and why proteinuria is an important prognostic factor for patients with hypertension (Bakris, 2005). This also explains why hypertension increases the risk of developing ESRD as progressive loss of podocytes is the most frequent cause of ESRD (Judd & Calhoun, 2015; Kriz et al., 2013).

Sustained podocyte injury has devastating outcomes that perpetuate progressive renal dysfunction. Upon initial insult to the glomerulus, a focal lesion develops and triggers apoptosis or detachment of podocytes and subsequent activation of the inflammatory response and fibrotic processes (López-Novoa et al., 2011). Fibrotic processes promote aberrant ECM synthesis in the spaces left behind by the podocytes which creates a connective pathway between the Bowman's capsule and intersititium that allows the protein-rich ultrafiltrate to access other glomeruli and tubules to induce further damage (López-Novoa et al., 2011). Since podocytes are terminally differentiated, they cannot regenerate and thus it is believed that glomerular injury can be initiated from a single injured podocyte that spreads the injury to neighbouring intact podocytes (cell-to-cell-spreading), setting up a vicious cycle that culminates into glomerulosclerosis (D'Agati, 2008; Fogo, 2007; Nagata, 2016).

Numerous mouse models have provided evidence for the critical role of podocytes in the pathogenesis of glomerulopathies, where podocyte-specific injury initiated by an extrinsic insult resulted in progressive sclerosis (Fogo, 2007). In one such model, the extrinsic insult was an injection of a toxin, with mice expressing the toxin receptor under

the control of a podocyte-specific promoter (Wharram et al. 2005). In these mice subjected to podocyte-injury, the number of depleted podocytes correlated closely with the severity of disease. Specifically, depletion of more than 40% of the podocyte population led to overt FSGS accompanied by high-grade proteinuria and renal insufficiency, establishing a disease threshold (Wharram et al. 2005). In another model, using chimeric mice, where only a portion of the podocytes were expressing the toxin receptor, podocyte injury and apoptosis spread to neighbouring podocytes that lacked the toxin receptor and initially escaped the extrinsic insult (Matsusaka et al., 2011). This provides support for the cell-to-cell spreading model, whereby a small subset of injured podocytes can propagate the initial injury to non-injured podocytes in a domino-like effect, resulting in glomerulosclerosis (Matsusaka et al., 2011).

The ability of hypertension to induce podocyte damage and progress into glomerulosclerosis has also been demonstrated by several models. *In vitro,* mechanical stretching of conditionally immortalized mouse podocytes facilitated by a computer-assisted stretch apparatus results in enhanced expression of proinflammatory cytokines including transforming growth factor beta (TGF-ß) (Durvasula et al., 2004). *In vivo,* using a uninephrectomy-desoxycorticosterone-trimethylacetate (UNX-DOCA) rat model of chronic hypertension and progressive renal disease, significant increases in blood pressure were observed 3 weeks after surgical kidney excision (Kretzler et al., 1994). By 7 weeks, these mice exhibit hypertrophied glomeruli and subsequent development of glomerulosclerosis. Common to all destructive glomerular profiles observed in the UNX-DOCA hypertensive rats was podocyte detachment, FPE, and pseudocyst formation directly leading up to glomerulosclerosis. While mesangial cell expansion was also frequently observed, no evidence for the pathological sequence of cell shape change and subsequent glomerulosclerosis was found (Kretzler et al., 1994). Mesangial cells function to structurally support the glomerular capillaries through their production of mesangial matrix components including collagen and fibronectin (Haraldsson et al., 2008). Interestingly, an unrelated study found that upon induction of podocyte injury, both endothelial and mesangial cells also exhibited cellular responses to stress marked by cell swelling and expansion of the ECM, which was then followed by the development of glomerulosclerosis (Ichikawa et al., 2005). Furthermore, the degree of endothelial and

mesangial cell response was dependent on the magnitude of podocyte injury, suggesting that podocytes may be capable of propagating injury to other cell types (Ichikawa et al., 2005). Thus, it could be the case that the mesangial cell expansion described in the study by Kretzler et al. (1999), was induced by podocyte damage.

A study using Dahl salt-sensitive (DS) rats that develop hypertension when fed a high-salt diet, foot process effacement and fusion were observed as early as 2 weeks into salt-loading concomitant with the onset of hypertension and before the development of glomerulosclerosis (Nagase et al., 2006). Furthermore, the degree of podocyte damage and consequent proteinuria was exacerbated with increasing exposure to the high-salt diet and manifested into glomerulosclerosis by 6 weeks. From these models of hypertensive renal injury, a common pattern of hypertension-induced podocyte damage characterized by FPE, cell body attenuation, bare areas of the GBM left behind by podocyte detachment and apoptosis, and formation of pseudocysts has emerged (Figure 1.3) (Endlich & Endlich, 2012).

1.2.6 Genome-Wide Association Studies (GWAS)

In keeping with other chronic multifactorial diseases, CKD is laden with complex aetiologies and comprises various environmental and lifestyle factors as well as an inherited component of susceptibility (Smyth et al., 2014). This inherited susceptibility usually exists in the form of genetic variants in the DNA sequence; identifying these susceptible disease variants is a central goal of genome-wide association studies (GWAS) (Bush & Moore, 2012; Smyth et al., 2014). Over the past decade, GWAS have been invaluable in elucidating the genetic component underlying CKD (Wuttke & Köttgen, 2016). GWAS analyze hundreds of thousands of single-nucleotide polymorphisms (SNPs) from across the human genome in order to find variants that are correlated to a particular disease or disease phenotype (Manolio, 2010). In the field of nephrology, GWAS have focused on identifying susceptibility variants associated with CKD aetiologies such as membranous nephropathy as well as CKD-defining traits such as eGFR and urinary albumin to creatinine ratio (UACR) (Wuttke & Köttgen, 2016). GWAS of CKD-defining traits have been conducted in whole populations rather than in

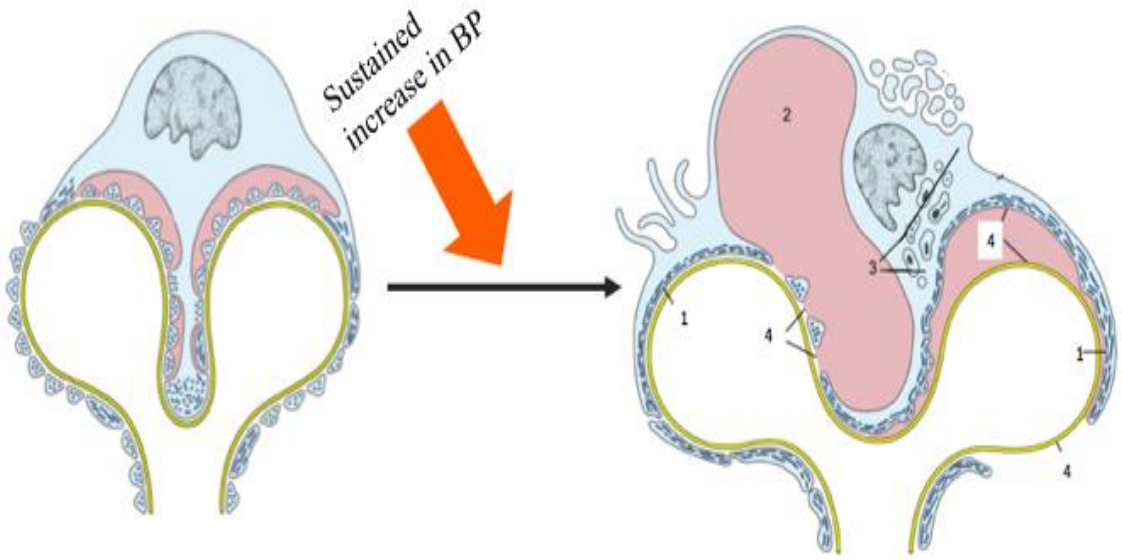

Figure 1.3 Podocyte injury induced by hypertension. Schematic diagram of a normal podocyte (left) and injured podocyte (right). Glomerular hypertrophy is induced by a sustained elevation in systemic blood pressure above a threshold causing the podocyte to also stretch and expand. In addition to podocyte hypertrophy, other injuries include: 1) Foot process effacement 2) pseudocyst formation 3) cell body attenuation 4) detachment and/or apoptosis resulting in naked GBM areas. Image modified from (Kriz et al., 2013).

case control studies like the GWAS of CKD aetiologies, making them more applicable to the general public (Wuttke & Köttgen, 2016). One gene that has consistently been identified by these GWAS as having a strong association with kidney function and disease is *SHROOM3*.

Meta-analyses of prevalent CKD and CKD-defining traits $eGFR_{cr}$ and $eGFR_{cys}$ from four large random populations of the Cohorts for Heart and Aging Research in Genomic Epidemiology (CHARGE) consortium found *SHROOM3* to have strong associations with all 3 measured parameters (Köttgen et al. 2009), only second to uromodulin (*UMOD*), a gene already established to play a role in CKD (El-Achkar et al., 2008; Lhotta, 2010; Pfistershammer et al., 2007; Vyletal et al., 2010a). These results were later replicated in a follow-up study of participants of European ancestry from 20 large population-based studies as well as in an independent consortium of European participants from 9 studies (Chambers et al., 2010; Köttgen et al., 2010). A separate study on five populations from the European Special Population Research Network (EUROSPAN) found a strong association between *SHROOM3* and serum creatinine levels, further confirming previous GWAS findings (Pattaro et al., 2010). While these GWAS identified genetic risk loci related to eGFR and prevalent CKD, defined by a eGFR < 60 ml/min/1.73m^2 at a single time point, they did not address whether the identified loci were involved in the initiation of CKD or in the progression of CKD to ESRD (Böger et al., 2011). To that end, a separate GWAS sought to determine whether the previously identified genetic loci associated with eGFR and prevalent CKD were also associated with initial CKD development and risk for progression to ESRD. Although *SHROOM3* was not found to be correlated with ESRD, it was found to be strongly associated with initiation of CKD (Böger et al., 2011).

Another GWAS interested in identifying loci associated with serum magnesium, potassium, and sodium concentrations found a SNP in *SHROOM3* that strongly correlated to serum magnesium concentrations and clinical hypomagnesemia in European descent participants from the CHARGE Consortium (Meyer et al., 2010). The kidney is an important regulator of ionic serum concentrations and serum magnesium has been

implicated in hypertension and diabetes, the main causes of CKD (Levey & Coresh, 2012; Meyer et al., 2010).

In light of these findings, a successive GWAS sought to assess whether the loci correlated to eGFR as identified by Köttgen et al. were also associated with albuminuria and urinary albumin-to-creatinine ratio (UACR) (Ellis et al., 2012). Albuminuria is the strongest known risk factor for the progression of CKD and UACR has a known inverse relationship with eGFR, with a decreased eGFR corresponding to an increased UACR. Participants of European ancestry from the CKDGen Consortium cohort and of African ancestry from the CARe Renal Consortium were tested for 16 eGFR-associated SNPs for association with UACR and albuminuria. In populations from the CKDGen Consortium and CARe Renal Consortium, *SHROOM3* was the only locus observed to have associations with UACR and albuminuria, respectively. Surprisingly, the association of *SHROOM3* to lower eGFR corresponded to a decreased UACR. This deviation from the typical inverse relationship may have two plausible explanations: *SHROOM3* may be exerting pleiotropic effects or is interacting with mechanisms that substantiate both a higher eGFR and a higher UACR, as in the case of hyperfiltration states (diabetes, hypertension, hyperuricemia) (Ellis et al., 2012). Given the role of hypertension and diabetes in the etiology of CKD, the latter is highly likely. The interaction between eGFR and albuminuria in diabetes was studied in patients with Type 2 diabetes from the Genetics of Diabetes Audit and Resaerch Tayside (GoDARTS) study. Results from the GWAS found that *SHROOM3* was strongly associated with eGFR in type 2 diabetes, and this association was specific to patients with diabetes accompanied by albuminuria (Deshmukh et al., 2013).

Despite the numerous GWAS postulating a correlation between *SHROOM3* and CKD, only recently was Shroom3's role in the kidney characterized. While pathogenic mutations in *UMOD*, the other candidate gene identified by GWAS, are known to cause autosomal dominant kidney diseases in humans including medullary cystic kidney disease 2 and familial juvenile hyperuricemic nephropathy, the potential role of *SHROOM3* in the pathophysiology of disease is still an emerging area that remains relatively incomplete (Vyletal et al., 2010; Zhu et al., 2002).

1.3 Shroom3

1.3.1 Identification

Shroom3 encodes for the actin-binding protein Shroom3 that was first identified in mice by gene trap mutagenesis as part of an ongoing screen for novel genes implicated in embryonic development (Hildebrand & Soriano, 1999). Gene trapping is a mutagenesis strategy that involves the insertion of a vector containing a splice acceptor site in front of a reporter such that if it inserts in an intron of a gene, it will express the reporter and potentially disrupt the gene at the insertion site (Stanford et al., 2001). This reporter becomes under the control of the trapped gene's endogenous promoter, allowing for accurate reporting of that gene's expression pattern. Depending on where the insertion takes place, the endogenous gene may no longer produce a functional protein. Sequencing of flanking genomic sequences upstream or downstream of the insertion site (depending on the type of gene trap vector used), allows one to then identify the gene trap insertion loci (Friedel & Soriano, 2010). Using this technique and the *B-galactosidase* reporter gene, Hildebrand and Soriano (1999) were able to characterize a novel recessive gene trap mutation that caused fully penetrant exencephaly in mice homozygous for the gene trap allele, herein referred to as Shroom3$^{Gt/Gt}$. Exencephaly is an embryonically lethal neural tube defect (NTD) resulting from failure of neural tube closure in which the brain protrudes out of the skull (Hildebrand & Soriano, 1999; Müller & O'Rahilly, 1991). Due to the appearance of the brain "mushrooming" from the skull, the mutation was accordingly named *Shroom* (shrm) and later renamed *Shroom3* in light of the presence of proteins with sequence similarities (Hagens et al., 2006; Hildebrand & Soriano, 1999) (see *1.3.2* below). The severity of the recessive lethal phenotype established Shroom3 as a critical factor for neural tube closure and subsequent studies primarily focused on defining its functional role in that process.

1.3.2 Shroom3 Protein Structure

1.3.2.1 Conserved Domains

The full-length human Shroom3 protein consists of 1996 amino acids and has a molecular mass of 217 kDa. In mice, there are two putative protein products of Shroom3

encoded by two different transcripts: a long isoform comprised of 1986 amino acids and a short isoform comprised of 1808 amino acids (Hildebrand & Soriano, 1999). Shroom3 is characterized by a specific linear array of sequence motifs that outlines three distinct domains (Figure 1.5): a N-terminal PSD/Dgl/ZO-1 (PDZ) domain, a centralized Apx/Shrm (ASD1) domain, and a C-terminal Apx/Shrm (ASD2) domain (Hildebrand & Soriano, 1999). The ASD1 domain directly binds to actin, while the ASD2 domain is characterized by a three-segmented coiled-coil region that binds to Rho-associated kinases 1 and 2 (ROCK1 and ROCK2) (Dietz et al., 2006; Hildebrand & Soriano, 1999; Mohan et al., 2012). The two ASD domains are critical for the function of Shroom3; deletion of either of the two domains leads to ablation of Shroom3-induced apical constriction. The PDZ domain of Shroom3 is not well-studied but is believed to be dispensable for apical constriction activity as the short isoform of Shroom3 in mice that lacks the PDZ domain phenocopies the long Shroom3 isoform containing the PDZ domain (Hildebrand & Soriano, 1999). These findings were recapitulated *in vitro* with deletion of PDZ having no effect on the ability of *Shroom3* to drive apical constriction (Dietz et al., 2006; Haigo et al., 2003).

1.3.2.2 Shroom Family

Shroom3 is a highly conserved protein with homologs found in 186 species including vertebrates such as the chick, mouse, chimpanzee, *Xenopus*, dog, cow, and rat as well as invertebrates such as *Drosophil*a and tunicate. The ASD domains of Shroom3 share no homology with any other known proteins and the conservation of at least one of the ASD domains is the defining feature of the Shroom family of proteins that Shroom3 belongs to (Hagens et al., 2006; Hildebrand & Soriano, 1999). The Shroom family consists of four family members that are numbered based on the order that they were identified (Hagens et al., 2006). Originally, the nomenclature for Shroom proteins was based on its discovery in *Xenopus* (Hagens et al., 2006). Correspondingly, Shroom1 was previously named apical protein in *Xenopus* (Apx) and Shroom2 was previously named apical protein *Xenopus*-like (APXL) as it was thought to be the human orthologue of Apx, but it has since been characterized as a distinct protein (Hagens et al., 2006). Shroom3 was previously named Shroom and Shroom4 was previously named KIAA1202; Shroom4 is

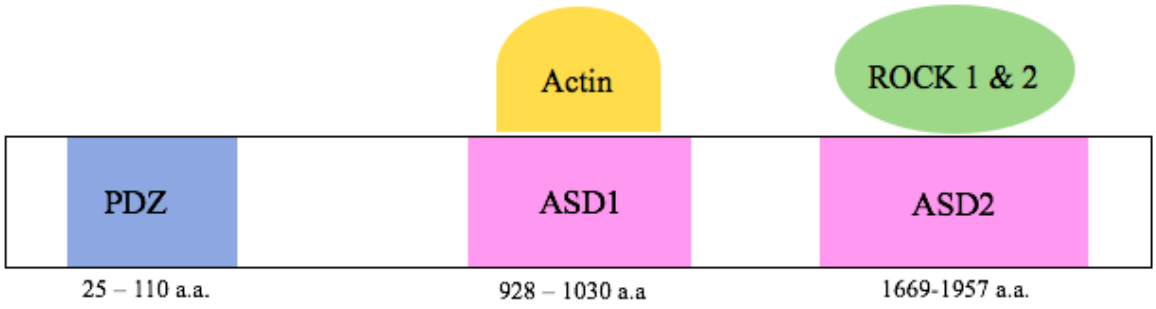

Figure 1.4 Conserved domains of Shroom3. Schematic diagram of Shroom3's three conserved domains: a N-terminal PSD/Dgl/ZO-1 (PDZ) domain, a centralized Apx/Shrm (ASD1) domain and a second C-terminal Apx/Shrm (ASD2) domain.

the only Shroom family member that does not possess both ASD domains, having only the ASD2 domain (Hagens et al., 2006; Lee et al., 2009). Collectively, the Shroom family proteins have been broadly linked to the regulation of cellular architecture through their interactions with cytoskeletal elements including actin filaments and microtubules (Lee et al., 2009). At this time, Shroom3 is unique in that it is the only family member that is known to be both necessary and sufficient for driving a specific cell shape change, namely apical constriction, required for the morphogenesis of epithelial tissues during development (Dietz et al., 2006).

1.3.3 Cellular Functions of Shroom3 and Mechanisms of Action

1.3.3.1 Apical Constriction

The cytoskeleton is a complex network consisting of actin filaments, microtubules, and intermediate filaments that establishes the structural framework of cells (Fletcher & Mullins, 2010). The regulation of the cytoskeletal elements underlies several aspects of cellular physiology including cell polarity, volume, division, and migration (Bezanilla et al., 2015; Fletcher & Mullins, 2010). Importantly, the dynamic properties of the actin cytoskeleton generate forces that enable cells to change shape and become motile (Bezanilla et al., 2015). The coordination of these cell shape changes and movements can lead to global alterations in tissue morphology (Heisenberg & Bellaïche, 2013; Martin & Goldstein, 2014).

Epithelial tissues rely on the coordinated cellular behaviors of their constituent cells in order to undergo remodeling events that are essential to tissue morphogenesis during development as well as maintaining tissue homeostasis throughout life (Martin & Goldstein, 2014). One important cell shape change that takes place in epithelial cells that are polarized along their apicobasal axis is apical constriction (Heisenberg & Bellaïche, 2013; Martin & Goldstein, 2014). Apical constriction is characterized by the narrowing of the cell surface at the apical end, inducing the cell to change from a columnar shape to a wedge shape (Martin & Goldstein, 2014). This occurs through the contraction of a filamentous actin (F-actin) meshwork at the apical surface by myosin (Sawyer et al., 2010). In a developmental context, tightly orchestrated apical constriction in distinct

populations of cells allows for bending and invagination of epithelial sheets, which are processes that govern neural tube closure, gut morphogenesis, and lens placode formation (Chung et al., 2010; Hildebrand & Soriano, 1999; Plageman et al., 2010; Sawyer et al., 2010). Additionally, apical constriction of epithelial cells has also been shown to contribute to cell ingression from epithelial tissue often accompanying epithelial-mesenchymal transition (EMT) (Anstrom, 1992; Williams et al., 2012). In a homeostatic context, apical constriction is involved in the extrusion of apoptotic cells from epithelial sheets as well as wound healing and closure (Davidson et al., 2002; Toyama et al., 2008). The critical importance of apical constriction to a variety of cellular and morphogenetic events has necessitated a greater understanding of its regulation.

It is now well established that Shroom3 is necessary and sufficient for inducing apical constriction in at least a significant subset of epithelial cells. Shroom3 achieves this through its two ASD domains that allow for apical subcellular localization as well as activation of the cellular machinery required to generate the mechanical force for contraction (Dietz et al., 2006; Hildebrand & Soriano, 1999; Nishimura & Takeichi, 2008). The ASD1 domain of Shroom3 directly binds to F-actin stress fibers, recruiting them to the apical surface and bundling them (Hildebrand, 2005; Hildebrand & Soriano, 1999). Prior to this, Shroom3 is recruited to the apical surface by RhoA, which is part of the Rho GTPase family of proteins that are broadly involved in organization of the actin cytoskeleton (Plageman et al., 2011; Sit & Manser, 2011). RhoA itself is activated upon catalytic conversion of its inactive GDP subunit to the active GTP form (Rossman et al., 2005). Concerning Shroom3 regulation, RhoA is specifically activated by the Rho guanine nucleotide exchange factor (GEF) Trio (Plageman et al., 2011).

Apical recruitment of Shroom3 by RhoA causes subsequent colocalization of Shroom3 and F-actin at the apical junctional complexes (AJCs) (Dietz et al., 2006). Once colocalized with actin at the AJCs, the ASD2 domain directly binds to Rho-associated kinases ROCK1 and 2 and recruits them to AJCs (Nishimura & Takeichi, 2008). ROCK1 and 2 possess a highly conserved coiled-coil Shroom3 binding domain while the ASD2 domain is composed of three canonical coiled-coil segments; the two domain structures allow for the formation of the Shroom3-ROCK complex (Mohan et al., 2012; Mohan et

al., 2013). In addition to its Shroom3 binding domain, ROCKs also possess a RhoA binding domain, and binding of RhoA was believed to be involved in ROCK activation (Plageman et al., 2011). However more recently, it has been shown that the ASD2 domain of Shroom3 can directly stimulate ROCK activity independently of RhoA (Zalewski et al., 2016). ROCKs are serine/threonine kinases that function as upstream regulators of non-muscle myosin II (Amano et al., 2010). Once recruited to the AJCs, ROCKs phosphorylate the myosin regulatory light chain (mRLC), activating the molecular motor non-muscle myosin II. Non-muscle myosin II then binds to actin filaments at the AJCs to assemble a contractile actomyosin network that contracts the cell at the apical surface, resulting in shrinkage of the apical end and thus apical constriction (Sawyer et al., 2010; Shutova et al., 2012). Deletion constructs lacking either of the two ASD domains abrogates Shroom3's ability to induce apical constriction in epithelial cells (Dietz et al., 2006; Haigo et al., 2003; Hildebrand, 2005).

1.3.3.2 Apicobasal Elongation

In addition to altering cellular architecture through its association with the actin cytoskeleton, Shroom3 also functions to regulate the microtubule cytoskeleton (Lee et al., 2007). Microtubules (MTs) are non-covalent polymers that consist of repeating α/β-tubulin heterodimers (Wiese & Zheng, 2006). Like actin, microtubules are highly dynamic and are involved in vital cellular processes such as cell transport, motility, division, as well as cell shape change (Nogales, 2001). Their dynamic nature is rooted in their ability to constantly switch between phases of growing and shrinking (Nogales, 2001). During MT assembly, the α/β-tubulin heterodimers align themselves in a head-to-tail fashion with the α tubulin on the slow growing "minus" end and the β-tubulin on the fast growing "plus" end (Wiese & Zheng, 2006). Nucleation of MTs mainly takes place at microtubule-organizing centers (MTOCs), which are located at the minus end (Nogales, 2001). Critical to the regulation of MT nucleation is the MTOC-associated protein γ-tubulin (Conduit, 2016). γ-tubulin forms a γ-tubulin ring complex that is recruited to MTOCs in order to catalyze MT assembly (Conduit, 2016).

An essential cell shape change that is regulated by MT assembly is apicobasal elongation (Kondo & Hayashi, 2015). In polarized epithelial cells, MT assembly occurs along the

apicobasal axis with the plus end of MTs pointing towards the basal end (Kondo & Hayashi, 2015). This apicobasal orientation of MTs is believed to regulate height control (Kondo & Hayashi, 2015). Shroom3 is sufficient to drive parallel MT assembly along the apicobasal axis in epithelial cells by controlling the distribution of γ-tubulin such that it is accumulated at foci at the apical end of cells (Lee et al., 2007). However, Shroom3 does not directly bind γ-tubulin nor does it alter the total γ-tubulin levels in tissues or non-apical MT arrays, suggesting that Shroom3 indirectly recruits γ-tubulin to the apical side and promotes assembly of a discrete population of MTs aligned apicobasally (Lee et al., 2007).

As mentioned previously, apical constriction contributes to epithelial invagination during embryogenesis. This decrease in apical surface area of epithelial cells is actually preceded by an increase in cell height (Kondo & Hayashi, 2015). Specifically, assembly of MTs along the apicobasal axis of cells causes elongation and a reduction in apical and basal surface areas, inducing cells to change from a cuboidal-shape to a columnar-shape (Kondo & Hayashi, 2015). This apicobasal elongation is subsequently followed by apical constriction, causing a decrease in the apical surface area of cells, and the adoption of a wedge-shape (Kondo & Hayashi, 2015). These two cellular processes are independent events that follow a conserved spatiotemporal pattern during neural tube formation (Kondo & Hayashi, 2015; Suzuki et al., 2012). Moreover, Shroom3 can mediate the two processes independently with apicobasal elongation occurring in the absence of apical constriction in some tissues and vice versa (Lee et al., 2007). The apical localization of both γ-tubulin and actin to drive MT and actin-based cell shape changes has established Shroom3 as a critical regulator of the cytoskeletal dynamics.

1.3.4 Tissue-Specific Activities of Shroom3

1.3.4.1 Neural Tube Closure

Neural Tube Formation. The pivotal work of Hildebrand and Soriano (1999) established Shroom3 as a novel regulator of neural tube morphogenesis. Herein, Shroom3's most

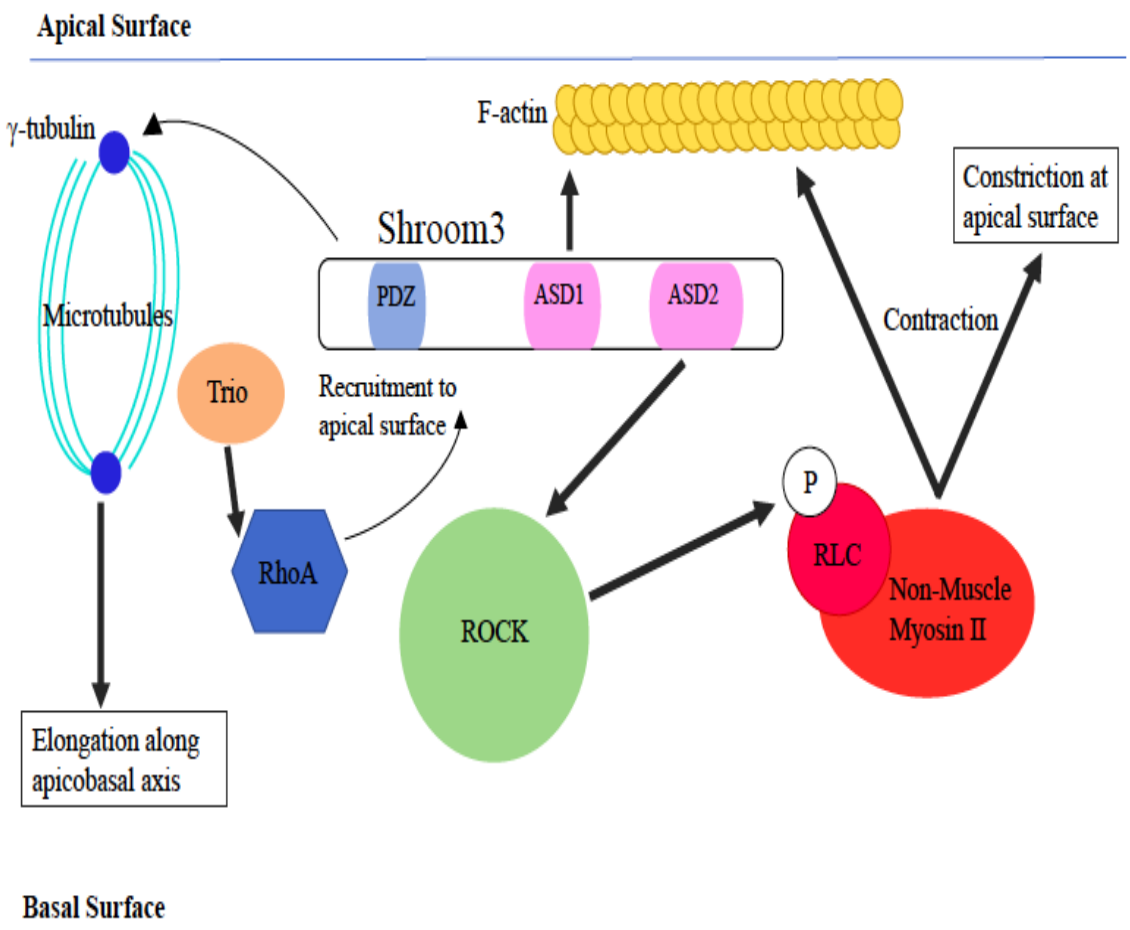

Figure 1.5 Schematic illustration of Shroom3's proposed mechanisms for apical constriction and apicobasal elongation. Activation of RhoA by Trio causes recruitment of Shroom3 to the apical surface. At the apical surface, Shroom3 binds to actin stress fibers with its ASD1 domain and bundles them. Its ASD2 domain binds to ROCK1 & 2, causing them to localize to the apical surface where they phosphorylate the non-muscle myosin II regulatory light chain. Active non-muscle myosin II then moves along actin filaments and causes contraction at the apical surface, resulting in apical constriction. Shroom3 can also recruit γ-tubulin to the apical surface, driving parallel assembly of MT arrays along the apicobasal axis, causing apicobasal elongation.

discernible function, inducing apical constriction in epithelial cells, was demonstrated by the fully penetrant exencephaly phenotype of Shroom3$^{Gt/Gt}$ mice. Apical constriction during neurulation is not uniformly applied to all neural plate cells, rather it occurs in discrete cell populations known as hingepoint cells (Haigo et al., 2003; Sawyer et al., 2010). Shroom3 is required for neural tube closure as it facilitates formation of dorsal lateral and medial hingepoints, which apically constrict to facilitate bending of the neuroepithelium towards the dorsal midline thereby forming the neural tube (Haigo et al., 2003). Concomitant with apical constriction during neural tube formation, Shroom3 also functions to increase cell height by inducing apicobasal elongation via assembly of MT arrays (Lee et al., 2007). Besides exencephaly, other consequences of failure of neural tube closure in Shroom3$^{Gt/Gt}$ mice were morphologically manifested as acrania, facial clefting, and spina bifida (Hildebrand & Soriano, 1999). Of note, mice containing only one copy of the gene trap allele (Shroom3$^{+/Gt}$) displayed partial (8%) penetrance of the exencephaly phenotype. Furthermore, although *Shroom3* is expressed along the entire neural tube, much of the spinal cord still closes in mice lacking functional *Shroom3* indicating that other mechanisms also facilitate neural tube closure.

Shroom3's ability to induce apical constriction during neural tube closure appears to be regulated by Lulu (also known as Epb41l5) (Chu et al., 2013). Lulu is a four-point-one, ezrin, radixin, moesin (FERM) domain containing protein and is critical for neurogenesis, with a loss of function mutation in mice causing aberrant neural plate morphology and failure of neural tube closure (Lee et al., 2007). In *Xenopus*, loss of endogenous Lulu leads to a significant decrease in Shroom3-induced apical constriction, a consequence attributed to reduced apical Shroom3 localization, with nearly all of Shroom3 remaining cytoplasmic rather than accumulating at the AJCs (Chu et al., 2013). On the contrary, co-injection of Shroom3 with Lulu resulted in enhanced apical constriction, indicating that the two proteins may be acting synergistically to induce apical constriction.

Planar Cell Polarity (PCP). Planar polarity is the establishment of polarity in any two-dimensional tissue that is orthogonal to apicobasal polarity (Zallen, 2007). In order to achieve planar polarity in tissues, the constituent cells must become asymmetric and coordinate their asymmetries with one another, a function that is regulated by the PCP

pathway (Zallen, 2007). Establishment of planar polarity is a necessary prerequisite for the cell shape changes involved in tissue morphogenesis, including apical constriction. The “core” PCP pathway confers polarity via noncanonical (β-catenin-independent) Wnt signaling and involves the transmembrane proteins Frizzled (Fzd), Van Gogh (Vang; also known as Strabismus/Stbm), and Celsr as well as the cytoplasmic proteins Dishevelled (Dvl), Prickle (Pk), and Inversin (Adler et al., 1997; Chae et al., 1999; Feiguin et al., 2001; Gubb & García-Bellido, 1982; J Taylor et al., 1998; Theisen et al., 1994; Usui et al., 1999; Vinson et al., 1989; Wolff & Rubin, 1998). Transduction of Wnt signaling occurs upon binding of Wnt ligands to Frizzled receptors, leading to activation of Dishevelled (Dvl) (Komiya & Habas, 2008). Active Dvl can then modify the actin cytoskeleton through activation of ROCK, which phosphorylates non-muscle myosin II (Habas et al., 2001; Marlow et al., 2002; Winter et al., 2001). The PCP pathway requires asymmetric localization of its key players and studies have shown that both Celsr and Dvl are planar polarized, localizing to the AJCs along the mediolateral axis (Tamako Nishimura et al., 2012). This subsequently causes polarization of ROCK and phosphorylated mRLC.

During neurulation, convergent extension of the neural plate that precedes neural plate bending critically depends on the PCP pathway (Wallingford et al., 2002). Convergent extension (CE) is driven by tightly coordinated cell intercalation, which proceeds through the formation of intermediary multicellular units known as rosettes (Williams et al., 2012). Apical constriction of distinct cell clusters within the primordium of the posterior lateral line is the primary mechanism underlying rosette assembly, a process that relies on FGF signaling (Lecaudey et al., 2008; Nechiporuk & Raible, 2008). Shroom3 is necessary for rosette formation in zebrafish by activating apical actomyosin contractility through ROCK and non-muscle myosin II downstream of FGF signaling (Ernst et al., 2012). Further, FGF is both necessary and sufficient for Shroom3 expression in the posterior lateral line, but not in any other regions, suggesting that FGF regulation of Shroom3 is specific to rosette formation (Ernst et al., 2012). These findings were recapitulated in *Drosophila*, where loss of functional Shroom led to disruption of rosette assembly accompanied by a decrease in ROCK and myosin planar polarity, decreased junctional tension, and consequent abrogation of CE (Simões et al. 2014).

Similar findings in zebrafish and *Drosophila* were also seen in mice that showed embryos lacking functional Shroom3 possessed rosettes with lower complexity, though they did not display a decrease in the total number of rosettes (McGreevy et al., 2015). This implicated that Shroom3 is not required for initial rosette formation but is necessary for formation of higher order rosettes, which are believed to facilitate apicobasal elongation and apical constriction at mediolateral junctions in the neural plate. Significant to this study was the finding that Shroom3 acts downstream of the PCP pathway in order to drive these cell shape changes required for CE in mice, in a manner dependent on Dvl2. First, genetic interactions between *Shroom3* and PCP components *Vangl* and *Wnt5a* were observed in mice as double mutants exhibited exacerbated NTDs and CE defects (McGreevy et al., 2015). Additionally, Shroom3's role in the PCP pathway appears to require the activity of Dvl2. The DEP domain of Dvl2 and an uncharacterized N-terminal region of Shroom3 were found to form a complex that is necessary for colocalization of Shroom3 and ROCK along mediolateral cell junctions in the neural plate, where it is postulated that apical constriction leads to higher order rosette assembly and subsequent induction of CE (McGreevy et al., 2015). Thus, Shroom3 appears to control various events during neurulation.

1.3.4.2 Neuronal Growth and Repair

Besides its role during neural tube closure, Shroom3 has been implicated in the adult vertebrate central nervous system (CNS) function. The inability of mature axons to spontaneously regenerate after injury is the central limiting factor underlying CNS damage and neurodegenerative diseases (Yiu, 2006). In the adult CNS, neural repair and regeneration is repressed by proteins that inhibit axon outgrowth (Dickson, 2010). One such protein is the multidomain scaffold protein Plenty of SH3s (POSH) composed of four Src homology (SH3) domains (Taylor et al., 2008). POSH promotes neuronal death by stimulating the proapoptotic JNK pathway (Xu et al., 2003). Shroom3 directly interacts with POSH's third SH3 domain (SH3-3) to jointly inhibit axon outgrowth in a manner that is dependent on ROCK (Taylor et al., 2008). Injection of either *Shroom3* or POSH RNAi into neurons derived from P19 cells, resulted in exuberant axon outgrowth (Taylor et al., 2008). Interestingly, repression of myosin II function reversed the axon

outgrowth seen in cells injected with Shroom3 or POSH RNAi. Thus, while myosin II activation is necessary for Shroom3 induced apical constriction, myosin II repression is required for POSH-Shroom3-mediated axon outgrowth inhibition (Taylor et al., 2008).

NogoA is another axon outgrowth inhibitory protein and possesses an inhibitory C-terminal domain, Nogo66 (Fournier et al., 2001). Nogo66 interacts with two different cell surface receptors, Nogo receptor 1 (NgR1) (Fournier et al., 2001) and paired immunoglobulin-like receptor B (PirB) (Atwal et al., 2008), that confer inhibitory signals through two distinct pathways. POSH has been found to act as a vital intracellular signal transducer in PirB-mediated Nogo66 neurite outgrowth inhibition by forming a complex with Shroom3, ROCK, and leucine zipper kinase (Dickson et al. 2010; Taylor et al. 2008). Blocking the interaction between Shroom3 and ROCK circumvents PirB-mediated Nogo66 axon outgrowth inhibition (Dickson et al., 2015). Utilizing an ELISA platform, a chemical inhibitor of Shroom3-ROCK interaction was identified (Dickson et al., 2015). This inhibitory compound, CCG-17444, irreversibly blocked binding of Shroom3 to ROCK, leading to release of axon outgrowth inhibition and increased neurite length, to a degree similar to the effect of RNAi-mediated POSH or Shroom3 repression (Dickson et al., 2015). Of importance, CCG-17444 fails to enhance neurite length in neurons lacking functional Shroom3 or POSH, suggesting that it acts on the same pathway as the two proteins. The ability to pharmacologically induce neurite outgrowth by blocking an inhibitory axon outgrowth pathway involving Shroom3 is potentially a tremendous first step in the uncovering of novel therapeutic strategies for CNS injury.

1.3.4.3 Lens Development

Early lens morphogenesis occurs through the formation of the lens placode that invaginates to form the lens pit and optic cup. The invagination of the lens placode is reliant on Shroom3 induced apical constriction of the epithelial cells of the prospective lens pit (Plageman et al., 2010). Lens placode invagination driven by Shroom3 is regulated by the lens-induction transcription factor Pax6 that activates *Shroom3* transcription in the surface ectoderm of the prospective lens (Plageman et al., 2010). A second regulator of Shroom3-mediated lens pit morphogenesis was later identified to be p120-catenin, which is required for Shroom3 localization to AJCs (Lang et al., 2014).

1.3.4.4 Thyroid Bud Morphogenesis

Shroom3-induced apical constriction is also necessary in the morphogenesis of the thyroid bud, which is an outgrowth of the gut endoderm (Loebel et al., 2016). Formation of the thyroid bud critically depends on bending of the foregut endoderm, that bending depends on apical constriction. Knockout of *Shroom3* in mouse embryos leads to ablation of apical constriction in the thyroid bud epithelium. Furthermore, knockout of the Rho GTPase protein Cdc42 has been shown to attenuate sub-cellular localization of Shroom3 to the apical surface of thyroid bud epithelial cells. It is therefore proposed that Shroom3 apical localization in the thyroid bud epithelium depends on concomitant Cdc42 localization, in a manner similar to the RhoA-dependent localization of *Shroom3* in the lens pit (Loebel et al., 2016).

1.3.4.5 Gut Morphogenesis

Shroom3 has also been shown to be critical for proper gut morphogenesis (Chung et al., 2010; Grosse et al., 2011; Plageman et al., 2011). In *Xenopus*, the V-shaped morphology of the archenteron floor requires both apical constriction and apicobasal elongation, which are driven by Shroom3 (Chung et al., 2010). Regulation of Shroom3 in the developing gut is dependent on the transcription factor Pitx1, which directly activates *Shroom3* transcription (Chung et al., 2010).

Another role for Shroom3 in gut morphogenesis arose from the observation that Shroom3$^{Gt/Gt}$ mice mutants displayed abnormal gut rotation (Plageman et al., 2011). Gut rotation requires the establishment of asymmetry within the dorsal mesentery (DM) (Davis et al., 2008). This asymmetry is generated by the constriction and lengthening of gut epithelial cells mediated by Shroom3, resulting in leftward DM tilting. A second Pitx family member, Pitx2, together with the adhesion molecule N-cadherin, has been found to be involved in Shroom3's activity within the DM, though Pitx2 in this case, unlike Pitx1 does not directly regulate *Shroom3*'s expression (Plageman et al., 2011).

A third function for Shroom3 during later stages of gut morphogenesis was seen in the fetal intestinal epithelium of mice (Grosse et al., 2011). The increasing girth of the early intestinal epithelium during development appears to occur through the progressive

apicobasal elongation of epithelial cells in a pseudostratified manner, rather than through the addition of stratified cell layers as previously believed. Shroom3 has been found to be a vital determinant in the maintenance of a single-layered pseudostratified intestinal epithelium, with Shroom3$^{Gt/Gt}$ mice displaying aberrant organization of the apical actomyosin network, expanded apical surfaces, decreased cell height, and temporarily stratified intestinal epithelium (Grosse et al., 2011).

1.4 Implications of Shroom3 in Disease

1.4.1 Human *SHROOM3* Variants

While the developmental roles of Shroom3 have been supported by multiple studies in different models, an increasing amount of evidence for the role of Shroom3 in complex human diseases is emerging. The National Heart, Lung, and Blood Institute (NHLBI) has established an Exome Sequencing Project (ESP) in order to document the range of gene variants within the human population and to classify the variants as benign, possibly damaging, or probably damaging. The goal of the ESP was to identify novel candidate genes associated with heart, lung, and blood disorders through next-generation sequencing of protein coding regions. Genomes from over 200 000 individuals across a diverse range of phenotype-rich populations have been analyzed. Predictions about how damaging a variant could be were made using the computer program Polymorphism phenotyping version 2 (PolyPhen-2), which analyzes the effect of a single amino acid substitution on the function of the protein based on several phylogenetic, structural, and sequence features. Several variants in *SHROOM3* have been predicted to be probably damaging by the NHLBI ESP (Table 1.3). Importantly, these variants could represent hypomorphic mutations with a phenotype analogous to *Shroom3*$^{Gt/t}$ mice, thus determining whether potentially damaging variants result in compromised Shroom3 function is important in understanding whether these variants represent mutations that might increase susceptibility to disease.

1.4.1.1 Heterotaxy

In a separate study, one variant identified by the NHLBI has already been correlated with a rare but severe congenital heart disease (CHD) in humans known as heterotaxy (Tariq

et al., 2011). Heterotaxy is defined by the aberrant arrangement of internal thoraco-abdominal organs caused by improper left-right (LR) patterning during development. The consequences of aberrant LR patterning are manifested as malformations in any of the organs asymmetric along the LR axis including the heart, spleen, and stomach (Kim, 2011). Currently, the majority of genes known to cause heterotaxy in humans are members of the Nodal signaling pathway involved in LR patterning. However, the heterogeneity of heterotaxy phenotypes coupled with its sporadic pattern of inheritance have necessitated the need to identify additional gene candidates (Tariq et al., 2011).

Using high-resolution SNP genotyping in combination with a whole-exome sequencing approach and homozygosity mapping, the authors identified several genetic variants in heterotaxy patients exhibiting multiple anomalies (Tariq et al., 2011). *SHROOM3* was one of the variants identified and has a recessive missense mutation at amino acid position 60 with valine substituted for glycine. Interestingly, this substitution is within the PDZ domain of *SHROOM3* indicating the need for further investigation of the PDZ domain with respect to Shroom3's cellular function. Further analysis in 96 sporadic heterotaxy patients revealed two additional homozygous variants and two heterozygous variants. One of the heterozygous variants, which has a glycine to aspartic acid substitution at amino acid position 1864, is also one of the variants identified by the NHLBI and is predicted to be probably damaging by PolyPhen-2. Moreover, this variant is within a known domain location, ASD2, suggestive of impaired actomyosin contractility. Given that Shroom3 acts downstream of Pitx2 and N-cadherin to drive gut looping (see *1.3.4.5*) and that ROCK2 has been found to be required for LR patterning in humans, the authors propose that the Pitx2-Shroom3-ROCK pathway could be a novel target for control of LR patterning. Functional analyses of the two aforementioned *SHROOM3* variants will be a necessary next step in establishing a mechanistic link between *SHROOM3* and heterotaxy.

Table 1.3 List of *SHROOM3* variants predicted to be probably damaging by PolyPhen-2 in known domain locations. SNPs found within a diverse range of populations from over 200 000 individuals from the USA. The variant allele on the left represents the less common SNP and the variant allele on the right represents the most common SNP; alleles frequencies follow correspondingly. *** denotes the homozygous G60V variant linked to the rare heterotaxy patient and ** denotes the heterozygous G1864D variant identified by (Tariq et al., 2011).

Amino Acid Position	Variant Allele	Allele Frequency	Amino Acid Change	Protein Change	Domain Location
35	T/G	T=1/G=13005	Val, Gly	Missense	PDZ
60	C/G	C=2/G=13004	Arg, Gly	Missense	PDZ
60* **	T/G	T=34/G=12972	Gly, Val	Missense	PDZ
80	T/A	T=2/A=13004	Tyr, Asn	Missense	PDZ
99	C/A	C=1/A=13005	Ser, Tyr	Missense	PDZ
106	C/G	C=15/G=12991	Lys, Val	Missense	PDZ
107	A/G	A=2, G=13004	Arg, His	Missense	PDZ
890	A/G	A=1/G=12725	Asn, Ser	Missense	ASD1
927	A/G	A=1/G=12705	Asn, Ser	Missense	ASD1
945	T/A	T=1/A=12393	Val, Asp	Missense	ASD1
1012	A/C	A=67/C=12581	Asn, Thr	Missense	ASD1
1058	A/G	A=1/G=12979	His, Arg	Missense	ASD1
1764	C/A	C=2/A=13004	Gln, Lys	Missense	ASD2
1778	C/G	C=1/G=13005	His, Asp	Missense	ASD2
1780	G/A	G=1/A=13005	Ser, Asn	Missense	ASD2
1812	C/A	C=1/A=13005	Thr, Asn	Missense	ASD2
1836	A/G	A=1/G=13005	Ile, Met	Missense	ASD2
1857	T/C	T=1/C=13005	Cys, Arg	Missense	ASD2
1857	A/G	A=1/G=13005	His, Arg	Missense	ASD2
1864* **	A/G	A=7/G=12999	Asp, Gly	Missense	ASD2

1892	T/C	T=1/G=13005	Trp, Arg	Missense	ASD2
1892	A/G	A=1/G=13005	Gln, Arg	Missense	ASD2
1935	T/A	T=1/A=13005	Lys, Gln	Missense	ASD2

1.4.1.2 Neural Tube Defects

NTDs affect 6% of all births worldwide and are a substantial public health challenge due to their complex etiology of genetic and environmental interactions (Wallingford et al., 2013). Folic acid supplementation in the diet of women who plan on conceiving has been widely endorsed as a preventative measure against NTDs (Pitkin, 2007). Several lines of evidence have shown the protective effects of folate against NTDs, specifically anencephaly, where exencephaly acts as the precursor, and spina bifida (Pitkin, 2007). Given Shroom3's role in neural tube closure and the NTDs resulting from loss of Shroom3, it is predictive that folic acid supplementation would reverse the consequences of Shroom3 loss. However, in pregnant mice possessing an ENU-induced Shroom3 mutation (*Shroom3*^{C5745T}), long-term folic acid supplementation actually led to increased prenatal lethality in mutant embryos. The ENU-induced mutation (*Shroom3*^{C5745T}) used in this study is a C to T transition in Exon 9 resulting in an arginine to cysteine substitution at amino acid position 1663; this mutation results in a hypomorphic allele. Interestingly, when the folic acid supplementation in the maternal diet was short-term, the effect was beneficial as evidenced by a significant decrease in mutant embryo lethality and a reduction in the prevalence of NTDs. These findings signify that the beneficial effects of FA supplementation, like NTDs themselves, are dependent on a number of factors including length of exposure to FA and the specific genetic background involved. It is not surprising that the complexity of NTDs and the multiple factors involved have resulted in the limited success of candidate gene studies in NTDs. Recently, *de novo* mutations (DNMs) have garnered increasing support as a common cause of birth defects and also explain why embryonically lethal diseases remain prevalent in the population (Veltman & Brunner, 2012). To identify potential candidate DNMs in novel genes associated with NTDs, exome data from 43 families consisting of one affected child and two unaffected parents with no other familial history of NTDs were analyzed. In two unrelated families, two loss-of-function heterozygous DNMs in *SHROOM3* were identified. The first variant identified harbors C to G transition at nucleotide position 1176 resulting in a nonsense mutation; the mother of the affected child supplemented FA in her diet. The second variant carries a frameshift mutation inserting G at nucleotide position 2843, leading to a

premature stop codon; the mother of the affected child did not supplement FA in her diet; this mutation is located within the ASD1 domain (Lemay et al., 2015).

Due to the linkage between heterotaxy and a recessive *SHROOM3* mutation and the fact that neither of the affected patients exhibited heterotaxy, it is believed that the LoF DNMs may be acting in a haploinsufficient or dominant negative manner (Lemay et al., 2015). Furthermore, the two affected children displayed different types of NTDs, with the first displaying anencephaly and craniofacial dysmorphism whereas the second displayed spina bifida (C1176G). Given that the more severe phenotype was associated with FA supplementation, and that long-term FA supplementation was found to be detrimental in the case of *SHROOM3*-related NTDs, it is possible that the mother was exposed to FA too long of a period. Irrespective of the role of FA in the maternal diet, this candidate gene study established, for the first time, a potential link between Shroom3's role in neural tube closure and human NTDs (Lemay et al., 2015).

1.4.2 Pulmonary Arterial Hypertension

In addition to Shroom3's association with congenital diseases due to its known roles in development, Shroom3 has been broadly implicated in adult disease. One of these diseases is pulmonary arterial hypertension (PAH), defined by a sustained elevation in pulmonary arterial pressure caused by injury to the pulmonary vasculature (Rubin, 2006). It is characterized by increased vascular proliferation and resistance leading to pulmonary vascular remodeling and decreased right ventricular function (Rubin, 2006). Histologically, it presents itself in lung tissue as intimal fibrosis, plexiform lesions, and increased medial thickness (Farber & Loscalzo, 2004). Of note, PAH is a separate disease from essential hypertension, which affects global blood pressure whereas PAH concerns only the blood pressure in the pulmonary arteries. Although the exact pathogenic mechanisms underlying PAH remain relatively uncharacterized, structural changes within the walls of the pulmonary arteries seem to play an essential role (Humbert et al., 2004). Similar to CKD, these changes are associated with ECM deposition and cell proliferation. Additionally, hypertrophy of pulmonary artery smooth muscle cells (PASMCs) caused by reorganization of the actin cytoskeleton has been strongly linked to PAH (Humbert et al., 2004; Stenmark et al., 2006).

Shroom3 has been found to be expressed in the lungs of mice and humans, exclusively in PASMCs (Sevilla-Pérez et al., 2008). In the same study, hypoxia-induced PAH in mice and primary cultured PASMCs revealed downregulation of *Shroom3*. In humans with idiopathic PAH, Shroom3 expression was found to be attenuated in PASMCs when normalized to levels of smooth muscle actin-binding protein alpha-actin (Acta2). Thus, Shroom3 has been proposed to be a novel protein involved in PAH pathogenesis perhaps due to its role in maintaining the cytoskeletal architecture of PASMCs.

1.4.3 HIV-Associated Neurocognitive Disorders (HAND)

As highlighted in *1.3.4.3*, Shroom3 has been shown to be involved in the adult CNS through inhibition of axon outgrowth. Recently, evidence of a potential role for Shroom3 in the onset of adult neurodegenerative diseases has been found in a study looking at the molecular mechanisms involved in the onset of HIV-associated neurocognitive disorders (HAND) resulting from HIV infection in the CNS (Ganief et al., 2017). HAND affects 70% of HIV-positive patients and encompasses a wide range of neuropathological disorders affecting cognitive, motor, and behavior functions (Antinori et al., 2007; Joska et al., 2011). Using proteomic analyses, *SHROOM3* expression was found to be downregulated in neuroblastoma cells infected with HIV transactivator of transcription (HIV-Tat), an established inducer of neuronal damage. Several of the other proteins identified by the study also function as cytoskeletal regulators. The aforementioned study analyzed an extremely specific subset of neurodisorders, but given the known role of Shroom3 in regulating axon outgrowth, there is rationale for Shroom3 playing a role in the pathophysiology of common neurodisorders. Thus, although sparse, the evidence for Shroom3's role in the onset of non-congenital diseases like pulmonary arterial hypertension and neural disorders is emerging.

1.4.4 Chronic Kidney Disease

The most significant evidence for Shroom3's role in non-congenital disease comes from the multiple GWAS (see *1.2.6*) that have identified *SHROOM3* as having a strong correlation to CKD prevalence and incidence. These GWAS necessitated subsequent studies aimed at elucidating the role of Shroom3 in kidney function and disease.

Yeo et al. (2016) explored the role of Shroom3 function in the kidney using a zebrafish and rat model, namely the Fawn-Hooded Hypertensive (FHH) rat, which is an established hypertension and renal injury model. The FHH rat is a useful animal model in this experiment because Shroom3 is located within a quantitative trait loci (QTL) previously identified in the FHH rat and the FHH rat has 14 protein-coding variants of *Shroom3* compared to the wild-type allele. The central objective of this study was to determine whether or not spontaneous renal injury in the FHH rat is associated with altered Shroom3 function was a central objective.

Introduction of a WT *Shroom3* allele was found to significantly reduce the glomerular defects typically exhibited by the FHH rat. Specifically, introduction of WT *Shroom3* was found to result in lower levels of albuminuria, glomerulosclerosis, and foot process effacement. Subsequent analysis of the FHH *Shroom3* allele revealed a variant within the ASD1 domain that disrupted binding to actin and could account for the FHH renal injury phenotype. These findings were further supported using zebrafish, in which Shroom3 is typically expressed in the pronephros during development. Global knockdown of Shroom3 using antisense morpholinos against Shroom3, was found to result in cardiac edema, a marker of pronephros dysfunction. Furthermore, RNA encoding the rat WT but not the FHH *Shroom3* allele was able to rescue glomerular function in these zebrafish. When the knockdown of Shroom3 was specific to podocytes, achieved using a vector containing a dominant negative *Shroom3* allele that ablates endogenous *Shroom3* function under the control of the podocyte-specific podocin promoter, zebrafish displayed foot process effacement and compromised GFB integrity (Yeo et al., 2015).

Kidney transplantation is the best available treatment for CKD patients who progress to ESRD. In these patients, the most prevalent cause of renal transplant failure leading to dialysis or retransplantation is chronic allograft nephropathy (CAN) (Paul, 1999). CAN is characterized by a progressive loss of renal function in the allograft, with common histopathological markers including glomerulosclerosis and tubulointerstitial fibrosis (Chapman et al., 2005). The intronic *SHROOM3* SNP rs17319271, identified by nearly all of the GWAS, has been implicated in the pathogenesis of tubulointerstitial fibrosis in CAN patients (Menon et al., 2015). This SNP has a G to A transition and presence of the

A allele in the donor but not the recipient correlated with decreased eGFR and increased allograft fibrosis in a prospective cohort of renal allograft recipients (GoCAR) at 12 months post-transplantation. This decline in renal function was correlated to increased *SHROOM3* expression in the allograft seen at 3 months post-transplant. Subsequent *in vitro* analyses of the *SHROOM3* SNP revealed that the sequence containing the A allele functions as an enhancer element for the transcription factor 7-like-2 (TCF7L2). This enhancer element increases binding of β-catenin to the DNA complex of TCF7L2 and *SHROOM3*, activating *SHROOM3* transcription. Downstream of the TCF7L2/β-catenin pathway, Shroom3 activity was found to be regulated by the transforming growth factor beta 1 (TGF-β1) (Menon et al., 2015). TGFβ1 is widely recognized as the primary pathological factor underlying fibrosis in CKD as it drives the expression of profibrotic genes. Importantly, when upregulated by TGF-β1, Shroom3 in turn, increases TGF-β1-mediated profibrotic gene expression. Knockdown of Shroom3 resulted in decreased profibrotic gene expression *in vitro* in renal epithelial cells and decreased interstitial fibrosis *in vivo* in a murine kidney injury model (Menon et al., 2015).

A study conducted by our lab and collaborators (Khalili et al., 2016), showed that Shroom3 is expressed in the developing kidney. Specifically, expression is found in the podocytes within the condensing mesenchyme, and in the medullary collecting ducts and podocytes of the adult kidney. The spatiotemporal expression of Shroom3 in the kidney was concomitant with a role for Shroom3 in glomerular development. Embryonic *Shroom3*$^{Gt/Gt}$ mice displayed aberrant glomerular morphology associated with the presence of cystic and collapsing glomeruli. At the ultrastructural level, these glomerular defects were characterized by abnormal podocyte morphology including foot process effacement attributed to abrogation of apical actin localization as well as loss of apical ROCK and myosin. The glomerular defects exhibited by Shroom3$^{Gt/Gt}$ mice were also observed in heterozygous *Shroom3*$^{+/Gt}$ mice.

An important finding in the above study was that the glomerular defects in early nephrogenesis associated with Shroom3 deficiency resulted in a dose-dependent decrease in glomerular number at birth. Due to the fact that Shroom3$^{Gt/Gt}$ mice are embryonically lethal, *Shroom3*$^{+/Gt}$ mice were used to determine whether this reduced glomerular number

translated into decreased kidney function later in life. At one year of age, *Shroom3*$^{+/Gt}$ mice displayed significantly increased levels of proteinuria measured by UPCR as well as glomerulosclerosis and foot process effacement. Thus, Shroom3 appears to be a significant determinant in proper kidney development as well as kidney function in adulthood, specifically owing to its maintenance of podocyte architecture.

Collectively, these studies have shed light on the role of Shroom3 in the kidney and have established functional support for the GWAS that have identified Shroom3 as a candidate gene for CKD. However, whether or not a deficiency in Shroom3 directly increases susceptibility to disease remains unclear.

1.5 Hypertension and CKD: Re-visited

While hypertension can cause CKD through a pathogenic mechanism involving progressive podocyte injury, the opposite is also true, as decreased kidney function can lead to increased systemic blood pressure. Hypertension is the leading global risk factor for mortality and affects more than 40% of adults worldwide, with this number projected to increase to 60% by 2025 (Kearney et al., 2005; World Health Organization, 2011) . Classification of blood pressure in adults is based on the average of BP measurements taken on two or more clinical visits (NHLBI, 2003). Hypertension is diagnosed on the basis of a systolic BP $\geq$ 140 mm Hg and/or diastolic BP $\geq$ 90mm Hg, with medical intervention beginning at the pre-hypertensive stage. Hypertension is the most frequent comorbidity of CKD, affecting 67-92% of patients (Center for Health Statistics, 2011).

1.5.1 Hypertension Induced by Renal Dysfunction

Nearly all cases of hypertension (90%) are of unknown cause, but there are a multitude of factors that clearly contribute to its pathogenesis (Oparil et al., 2003). Examples of pathophysiologic factors implicated in the onset of hypertension include long-term high sodium intake, deficiencies of vasodilators, overproduction of vasoconstrictors and sodium-retaining hormones, and increased sympathetic nervous system activity (Oparil et al., 2003). Collectively, these factors potentiate sustained elevation in blood pressure levels by increasing systemic vascular resistance and stiffness, as well as cardiac output (Foëx & Sear, 2004).

Table 1.4 Classification of hypertension. From the 7th Report of the Joint National Committee on Prevention, Detection, Evaluation, and Treatment of High Blood Pressure (JNC 7) (NHLBI, 2003).

Blood Pressure Classification	**Systolic Blood Pressure (mm Hg)**	**Diastolic Blood Pressure (mm Hg)**
Normal	< 120	and < 80
Pre-hypertension	120 – 139	or 80 – 89
Stage 1 Hypertension	140 – 159	or 90 – 99
Stage 2 Hypertension	≥ 160	or ≥100

Kidneys play an essential role in blood pressure regulation through their function of sodium excretion. The importance of renal mechanisms in the pathophysiology of hypertension has been evidenced by several experimental and clinical hypertensive models, which have all been linked to a reduced ability of the kidneys to excrete sodium (Tedla et al., 2011). Excess sodium and water retention caused by renal injury leads to an increased production of vasoconstrictors such as angiotensin II, and a simultaneous decrease in the expression of vasodilators such as nitric oxide. The resulting imbalance towards the upregulation of vasoconstriction systems leads to an increase in renal vascular resistance, cardiac output, and consequently blood pressure (Oparil et al., 2003).

1.5.2 Developmental Origins for Hypertension: The Brenner Hypothesis

In 1988, Brenner put forth a hypothesis that nephron number and systemic blood pressure are inversely related based on his observation that hypertensive patients had reduced nephron number. The total number of nephrons present at birth or shortly after (as in the case of mice), is referred to as nephron endowment (Brenner et al., 1988; Didion, 2017). In contrast, the total number of nephrons measured at any given time post-birth is the nephron number (Didion, 2017). Due to the fact that nephrogenesis ceases at 36 weeks of gestation, nephron endowment represents the maximum amount of nephrons an individual can have in life with nephron number only declining afterwards. Glomerular number is used as an index for nephron number (Hoy et al. 2005). As mentioned in *1.2.2.1*, GFR is based on nephron number and the filtration rate within each individual nephron. When the GFR falls below a certain threshold, a pathological and progressive cycle of glomerular injury is initiated (Brenner and Mackenzie, 1997). The cycle begins with a reduction in nephron number and GFR that induces residual nephrons to compensate by increasing single-nephron GFR and glomerular surface area, resulting in high glomerular volume (Brenner et al., 1988). While this fulfills a compensatory function in the short-term, sustained glomerular hypertrophy and hyperfiltration result in increased fluid and sodium retention, increased extracellular fluid volume, and consequently contribute to the onset of hypertension (Brenner et al., 1988). Chronic hypertension then perpetuates glomerular injury by increasing renal blood flow and

glomerular capillary pressure leading to sclerosis, further nephron loss, and even higher blood pressure, perpetuating the cycle (Figure 1.6) (Didion, 2017). As explained in *1.2.5.1*, the degree of renal damage caused by hypertension-induced pathogenic mechanisms depends on local susceptibility factors, one of which includes glomerular hypertrophy. In individuals with reduced nephron endowment, glomerular hypertrophy then not only promotes hypertension but also increases the extent of kidney injury once hypertension develops.

1.5.2.1 Determinants of Nephron Endowment

Although the "average" number of nephrons per human kidney is approximately 1 million, this is not a true representation of nephron number as the actual values range from 200 000 to 2.7 million (Bertram et al., 2011). The significant degree of variation reflects the diversity of factors that are involved in determining nephron number, including complex environmental and genetic factors (Gurusinghe et al., 2017). Birth weight has been recognized as a primary nephron number determinant. In humans, low birth weight attributed to intrauterine growth restriction or premature birth has been directly associated with reduced nephron endowment (Manalich et al., 2000). Genetics also play an important role, particularly those involved in regulating branching of the ureteric bud. Loss of fibroblast growth factor-7 (FGF-7), belonging to the FGF family of proteins, results in a 30% reduction in nephron number, abnormal renal papilla morphology, and smaller overall kidney size in mature FGF-7-null mice (Qiao, 1999). In addition, environmental factors such as maternal diet have been found to play an important role (Gurusinghe et al., 2017).

1.5.3 Regulation of Blood Pressure by the Kidney

1.5.3.1 Renin-Angiotensin-Aldosterone System (RAAS)

The kidneys play an essential role in regulating systemic blood pressure through a number of mechanisms. The renin-angiotensin-aldosterone system (RAAS) is one such established mechanism involved in the regulation of blood pressure and is a target for hypertension management (Weir and Dzau, 1999). Renin is secreted by renal juxtaglomerular cells in response to decreased blood pressure and converts

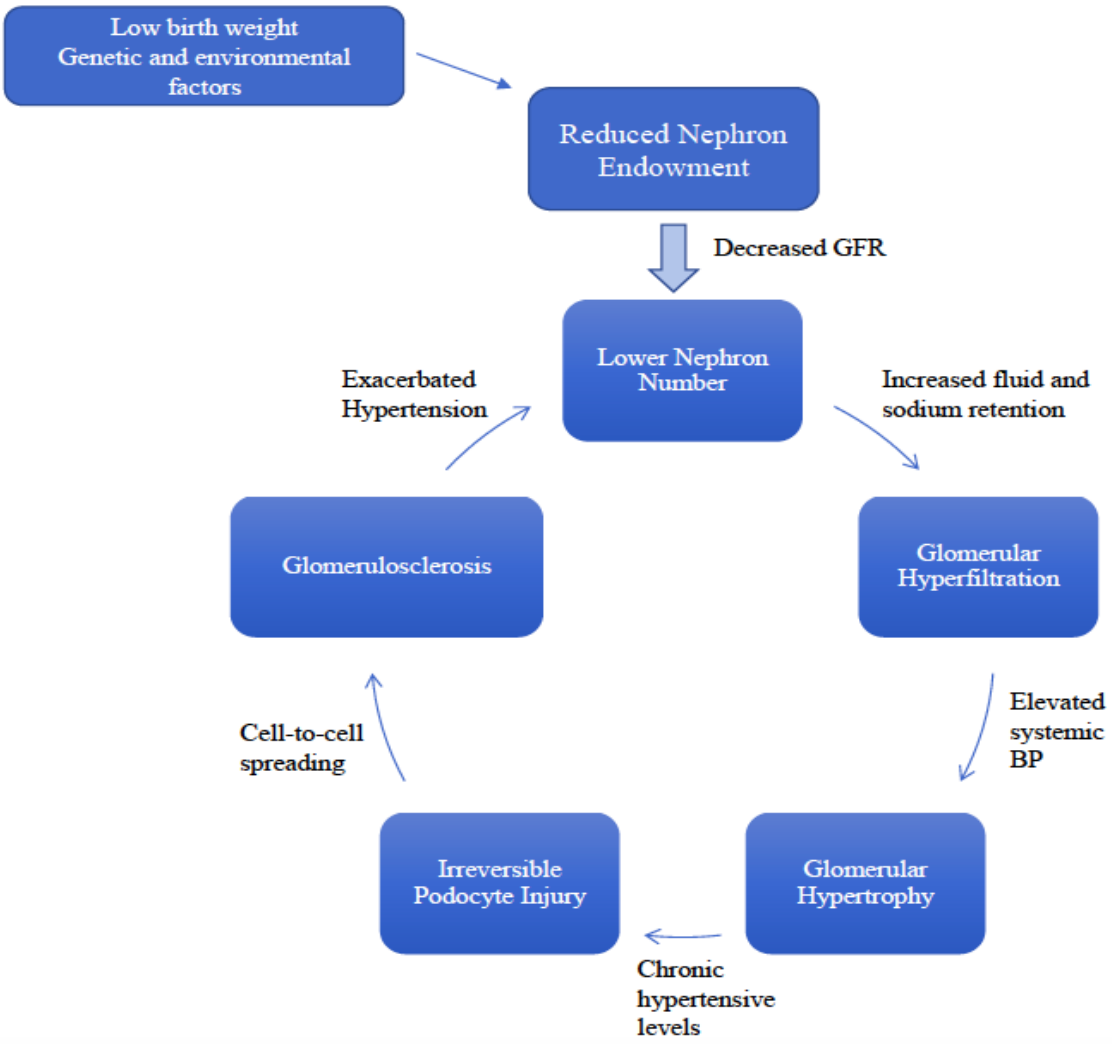

Figure 1.6 Progressive cycle of hypertension and CKD. Flowchart demonstrating the interdependence between kidney function and hypertension. Reduced nephron endowment due to factors such as low birth weight results in a lower nephron number. A lower nephron number leads to decreased GFR. When this decreased GFR falls below a threshold, the residual nephrons compensate by hyperfiltrating, leading to increased fluid and sodium retention and increased systemic BP. Increased systemic blood pressure then increases glomerular capillary pressure leading to hypertrophy and podocyte injury. Sustained increases in systemic BP result in irreversible podocyte injury that eventually manifests as glomerulosclerosis through cell-to cell-spreading. Glomerulosclerosis leads to further nephron loss and hyperfiltration in the residual glomeruli, exacerbating hypertension and perpetuating progressive renal dysfunction. Adapted from (Didion, 2017).

angiotensinogen, secreted by the liver, into angiotensin I (Weir and Dzau, 1999). Angiotensin I is then converted into RAAS' main effector Angiotensin II (AngII) by the angiotensin-converting enzyme (ACE), after which active AngII binds to Ang II type 1 receptor sites in a variety of target tissues to exert its effects (Weir and Dzau, 1999). While under normal conditions, RAAS maintains water and sodium homeostasis and regulates tissue growth in the kidney, aberrant activation of RAAS leading to overactivity has been shown to be involved in the pathogenesis of both hypertension and CKD (Brewster and Perazella, 2004). Importantly, Ang II acts as a vasoconstrictor that promotes increases in blood pressure by elevating extracellular fluid volume and sodium reabsorption in the kidney (Weir and Dzau, 1999). Furthermore, AngII promotes fibrotic processes in the kidney by stimulating growth factors such as TGF-ß and FGF, inducing renal injury (Fogo, 2007).

AngII also regulates renal hemodynamics and thus blood pressure through its action on the tubuloglomerular feedback system (Kobori et al., 2007). The tubuloglomerular feedback system regulates the GFR through the macula densa, which senses changes in the tubular fluid flow rate and NaCl concentrations and transmits signals to the juxtaglomerular cells in the afferent and efferent arterioles (Carroll, 2007). In this feedback system, the negative feedback signal is the delivery of NaCl to the distal tubule. A decrease in the NaCl concentration at the distal tubule is sensed by the macula densa, which causes the afferent arterioles to undergo vasodilation while simultaneous secretion of renin by the juxtaglomerular cells promotes vasoconstriction of the efferent arterioles (Carroll, 2007). Together, the actions of the arterioles increase glomerular capillary hydrostatic pressure and GFR, restoring the level of NaCl delivery to the distal tubule (Carroll, 2007). The sensitivity of the tubuloglomerular feedback system is enhanced by increased intrarenal AngII levels (Kobori et al, 2007). Augmented AngII levels increase proximal tubular reabsorption while decreasing NaCl delivery to the distal tubule, thereby decreasing urinary sodium excretion, and ultimately elevating extracellular fluid volume and blood pressure (Kobori et al., 2007). In the presence of an increased dietary sodium intake, salt excretion is further impaired, exacerbating elevations in blood pressure.

1.5.4 Sodium Intake and Hypertension

Salt plays a central role in the development of hypertension and excess salt intake results in greater renal impairment of sodium excretion and exacerbation of hypertension. Long-term blood pressure regulation critically depends on sodium and water balance. Impaired sodium excretion leads to increased water and sodium retention, which consequently elevates plasma volume and thus inevitably blood pressure (Blaustein et al., 2006). Sustained elevations in blood pressure then promote systemic hypertension through pressure natriuresis, as normal plasma volume is restored at the expense of increased blood pressure (Blaustein et al., 2006). Chronic hypertension can then potentiate further declines in kidney function through the pathogenic mechanisms discussed earlier. Rats placed on a high-salt diet exhibit significantly augmented levels of TGF-β in the kidneys, suggesting the promotion of pathways that lead to kidney fibrosis. Furthermore, salt-restriction has been shown to have protective effects in uninephrectomized spontaneously hypertensive rats. After surgery, rats were placed on either a standard chow, low-sodium chow, or standard chow with sodium added to drinking water. All rats developed severe hypertension but 42 weeks after uninephrectomy, rats that were placed on the low-sodium diet displayed significantly lower levels of proteinuria and glomerulosclerosis (Benstein et al., 1990) .

In addition, a link between high-salt and the consequences of lower nephron endowment has been established. In a mouse model for reduced nephron number, mice were seen with 25% and 65% lower nephron counts compared to WT (Ruta et al., 2010). When placed on an acute 7-day 5% high-salt diet, mice with decreased nephron numbers showed greater increases in blood pressure and lower creatinine clearance in a dose-dependent manner.

High sodium diets are commonly used to study hypertension and renal injury in animal models that are not spontaneously hypertensive. They are particularly useful for assessing susceptibility to hypertension in heterozygous animals or homozygous mutants that are not embryonically lethal, in which the addition of an insult is needed to produce a phenotype. This is under the assumption that some form of underlying kidney stressor (i.e. reduced nephron endowment) provides the “first hit” increasing susceptibility to

external insults and the addition of a salt provides the “second hit,” thereby eliciting sustained injury (Ruta et al., 2010).

1.6 Rationale, Hypotheses, Objectives

1.6.1 Rationale

Shroom3 has been shown to play a role in glomerular development and function, providing evidential support for the GWAS that have strongly associated Shroom3 with CKD. Importantly, even partial loss of Shroom3 in heterozygous *Shroom3*$^{+/Gt}$ mice, a model for hypomorphic *Shroom3*, was sufficient to produce glomerular defects in older mice. As I would not expect a complete loss of Shroom3 function in humans due to its requirement for neural tube closure, the observation that heterozygous *Shroom3*$^{+/Gt}$ mice exhibit compromised kidney function suggests that human *SHROOM3* hypomorphs may be at risk for diseases dependent on the renal system. Hypertension is the most common comorbidity of CKD and is also a leading cause. This cause-and-effect relationship between the two diseases is attributed to a shared dependence on the glomerulus. The lower glomerular number coupled with abnormal podocyte morphology observed *Shroom3*$^{+/Gt}$ would suggest an increased susceptibility to hypertension. Furthermore, because hypertension induces kidney damage specifically through podocyte injury, podocytes with inherent structural defects should be more vulnerable to the mechanical and shear forces that accompany higher blood pressure. As a leading cause of CKD and as a significant risk factor for progression to ESRD and mortality, determining whether loss of Shroom3 predisposes individuals to hypertension will be important.

The overarching goal of my project is to investigate how Shroom3 contributes to human health and disease by determining the potential consequences of altered Shroom3 activity using *in vivo* and *in vitro* models.

1.6.2 Hypothesis and Objectives

The hypothesis for my *in vivo* analysis is that partial loss of Shroom3 activity increases susceptibility to CKD. I will address this hypothesis through the following objectives:

1) Determine if *Shroom3*$^{+/Gt}$ mice are more susceptible to hypertension

2) Determine if a high-salt diet exacerbates renal injury in *Shroom3*$^{+/Gt}$ mice

For my *in vitro* analysis, I hypothesize that potentially damaging *SHROOM3* variants identified by the NHLBI with mutations in known domain locations will have compromised Shroom3 function. I will address this through the following objective:

3) Examine the ability of potentially damaging *SHROOM3* variants to induce apical constriction in cultured epithelial cells

Chapter 2

2 Materials and Methods

2.1 Mice

All mice used in this study were bred from the *Shroom3* gene trap line (B6.129S4-*Shroom3Gt(ROSA53)Sor/J*) purchased from the Jackson Laboratory. The mice are derived from the original line generated by Hildebrand and Soriano (1999). The line was bred onto the C57BL/6 background and is considered congenic with that strain. The gene trap mutation inserted an adenovirus splice acceptor (Friedrich & Soriano, 1991), a bifunctional gene fusion between β-galactosidase and Cre recombinase, and the MC1 polyadenylation (pA) sequence. This results in elimination of the short isoform and a severe truncation of the long isoform of Shroom3. Due to the embryonic lethality of homozygous *Shroom3* mutants, the line is maintained using *Shroom3* gene trap mice only carrying one copy of the gene trap allele (*Shroom3*$^{+/Gt}$). All mice were housed in an animal care facility and maintained on standard rodent chow prior to the experimental period. All studies were approved by the University of Western Ontario's Animal Care Committee (Protocol #: 2015-026) and were in accordance with the guidelines of the Canadian Council on Animal Care (CCAC).

2.2 Genotyping

The genotypes of all mice were analyzed by PCR using primers specific for the Shroom3 gene-trap allele. DNA was extracted from the ear clips of 21 day-old pups and immediately lysed in tissue lysis buffer (100mM Tris-Cl pH 8.5, 5mM EDTA pH 8.0, 200mM NaCl, 0.2% SDS (w/v) in dH_2O) containing 100µg/mL of Proteinase K overnight at 55°C. The following day, phenol/chloroform extraction was used to separate the remaining protein from the DNA samples. The samples were subjected to PCR for 30 cycles of the following parameters: 95°C for 45 seconds, 60°C for 45 seconds, and 72°C for 45 seconds. The sequences of the primers: a forward primer 5'-GGTGACTGAGGAGTAGAGTCC -3' (F11) and a reverse primer R1 (5'-GAGTTTGTGCTCAACCGCGAGC -3' (R1) amplified the *Shroom3* gene trap allele. To detect the wild-type Shroom3 allele, the forward primer (F11) was paired

with the reverse primer R4 (5'- GCAACCACATGGTGGGAGACAAGC -3'). The expected amplicon size of the gene-trap allele was 1500 bp and only mice that were heterozygous were expected to display a band. The expected amplicon size for the wild-type allele was 1000 bp and both heterozygous and wild-type mice were expected to display a band.

2.3 High-Salt Model

Congenic WT (C57BL/6) and *Shroom3*$^{+/Gt}$ male mice were bred and raised on standard rodent chow prior to the experimental period. Only male mice were considered for this study as female mice are more resistant to developing hypertension (Hyndman and Pannabecker, 2015). Animals were randomly assigned to either a normal salt diet continuing with the same standard rodent chow (NS) or a high-salt diet (HS) consisting of 8% NaCl with 1% NaCl in drinking water. Mice were able to freely access food and water at all times. The experimental groups were as follows: wild-type mice on NS, wild-type mice on HS, *Shroom3*$^{+/Gt}$ mice on NS, and *Shroom3*$^{+/Gt}$ mice on HS. Both the normal salt diet (cat. no. 2019) and high-salt diet (cat. no. TD92012) were purchased from Harland Teklad (Madison, WI, U.S.A). The high-salt diet groups were initiated on the diet after basal level systolic blood pressure was measured; normal salt diet groups remained on the standard chow for the duration of the basal and experimental periods. Mice were between the ages of 5-7 months at the start of the experimental period. Studies were conducted in three sequential rounds, and data from each round was pooled for each experimental group.

2.4 Blood Pressure Measurements (Tail-Cuff)

Blood pressures of conscious mice were measured using a CODA 6-Channel High Throughput Non-Invasive Blood Pressure system (CODA-HT6, Kent Scientific, Torrington, CT, USA) according to the manufacturer's instructions. The apparatus applies the tail-cuff method to determine blood pressure. Mice were placed into holders that restrained movement; the head was secured with a nose cone while the tail extended out of the rear end of the holder. The holders were kept on a warming platform to maintain the mice at a minimum temperature of 32°C for the duration of

the experiment. Two cuffs were placed around the tail: an occlusion cuff which impedes blood flow by inflation, and a Volume Pressure Recording (VPR) cuff which measures the swelling of the tail that occurs as a result of returning blood flow upon deflation of the occlusion cuff. The VPR sensor measures and outputs six different physiological readings: systolic and diastolic blood pressure, mean arterial pressure, heart rate, tail blood flow, and tail blood volume. In order to condition the mice and minimize the level of stress caused by the tail-cuff apparatus, mice were trained on a daily basis for 2-3 weeks prior to taking the basal blood pressure measurement. Blood pressures were monitored over two sets of 15 cycles each, with 5 additional acclimatization cycles at the start of the first set; measurements were taken at the same time each day.

2.5 Tissue Collection

At the end of each experimental period, mice were weighed then euthanized by CO_2. The heart was extracted, trimmed of excess cardiac and atrial tissue, and washed in ice-cold 1xPBS. Hearts were blotted dry and weighed on the same scale used to measure body weight, and heart weight to body weight ratios were calculated. In addition, the kidneys were dissected out, cut longitudinally, and rinsed in ice-cold 1x PBS. Kidneys were then fixed for at least 24 hours at 4°C in either 4% PFA or 10% formalin. Samples were then transferred to tissue cassettes and sent to our collaborators at University Hospital (London, ON) to be dehydrated, embedded in paraffin, and subsequently sectioned. Sections were cut at a thickness of 4μm and stained with hematoxylin and eosin to visualize tubules and glomeruli, and with Masson's Trichome to visualize interstitial fibrosis. All slides were visualized using a Leica DM5500 B microscope (cat. no. 380492, Leica Camera AG, Wetzlar, Germany).

2.6 Urinalysis

Urine was collected on various days during the course of the diet treatment; collection always occurred at the same time each day (9 am). To induce urination, the mouse was scruffed and pressure was directly applied to the bladder area. The urine was

collected on a piece of Parafilm® M then transferred to an Eppendorf tube and stored at -80°C until ready for analyses. Urine was analyzed for urinary protein and creatinine levels (University Hospital, London, ON, Canada).

2.7 Generation of *SHROOM3* Variants

The substitution mutations corresponding to the human *Shroom3* variants of interest were introduced into the full-length *Shroom3* construct using a Quikchange II XL Site-Directed Mutagenesis Kit (Agilent Technologies, Santa Clara, CA, USA) according to the manufacturer's instructions. PCR amplification of oligonucleotide primers containing the desired substitution was used to generate mutated plasmids (see Table 2.1 for primer sequences). The resulting PCR products were digested with a *Dpn* I treated endonuclease to digest the parental DNA template and to select for newly synthesized DNA carrying the desired mutation.

The mutated DNA generated by PCR amplification was transformed into XL10-Gold Ultracompetent cells (Agilent Technologies, Santa Clara, CA, USA) and plated on LB-ampicillin agar plates. The following day, colonies were selected from the plates and inoculated in LB broth overnight at 37°C. Plasmid DNA was then isolated from the bacterial inoculates using a standard plasmid miniprep kit (Qiagen, Valencia, CA, USA). To confirm that the plasmid DNA was carrying the mutation of interest, all plasmid DNA samples were sequenced at Robarts Research Institute (University of Western Ontario, London, ON, Canada).

2.8 Cell Culture and Transfection

The Madin-Darby canine kidney (MDCK) epithelial cell line was obtained from ATCC (Manassas, VA, USA). Importantly, this cell line is epithelial rather than mesenchymal and has been used for apical constriction assays by several previous studies that have looked at *Shroom3* function; the cells do not endogenously express *SHROOM3* (Dietz et al., 2006; Hildebrand, 2005; Plageman et al., 2011). The cell line was maintained in DMEM (Thermo Fisher Scientific, Waltham, MA, USA) supplemented with 10% FBS and grown in 55 cm^2 petri dishes at 37°C, in a

Table 2.1 Primer sequences for PCR used to generate *SHROOM3* variants

Variant	**Forward Primer (5' to 3')**	**Reverse Primer (5' to 3')**
G60V	TCTAAGGTCGAAGAAGTGGG CAAAGCAGACACC	GGTGTCTGCTTTGCCCACTTCTTCGACC TTAGA
T1012N	CTCGCCGGCGCCTGAATCCCG AGC	GCTCGGGATTCAGGCGCCGGCGAG
G1864D	GAGAATGTCCTTAGCGACCTT GGTGAAGATGC	GGCATCTTCACCAAGGTCGCTAAGGAC ATTCTC

humidified 5% CO_2 incubator. Cells were passaged every other day until they reached 70% confluency and appeared to be cobblestone-like in shape and structure. Cells were seeded on glass coverslips in a 6-well plate at a density of 0.5-1 x 10^7 cells/mL one day before transfection and grown to 80-90% confluency prior to transfection. One hour prior to cell seeding, fibronectin (Sigma-Aldrich, St. Louis, MI, USA) was added to each glass coverslip at a 1:750 dilution in 1x PBS to enhance cellular adhesion. To transfect cells, the DMEM + 10% FBS that the cells were plated in was first aspirated from each of the six wells and replaced with pre-warmed Opti-MEM reduced serum medium (Invitrogen, Carlsbad, CA, USA). All transfections were carried out using the plasmid vector pEF-I-GFP-GX (Plasmid #45443, Addgene, Cambridge, MA, USA) that contains an internal ribosome entry site (IRES) that allowed for bicistronic expression of both GFP and *SHROOM3* from a single transcript while circumventing the potential disruption of function that could arise from the production of a GFP fusion protein. All transfections were carried out with the inclusion of a negative control, an empty GFP plasmid vector, and a positive control, a vector harboring WT *SHROOM3.*

Cells were transfected using the transfection agent Lipofectamine 3000, according to the manufacturer's protocol (Invitrogen). Two sets of solutions were prepared in separate tubes for transfection. The first set contained 7.5 µl of Lipofectamine 3000 diluted in 125 µl of Opti-MEM. The second set contained 2µg of plasmid DNA diluted in 125 µl of Opti-MEM with 4 µl of P3000 Enhancer Reagent (Invitrogen). An equal 1:1 ratio of each solution (125 µL each) was pooled together and incubated for 5 minutes at room temperature to allow proper lipoplex formation. The complex was then added to each of the wells containing cells and Opti-MEM, and the plate was incubated at 37°C for 48 hours.

2.9 Immunofluroescence

Cells were washed three times in 1x PBS 48 hours post-transfection and subsequently fixed in 4% PFA for 15 minutes at room temperature. After, cells were washed three more times in 1x PBS and permeabilized in 0.2% Triton-X100 diluted in PBS for 5

minutes at room temperature. Cells were then left in 0.1% Tween 20 diluted in 1x PBS for 30 minutes at room temperature to allow blocking. The blocking buffer was removed and cells were incubated with the mouse anti ZO-1 monoclonal antibody (ZO1-1A12) conjugated to Alexa Fluor 594® for 1 hour at room temperature to enable visualization of intercellular boundaries (cat. no. 339194, 1:100, Thermo Fisher Scientific, Waltham, MA, USA). ZO-1 is a tight junction protein that can be stained to outline apical cell-cell boundaries. Cells were washed three times in 1x PBS then counterstained with DAPI (1:1000 in 1x PBS) for 7 minutes at room temperature. After a final three washes, slides were mounted with PermaFluor Aqueous Mounting Medium (Thermo Fisher Scientific) and stored at 4°C. All slides were visualized by fluorescence microscopy using a Leica DM5500 B microscope.

All microscope images were analyzed using ImageJ software (National Institutes of Health, Bethesda, MD, USA). To quantify apical constriction, cell profiles were traced and measured using ImageJ similar to previously described methods (Das et al., 2014; Plageman et al., 2010). The apical area was defined as the area of the cell outlined by red ZO-1 staining. Between 22 – 25 randomly picked cells from 2 – 4 independent experiments were analyzed (see Appendix F).

2.10 Statistical Analysis

All statistical analysis was performed using GraphPad Prism 7 (GraphPad Software Inc., San Diego, CA, USA). For physiological measurements, statistical analysis between genotypes at baseline was conducted using an unpaired Student's t-test. Differences between experimental groups during the dietary treatment period were analyzed using two-way ANOVA, followed by a Tukey's post-hoc test. A one-way ANOVA with repeated measures followed by a Dunnett's multiple comparisons test was used to determine statistical significance within experimental groups; three individual mice were omitted from analysis (see Appendix A). For apical constriction assays, statistical differences between controls and variants were analyzed using one-way ANOVA followed by a Dunnett's multiple comparison test while statistical differences between transfected cells and neighboring cells were analyzed by an unpaired t-test. P-values < 0.05 were considered statistically significant.

Chapter 3

3 Results

3.1 Physiological effects of *Shroom3* loss

Previous work in our lab has revealed that loss of Shroom3 is associated with glomerular defects during development that result in compromised renal function later in adulthood (Khalili et al., 2016). Importantly, the reduced glomerular number found in *Shroom3*$^{+/Gt}$ mice, would suggest an increased risk for developing adult onset hypertension. To determine whether loss of Shroom3 increases susceptibility to hypertension, congenic wild type (WT; *Shroom3*$^{+/+}$) and heterozygous *Shroom3*$^{+/Gt}$ mice were treated with either a high-salt (HS) diet or normal-salt (NS) diet for four weeks. Initially, a HS diet consisting of 4% NaCl in chow was chosen for my study. However, this diet was not sufficient to produce any observable changes in blood pressure in any of the four mice cohorts (data not shown). A more commonly used diet to generate high blood pressure in experimental models is the 8% NaCl diet (Bohlooly et al., 2001; Mathis et al., 2011; Nakagawa et al., 2006; Obih & Oyekan, 2008; Oliver et al., 1997; Watanabe et al., 2005; Yu et al., 2004), sometimes supplemented with 1% NaCl in drinking water (Brochu et al., 2002; Greenwald et al., 1988; Hernandez et al., 2015; Ofem et al., 2014). As such, I treated mice with either 8% NaCl in chow with 1% NaCl in drinking water or standard chow over a period of four weeks and assessed six different physiological parameters using the CODA 6-Channel High Throughput Non-Invasive Blood Pressure system. Weeks 1, 2, 3 and 4 correspond to measurements taken on days 7, 14, 21, and 28 of treatment, respectively. However, when mice exhibited signs of high-stress on any given day, including resistance to being placed in the holders or frequent movement while measurements were being taken, blood pressure measurements were taken the next day.

To determine whether loss of *Shroom3* has physiological effects under basal conditions, baseline measurements of body weight, heart rate, and blood pressure for 5-7 month old congenic male WT and *Shroom3*$^{+/Gt}$ mice were analyzed. Baseline values were calculated by averaging recordings obtained from at least two different days during the week preceding the first day of treatment. There was no significant difference in body weight,

heart rate (HR), diastolic blood pressure (DBP), mean arterial blood pressure (MAP), or systolic blood pressure (SBP) between WT and *Shroom3*$^{+/Gt}$ mice at baseline (Figure 3.1). These results suggest that loss of *Shroom3* does not have physiological consequences under normal conditions at 5-7 months of age.

3.1.1 Body weight and heart rate

Upon treatment with a high-salt diet, no significant differences in body weight were seen between the experimental groups at any of the weekly time points throughout the four-week period (Figure 3.2). WT and *Shroom3*$^{+/Gt}$ mice on a normal-salt diet generally appeared heavier than mice on a HS diet, however, this was not statistically significant (Figure 3.2A, C). Surprisingly, both WT and *Shroom3*$^{+/Gt}$ mice on a NS diet were found to be significantly heavier at four weeks compared to the baseline (WT $p=0.0079$, *Shroom3*$^{+/Gt}$ $p = 0.0343$; Figure 3.2E). This unexpected finding may be explained, at least in part for the WT mice, by one of the mice from the cohort gaining a substantial amount of weight near the last two weeks of the experimental period; this mouse was also found with extremely high blood pressure by week 4 (see Appendix B). There was no significant difference found within either of the two HS experimental groups throughout the duration of the treatment period.

There were no significant differences seen in heart rate between the four experimental groups at any of the weekly time points during the dietary period (Figure 3.3). In addition, no significant changes in heart rate were seen within the experimental groups during the four-week period when compared to baseline measurements.

3.1.2 Blood Pressure

Diastolic blood pressure (DBP), defined as the minimum blood pressure recorded when the heart is at rest between contractions, systolic blood pressure (SBP) defined as the maximum blood pressure recorded when the heart contracts, and mean arterial pressure (MAP), which is calculated using the DBP and SBP, were assessed to determine the effects of *Shroom3* loss in the presence of a high-salt diet (Brzezinski, 1990).

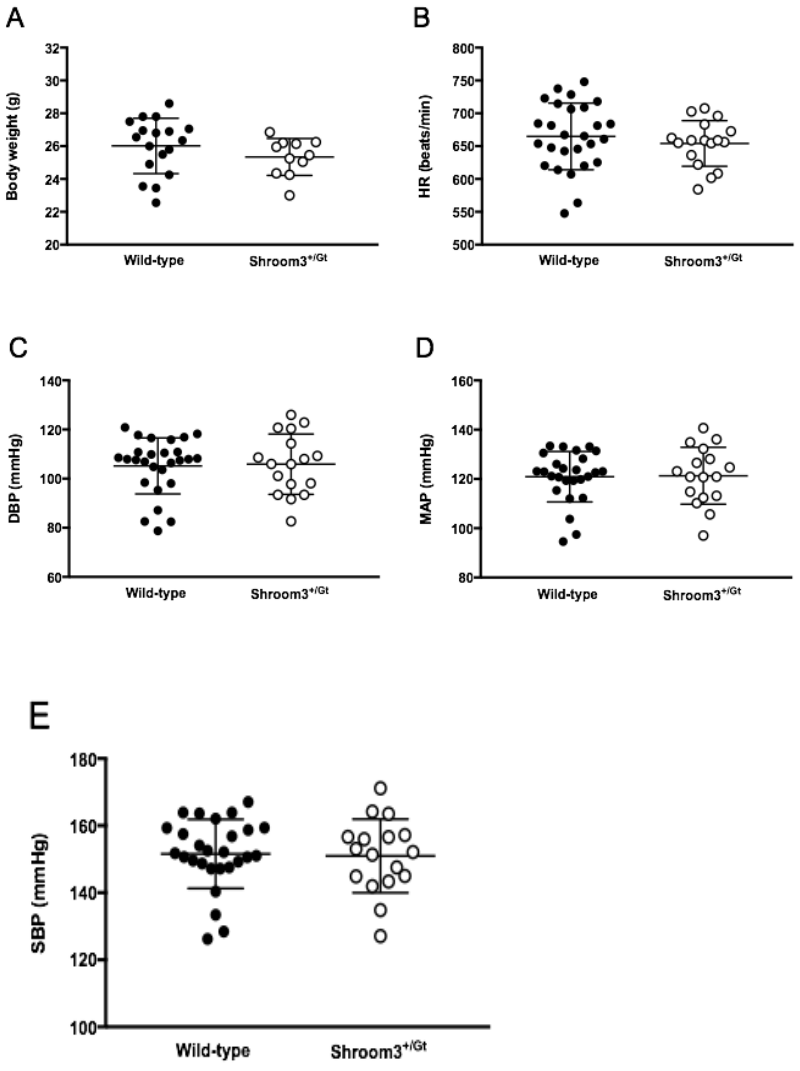

Figure 3.1 Comparison of baseline physiological parameters between WT and *Shroom3*$^{+/Gt}$ mice. Measurements for body weight (A), heart rate (B), diastolic blood pressure (C), mean arterial pressure (D), and systolic blood pressure (E), taken prior to the dietary period are shown. Individual dots represent the average of measurements taken from 2 or 3 different days in the week prior to the start of the NS or HS diet. Mice were trained for use of the tail-cuff system for a minimum of 2 weeks before recording baseline measurements. Data expressed as mean ± SEM; n = 27 for WT, n=17 for *Shroom3*$^{+/Gt}$ mice for all panels with the exception of body weight (n=17 for WT, n=11 for *Shroom3*$^{+/Gt}$ mice; body weight was not measured in the first independent experiment).

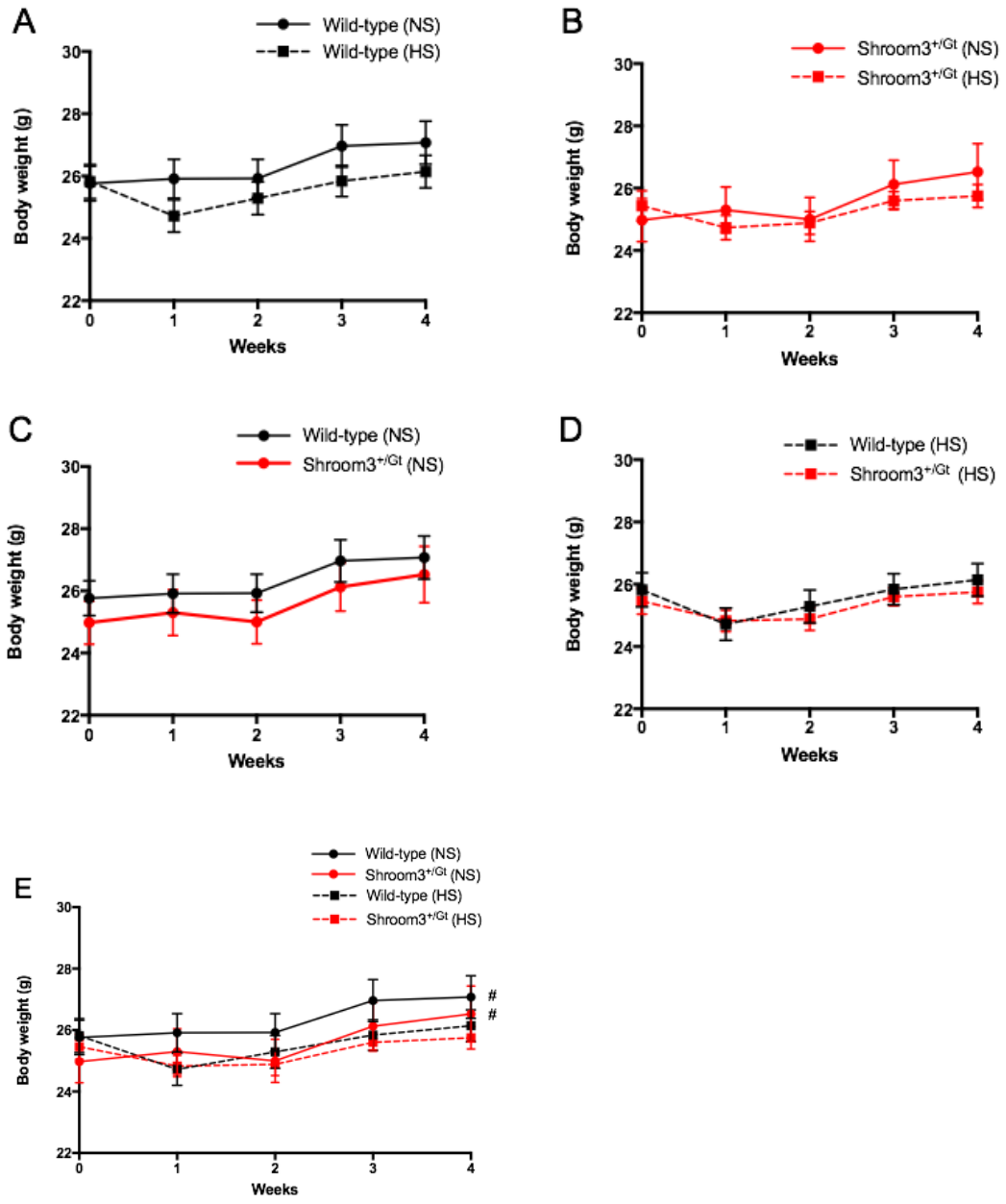

Figure 3.2 Effects of high-salt diet and *Shroom3* loss on body weight. Time-course of body weight of WT and *Shroom3*$^{+/Gt}$ mice on a NS (C) and HS (D) diet. A summary of all four groups is shown in (E). The data was grouped in multiple ways to depict the comparison between diet as well as genotype. Data expressed as mean ± SEM; n= 4-8 for NS groups and n= 7-10 for HS groups. ($^{\#}$ $p < 0.05$ vs. baseline, repeated measures one-way ANOVA with Dunnett's multiple comparisons test).

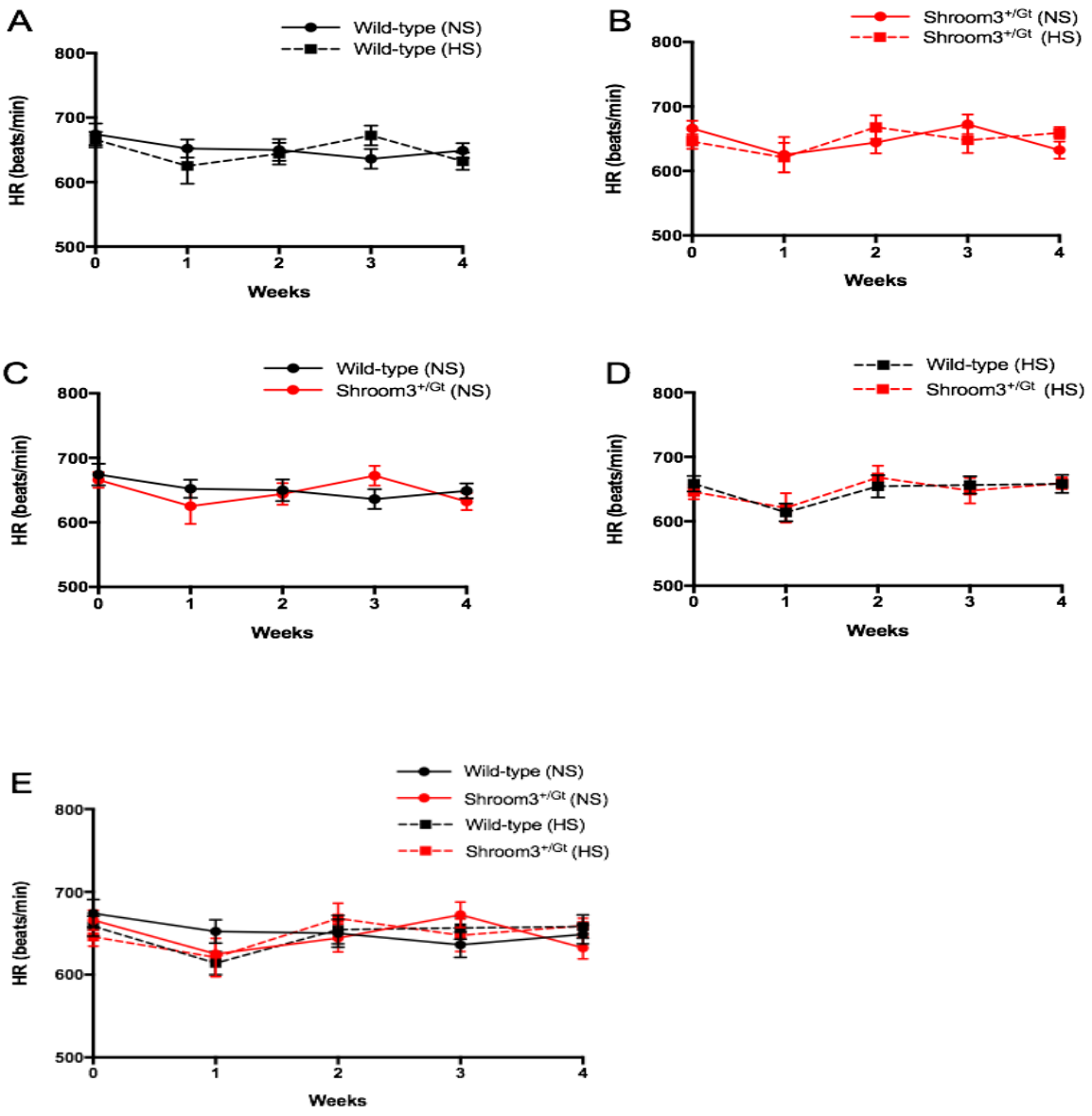

Figure 3.3 Effects of high-salt diet and *Shroom3* loss on heart rate. Time-course of HR from baseline (week 0) to the end of the treatment period (week 4) for WT (A) and *Shroom3*$^{+/Gt}$ (B) mice on a NS and HS diet, as well as WT and *Shroom3*$^{+/Gt}$ mice on a NS (C) and HS (D) diet. Measurements were taken 7, 14, 21, and 28 days after the start of the dietary period using the tail-cuff blood pressure system. A summary of all four groups is shown in (E). No significant differences were found between groups (two-way ANOVA with Tukey's post-hoc) or within groups (repeated measures one-way ANOVA with Dunnett's multiple comparison test). Data expressed as mean ± SEM; n= 7-11 for NS groups and n= 9-16 for HS groups.

Increased dietary salt intake did not lead to a significant difference in the DBP (Figure 3.4) or MAP (Figure 3.5) of WT mice compared to WT mice on a normal salt diet. However, when *Shroom3*$^{+/Gt}$ mice were placed on a HS diet, they exhibited a significant decrease in DBP compared to *Shroom3*$^{+/Gt}$ on a NS diet at week 2 (p=0.0129) and 3 (p=0.0319) and WT mice on a NS diet at week 2 (p=0.0140) of the treatment period (Figure 3.4B). *Shroom3*$^{+/Gt}$ mice on a HS diet also displayed significantly decreased MAP at weeks 2 (p=0.0108) and 3 (0.0388) compared to *Shroom3*$^{+/Gt}$ mice on a normal salt diet (Figure 3.5B). Generally, increased sodium intake led to a decrease in DBP and MAP for both WT and *Shroom3*$^{+/Gt}$ mice, but this difference was significantly greater in *Shroom3*$^{+/Gt}$ mice at weeks 2 and 3 compared to WT mice, suggesting that when challenged with a HS diet, loss of *Shroom3* may lead to decreased ability to regulate blood pressure. No significant differences were seen within the experimental groups when compared to baseline measurements.

SBP is believed to be a more important predictor of cardiovascular risk than DBP, with many studies suggesting that SBP should be the primary focus of antihypertensive therapy (Kannel, 2000; Leonetti et al., 2000; Wilkinson & Cockcroft, 2000). SBP is also considered the most useful and accurate cardiac parameter measured by the tail-cuff technique (Feng et al., 2008). Therefore, the majority of my blood pressure data will primarily focus on SBP. As expected, no significant differences in SBP levels were observed between WT and *Shroom3*$^{+/Gt}$ mice on a NS diet over the four-week period (Figure 3.6A). Surprisingly, a HS diet did not cause a significant increase in the SBP of *Shroom3*$^{+/Gt}$ mice over the course of the treatment period compared to baseline SBP levels (Figure 3.6B). However, interestingly, *Shroom3*$^{+/Gt}$ mice on a NS diet had significantly higher SBP at week 3 compared to the baseline level (Figure 3.6B). Similar to DBP and MAP findings, a HS diet appeared to cause lower SBP levels compared to a NS diet in both *Shroom3*$^{+/Gt}$ mice and WT mice, with a greater difference seen in *Shroom3*$^{+/Gt}$ mice compared to WT mice, although not statistically significant. The finding that a HS diet does not lead to an increase in blood pressure levels in WT mice is consistent with previous studies that have used a 8% HS model (Bao et al., 2014; Daumerie et al., 2010; Davenport et al., 2015; Iida et al., 2005; Ye et al., 2006).

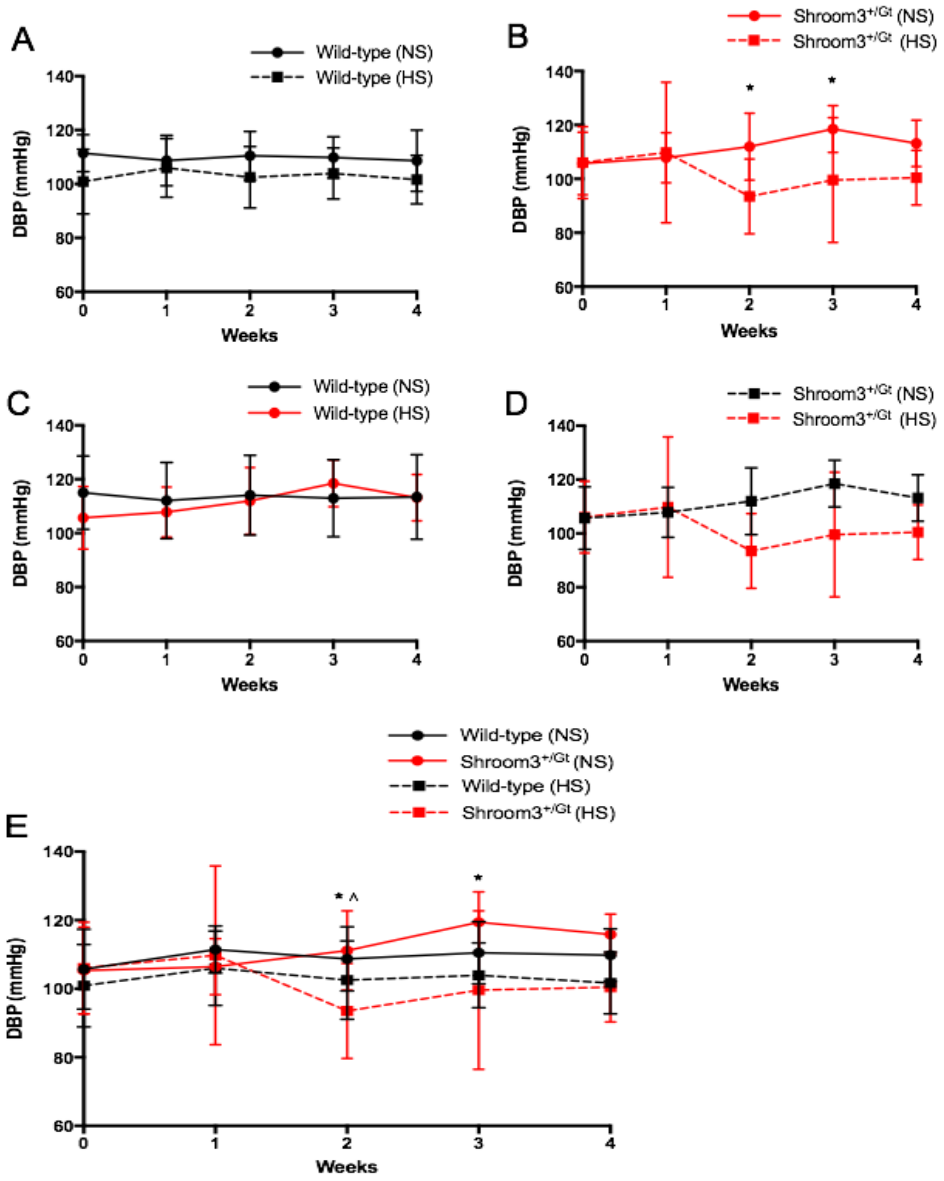

Figure 3.4 Effects of high-salt diet and *Shroom3* loss on diastolic blood pressure. Time-course of DBP from baseline (week 0) to the end of the treatment period (week 4) for WT (A) and *Shroom3*$^{+/Gt}$ (B) mice on a NS and HS diet, as well as a time-course of DBP of WT and *Shroom3*$^{+/Gt}$ mice on a NS (C) and HS (D) diet. Measurements were taken 7, 14, 21, and 28 days after the start of the dietary period using the tail-cuff blood pressure system. A summary of all four groups is shown in (E). DBP was significantly lower in *Shroom3*$^{+/Gt}$ mice on a HS diet compared to WT and *Shroom3*$^{+/Gt}$ mice on a NS diet (*$p < 0.05$ vs. *Shroom3*$^{+/Gt}$ mice, ^$p < 0.05$ versus WT mice). Data expressed as mean ± SD; n= 7-11 for NS groups and n= 9-16 for HS groups.

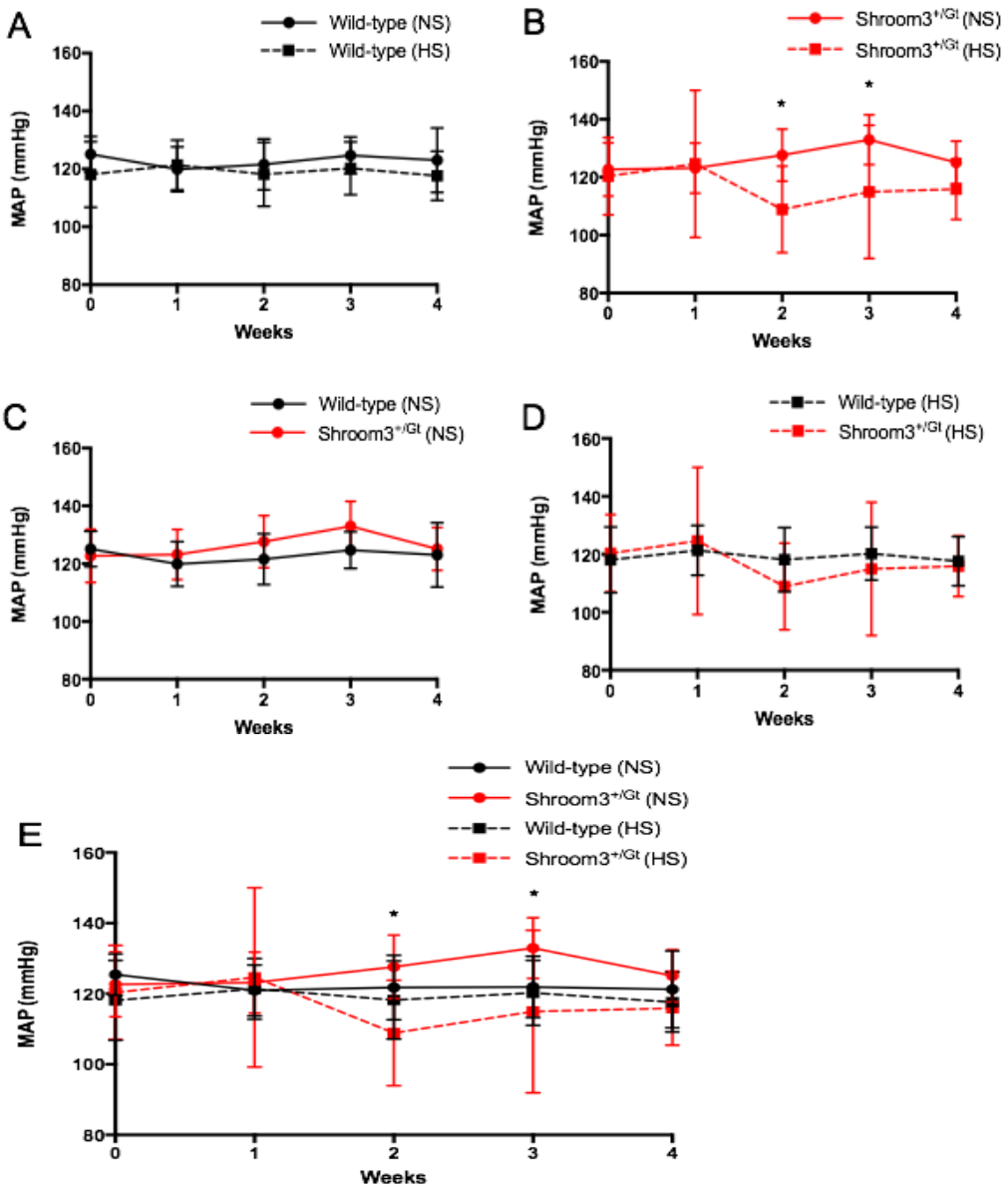

Figure 3.5 Effects of high-salt diet and *Shroom3* loss on mean arterial pressure. Time-course of MAP from baseline (week 0) to the end of the treatment period (week 4) for WT (A) and *Shroom3*$^{+/Gt}$ (B) mice on a NS and HS diet, as well as a time-course of MAP of WT and *Shroom3*$^{+/Gt}$ mice on a NS (C) and HS (D) diet. Measurements were taken 7, 14, 21, and 28 days after the start of the dietary period using the tail-cuff blood pressure system. A summary of all four groups is shown in (E). MAP was significantly higher in *Shroom3*$^{+/Gt}$ mice on a HS diet compared to *Shroom3*$^{+/Gt}$ mice on a NS diet (*$p < 0.05$ two-way ANOVA with Tukey's post-hoc test). Data expressed as mean ± SD; n= 7-11 for NS groups and n= 9-16 for HS groups.

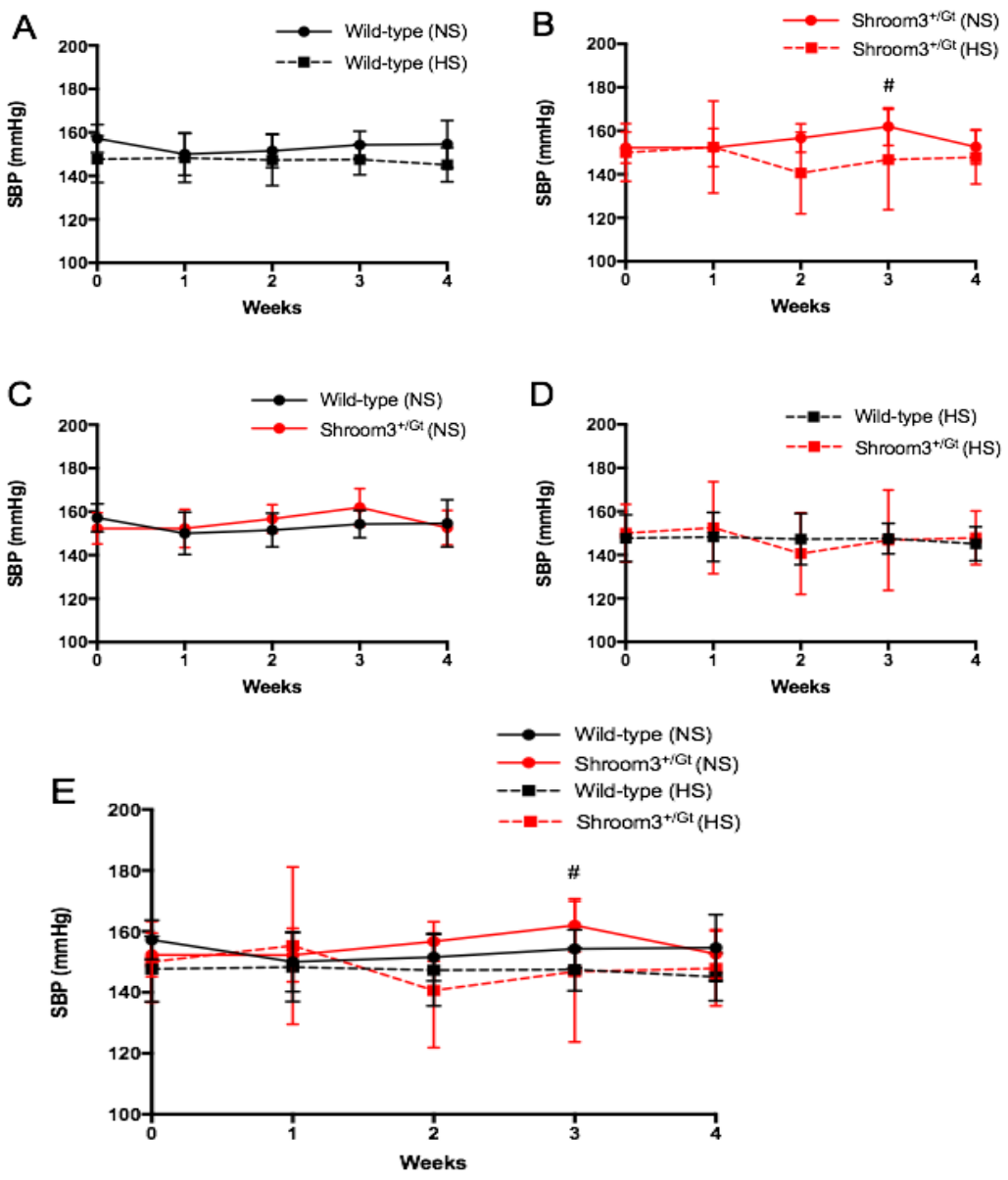

Figure 3.6 Effects of high-salt diet and *Shroom3* loss on systolic blood pressure. Time-course of SBP from baseline (week 0) to the end of the treatment period (week 4) for WT (A) and *Shroom3*$^{+/Gt}$ (B) mice on a NS and HS diet, as well as a time-course of SBP of WT and *Shroom3*$^{+/Gt}$ mice on a NS (C) and HS (D) diet. Measurements were taken 7, 14, 21, and 28 days after the start of the dietary period using the tail-cuff blood pressure system. A summary of all four groups is shown in (E). SBP was significantly higher in *Shroom3*$^{+/Gt}$ mice on a NS diet at week 3 in comparison to the baseline. ($^{\#}p < 0.05$ versus baseline). Data expressed as mean ± SD; n= 7-11 for NS groups and n= 9-16 for HS groups.

Surprisingly, however, results thus far would suggest that a HS diet does not induce elevations in blood pressure in *Shroom3*$^{+/Gt}$ mice, but may rather lead to decreased blood pressure levels.

3.1.3 High-salt diet increases blood pressure variability in *Shroom3*$^{+/Gt}$ mice

A closer look at the SBP trends of *Shroom3*$^{+/Gt}$ mice on a HS diet may at least in part explain the unexpected SBP findings that a HS diet leads to a decrease in blood pressure. Throughout the period of high-salt treatment, I noticed that the SBP of *Shroom3*$^{+/Gt}$ mice on a high-salt diet varied considerably over time and between individual mice (see Appendix B). Specifically, some mice consistently exhibited noticeable increases in SBP, while others exhibited a consistent decrease, and yet some mice exhibited both an increase and decrease over the course of the high-salt diet, leading to a large range in SBP values in *Shroom3*$^{+/Gt}$ mice on a HS diet compared to the baseline range (Figure 3.7A). Moreover, the variance of *Shroom3*$^{+/Gt}$ mice was significantly higher than the variance of WT mice at week 1 and 3 of salt loading, as determined by the F-test for equality of variances (week 1 p=0.0254, week 3 p=0.0001; Figure 3.7B, D).

To assess the degree of change in blood pressure and to determine whether such changes were significantly different between experimental groups, I compared the change in SBP from the baseline level for each week of the treatment period. An absolute value for change was used to account for both increases and decreases in blood pressure over time, as a large negative and a large positive value would cancel each other out and reflect minimal change, and I was interested in the magnitude of change rather than the direction. As shown in Figure 3.8, *Shroom3*$^{+/Gt}$ mice showed significantly higher changes in SBP compared to WT mice at all four weekly time points during the HS diet (week 1 p=0.0133, week 2 p=0.0029, week 3 p=0.0459, week 4 p=0.0460). *Shroom3*$^{+/Gt}$ mice on a HS diet also had significantly higher changes in SBP compared to *Shroom3*$^{+/Gt}$ mice on a NS diet in the first two weeks of the HS diet (week 1 p=0.0345, week 2 p=0.0136) and compared to WT mice on a NS diet in the last three weeks of the HS diet (week 2 p=0.0054, week 3 p=0.0024, week 4 p=0.0203). No significant differences between the

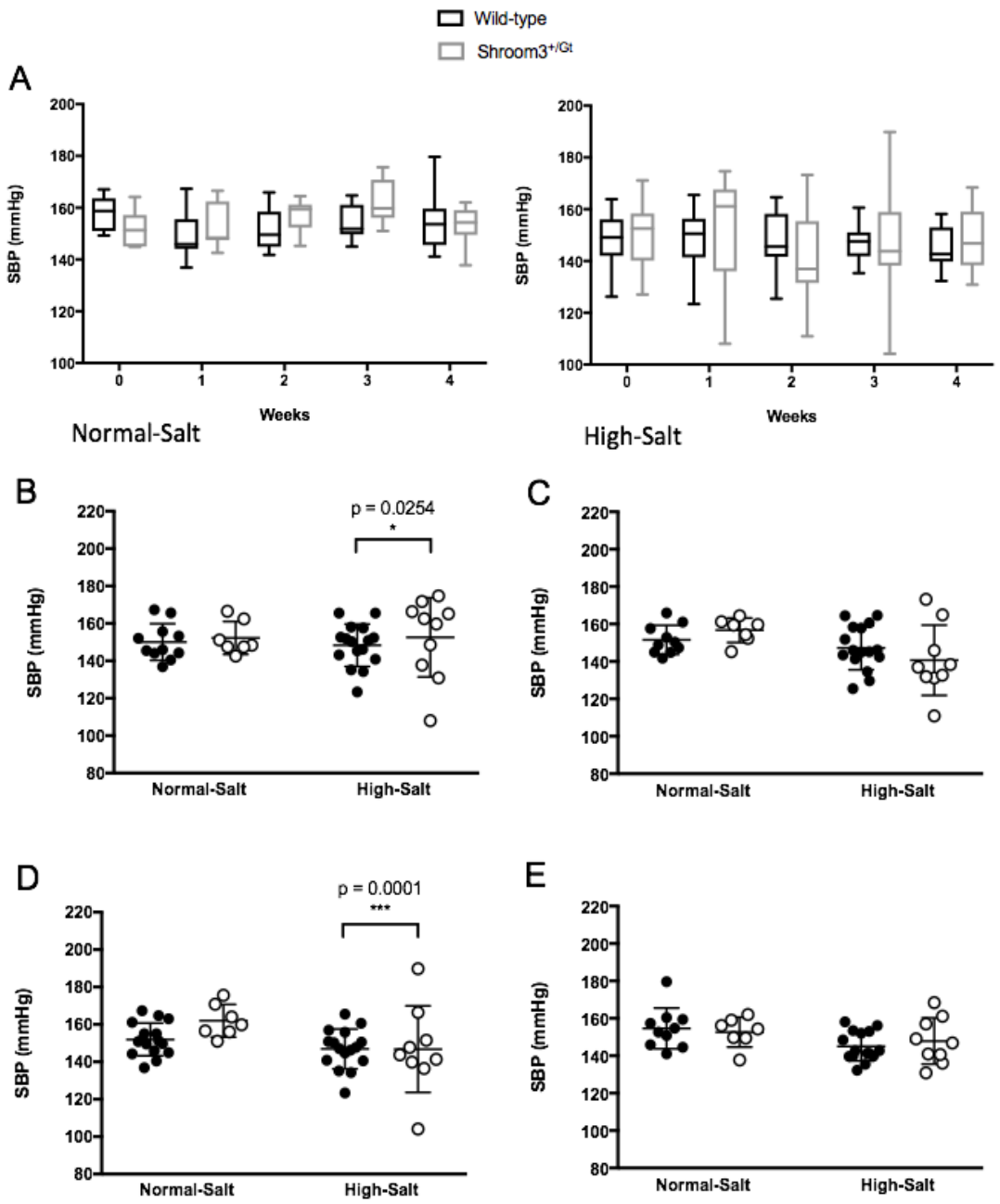

Figure 3.7 A high-salt diet increases SBP variance in *Shroom3*$^{+/Gt}$ mice. Box plots depicting the range in SBP values (A) and interleaved scatter plots depicting the high variability in SBP values in HS *Shroom3*$^{+/}$Gt mice at week 1 (A), 2 (B), 3 (C), and 4 (D), of the dietary period. On a HS diet, *Shroom3*$^{+/}$Gt mice exhibit a significant increase in variance in SBP measurements compared to WT mice (**p=0.0254, ***p=0.0001, F-test to compare equality of variances). Data expressed as mean ± SD; n= 7-11 for NS groups and n= 9-16 for HS groups.

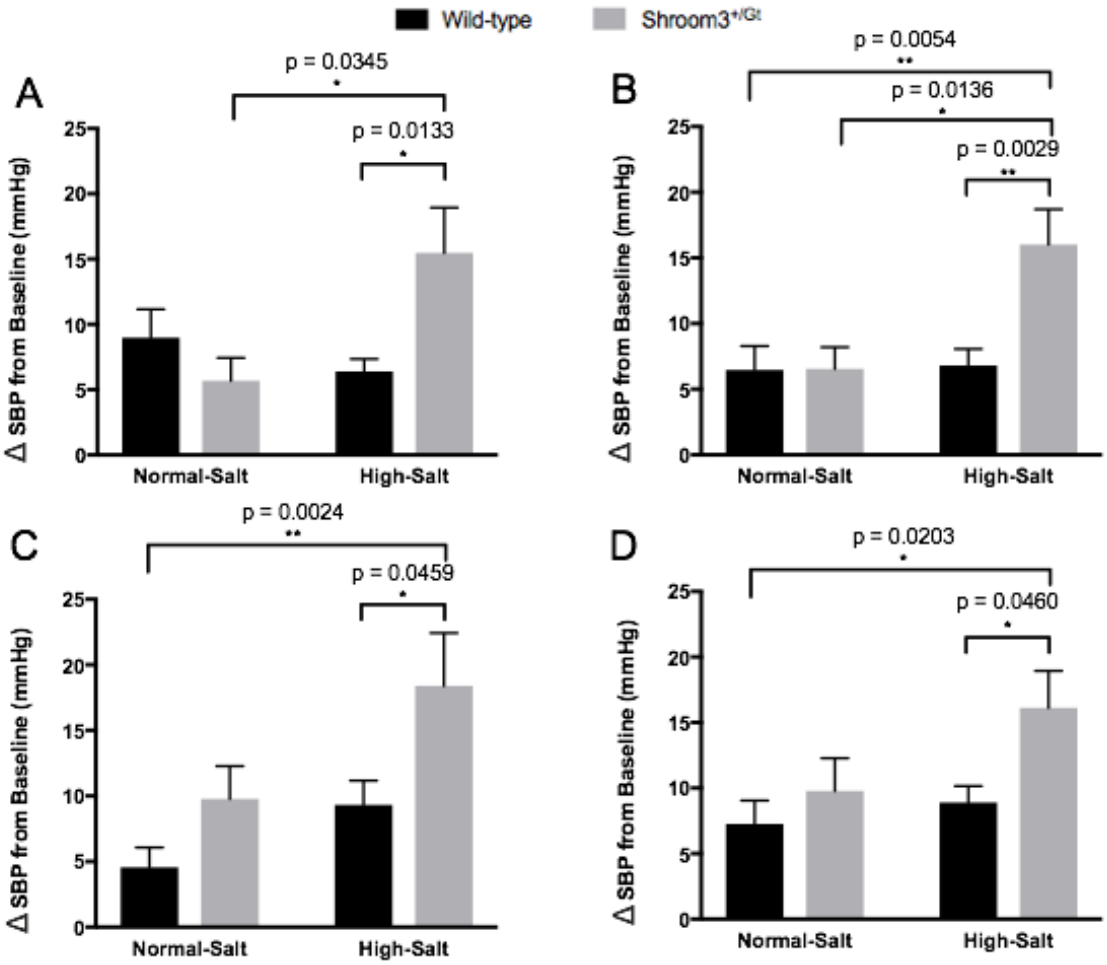

Figure 3.8 Absolute change in systolic blood pressure in response to a high-salt diet. SBP measurements at one week (A), two weeks (B), three weeks (C), and four weeks (D) after the start of the dietary treatment period were subtracted from baseline SBP values. Delta SBP reflects an absolute value; negative delta values were considered to be positive in calculations as I was only interested in the magnitude of change not the direction, due to mice reflecting both increases and decreases in SBP throughout the treatment period. A high-salt diet caused a greater change in SBP from baseline in *Shroom3*$^{+/Gt}$ mice compared to WT mice and *Shroom3*$^{+/Gt}$ mice on a NS diet and WT mice on a HS diet (*$p < 0.05$, **$p < 0.01$, two-way ANOVA with Tukey's post-hoc test). Data expressed as mean ± SD; n= 7-11 for NS groups and n= 9-16 for HS groups.

other experimental groups were observed, suggesting that a HS diet induces greater fluctuations in blood pressure in *Shroom3*$^{+/Gt}$ mice in a manner dependent on loss of *Shroom3*.

The high SBP variance observed in *Shroom3*$^{+/Gt}$ mice on a HS diet is reflected by the high standard deviation within this group, an outcome of the discrepancy in the directional change in blood pressure, with mice exhibiting both increases and/or decreases. For this reason, the SBP data was expressed as mean ± SD rather than SEM to depict variability. Both long-term and short-term blood pressure variability (BPV) are associated with cardiovascular and renal disease outcomes as well as all-cause mortality in humans (Mancia, 2012). The SD of the mean SBP calculated from sequential blood pressure measurements is an established index for BPV (Dolan & O'Brien, 2010; Kikuya et al., 2008; Rothwell et al., 2010; Stevens et al., 2016). A previous study that assessed day-to-day variability of blood pressure and heart rate as a novel predictor of cardiovascular mortality in humans proposed that at least 10 blood pressure measurements taken on 10 different days are necessary to provide a reliable SD of blood pressure (Kikuya et al., 2008). Therefore, the SD of blood pressure measurements taken on various days throughout the four-week dietary period was calculated; 11 different blood pressure measurements were used in total (see Appendix C). A HS diet significantly elevated BPV in both WT and *Shroom3*$^{+/Gt}$ mice compared to WT mice on a NS diet (WT $p=0.0482$, *Shroom3*$^{+/Gt}$ $p<0.0001$; Figure 3.9). However, this increase in BPV associated with a HS diet was significantly higher in *Shroom3*$^{+/Gt}$ mice compared to WT mice ($p<0.0001$). Furthermore, *Shroom3*$^{+/Gt}$ mice also had significantly higher BPV compared to *Shroom3*$^{+/Gt}$ mice on a NS diet, indicating that this increase in BPV was dependent on increased dietary sodium ($p<0.0001$). These results strongly suggest that loss of *Shroom3* is associated with alterations in blood pressure leading to greater blood pressure variability in the presence of a sodium insult.

3.2 A short-term high-salt diet does not promote renal injury in *Shroom3*$^{+/Gt}$ mice

High dietary sodium plays a central role in the pathophysiology of chronic kidney disease. In order to determine whether a high-salt diet promotes renal injury in Shroom3

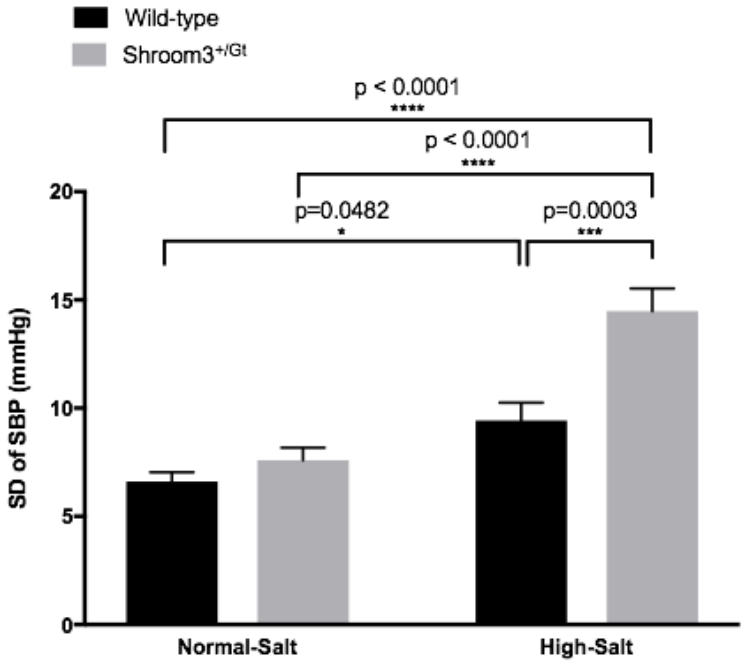

Figure 3.9 Loss of *Shroom3* leads to elevated blood pressure variability on a high-salt diet. The standard deviation of SBP is an established index of blood pressure variability. SD was calculated from the average SBP value of measurements taken at week 1, 2, 3, and 4 of the dietary treatment period. When placed on a HS diet, WT and *Shroom3*$^{+/Gt}$ mice exhibit significantly higher blood pressure variability compared to WT mice on a NS diet, but this increase in BPV caused by the HS diet is significantly higher in *Shroom3*$^{+/Gt}$ mice (*p<0.05, ***p<0.001, ****p<0.0001, two-way ANOVA with Tukey's post-hoc test). Data expressed as mean ± SEM; n= 7-11 for NS groups and n= 9-16 for HS groups.

deficient mice, kidneys were assessed by histology directly following the end of the dietary treatment period. Staining of kidneys with H&E revealed no overt signs of kidney damage in high-salt treated *Shroom3*$^{+/Gt}$ mice compared to high-salt treated WT mice, including no glomerulosclerosis, glomerular cysts, tubular atrophy, or increased glomerular size (Figure 3.10). Additional staining with Masson's Trichrome for assessment of tissue fibrosis also revealed no differences in the level of fibrotic injury between *Shroom3*$^{+/Gt}$ mice and WT mice on a HS diet (Figure 3.10). No gross markers of kidney damage were seen across any experimental groups. Kidneys were further blindly examined by a renal pathologist (Dr. Aaron Haig, University Hospital, London, ON) who confirmed the absence of kidney damage.

3.3 Effects of *Shroom3* loss under prolonged exposure to high dietary salt intake

3.3.1 Blood Pressure

While the HS diet was not expected to promote kidney damage in WT mice, the absence of renal damage seen in *Shroom3*$^{+/Gt}$ mice was surprising as these mice have been previously shown to exhibit glomerulosclerosis at one year of age (Khalili et al., 2016). However, the mice in this study were younger than one year at the start of the experimental period (5-7 months), therefore I sought to determine whether extending the salt loading period from 4 weeks to 14 weeks would produce a kidney phenotype. At the time of my decision to extend the dietary period to 14 weeks, my second independent experiment was just nearing the end of cessation, thus these mice were kept on the diet for an additional 10 weeks. However, my n-value for *Shroom3*$^{+/Gt}$ mice on a NS diet was insufficient to allow for statistical comparison (n=2) with *Shroom3*$^{+/Gt}$ mice on a HS diet. Thus, statistical analyses for my long-term study was carried out between *Shroom3*$^{+/Gt}$ mice on a HS diet and WT mice on a NS and HS diet.

Continuation of the HS diet led to a further reduction in SBP in *Shroom3*$^{+/Gt}$ mice, with significant differences in SBP seen between *Shroom3*$^{+/Gt}$ mice and WT on a HS diet at week 8 ($p=0.0168$; Figure 3.11D,E) at week 8 and with WT NS mice at weeks 7 and 8

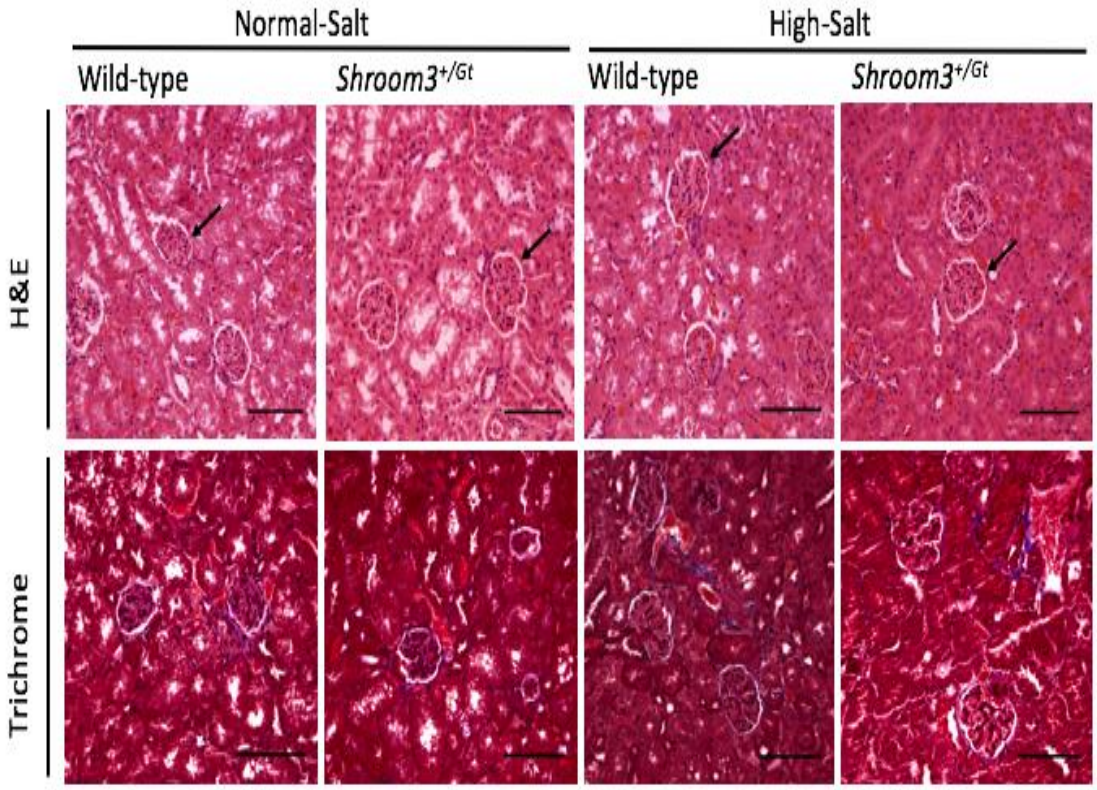

Figure 3.10 Histological assessment of kidneys from WT and *Shroom3*$^{+/Gt}$ mice on a short-term high-salt diet. Representative images of kidney sections stained with H&E (top panel) and Masson's Trichrome (bottom panel). Kidneys were extracted from mice after the cessation of the four-week dietary period and examined for markers of kidney damage. No signs of kidney damage were seen in any of the experimental groups. Black arrows in top panel indicate glomeruli that appear to be healthy; no dilation of Bowman's capsule (associated with cystic glomeruli), enlarged glomerular area, or scarring was observed. Staining with Masson's Trichrome revealed no increase in collagen deposition, which would be indicated by blue colouring. Findings were confirmed by a renal pathologist who did not observe any signs of injury in the experimental groups. n= 2-4 for NS groups and n= 4-6 for HS groups. Black scale bars = 100 μm.

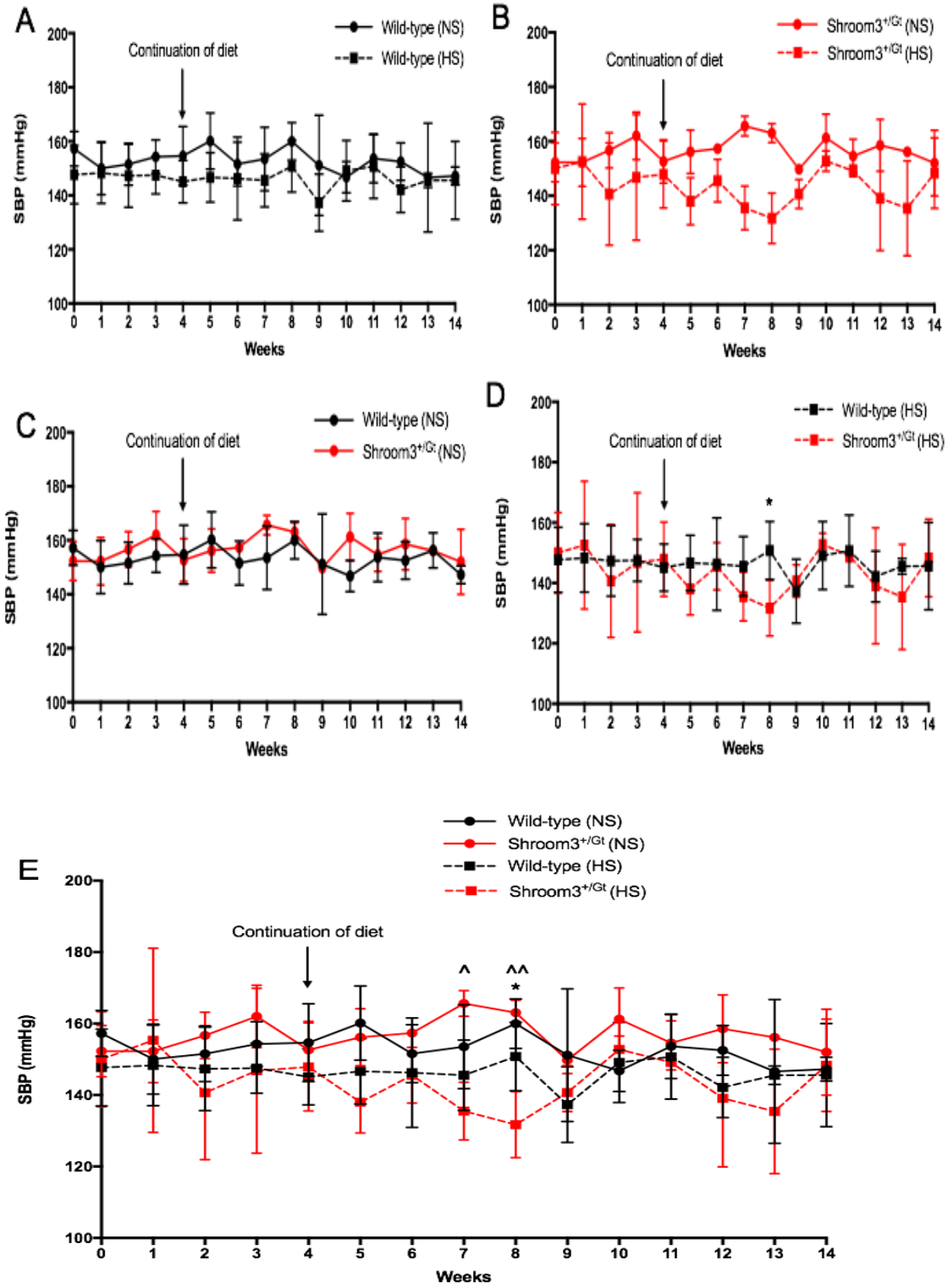
A
Wild-type (NS)
Wild-type (HS)
Continuation of diet
SBP (mmHg)
Weeks
B
Shroom3+/Gt (NS)
Shroom3+/Gt (HS)
Continuation of diet
SBP (mmHg)
Weeks
C
Wild-type (NS)
Shroom3+/Gt (NS)
Continuation of diet
SBP (mmHg)
Weeks
D
Wild-type (HS)
Shroom3+/Gt (HS)
Continuation of diet
*
SBP (mmHg)
Weeks
E
Wild-type (NS)
Shroom3+/Gt (NS)
Wild-type (HS)
Shroom3+/Gt (HS)
Continuation of diet
^
^^
*
SBP (mmHg)
Weeks

Figure 3.11 Effects of a long-term high-salt diet and *Shroom3* loss on systolic blood pressure. Time-course of SBP from baseline (week 0) to the end of the prolonged treatment period (week 14) for WT (A) and *Shroom3*$^{+/Gt}$ (B) mice on a NS and HS diet, as well as a time-course of SBP of WT and *Shroom3*$^{+/Gt}$ mice on a NS (C) and HS (D) diet. Measurements were taken at weekly time points after the continuation of the dietary period using the tail-cuff blood pressure system. A summary of all four groups is shown in (E). SBP was significantly lower in *Shroom3*$^{+/Gt}$ mice on a HS diet compared to WT mice on the same diet and WT mice on a NS diet at week 8 (*p=0.0168 vs. WT-HS, ^^p=0.0023 vs. WT-NS) and compared to WT mice on a NS diet at week 7 (^p=0.0167); statistical analysis between groups was conducted using one-way ANOVA with Tukey's post-hoc test. Statistical comparisons to *Shroom3*$^{+/Gt}$ mice on a NS diet could not be conducted due to low n-value (n=2). Data expressed as mean ± SD; n= 4 for WT-NS and n=4-6 for HS groups.

(week 7 p=0.0167, week 8 p=0.0023; Figure 3.11E). However, those differences were not maintained in later weeks. Furthermore, blood pressure variability remained significantly higher in *Shroom3*$^{+/Gt}$ mice compared to WT mice upon prolonged exposure to increased dietary sodium intake (p=0.0155 vs. WT HS, p=0.0098 vs. WT NS; Figure 3.12).

3.3.2 Urinalysis

To assess kidney function in mice on a long-term HS diet, random spot urine was collected from mice and analyzed for urinary protein and creatinine levels at 14 weeks from the start of the treatment period. No significant difference in urinary protein to creatinine ratio (UPCR) was found between *Shroom3*$^{+/Gt}$ mice on a HS diet and WT mice on a HS and NS diet (Figure 3.13A). *Shroom3*$^{+/Gt}$ mice on a NS diet exhibited the highest UPCR, although the n-value did not allow for analysis of statistical significance. When looking at independent values for total urinary protein and creatinine levels, a HS diet resulted in significantly decreased urinary creatinine and protein levels in both WT (creatinine p=0.0001, protein p=0.0001) and *Shroom3*$^{+/Gt}$ mice compared to WT mice on a NS diet (creatinine p=0.0001, protein p=0.0001; Figure 3.13B,C). Concomitant with these results, I noted that a HS diet caused more frequent urination and consequently increased water intake in both WT and *Shroom3*$^{+/Gt}$ mice. This was evidenced by extreme dampening of cage bedding that needed to be changed almost daily as well as frequent replenishment of drinking water. These observations might also explain the decrease in blood pressure observed in some HS mice as increased urine production would be accompanied by a decrease in fluid volume and thus blood pressure. In addition, although statistical comparisons could not be made, *Shroom3*$^{+/Gt}$ mice on a NS diet exhibited the highest UPCR and total urinary protein levels, which is consistent with previous studies that showed loss of *Shroom3* caused increased proteinuria in mice at one year of age (Khalili et al., 2016). Taken together, these findings suggest that a HS diet decreases urinary protein and creatinine levels, that is likely an outcome of the increased water intake and urinary output due to salt loading.

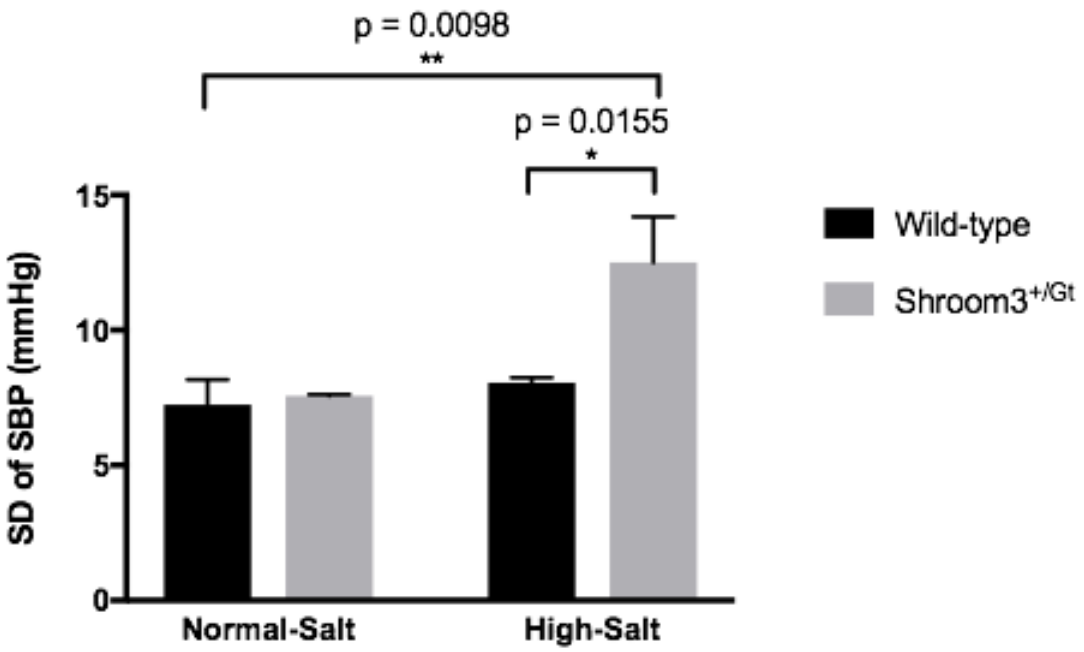

Figure 3.12 Loss of *Shroom3* leads to sustained increases in blood pressure variability on a prolonged high-salt diet. The SD of the average SBP value calculated from measurements taken weekly throughout the 14-week period of the dietary treatment was calculated. When placed on a long-term HS diet, *Shroom3*$^{+/}$Gt mice exhibit a sustained elevation in pressure variability compared to WT mice on the same diet and WT mice on a NS diet (*p=0.0155 vs. WT-HS, ***p=0.004 vs. WT-NS, one-way ANOVA with Tukey's post-hoc test). Statistical comparisons to *Shroom3*$^{+/Gt}$ mice on a NS diet could not be conducted due to low n-value (n=2). Data expressed as mean ± SD; n= 4 for WT-NS and n=4-6 for HS groups.

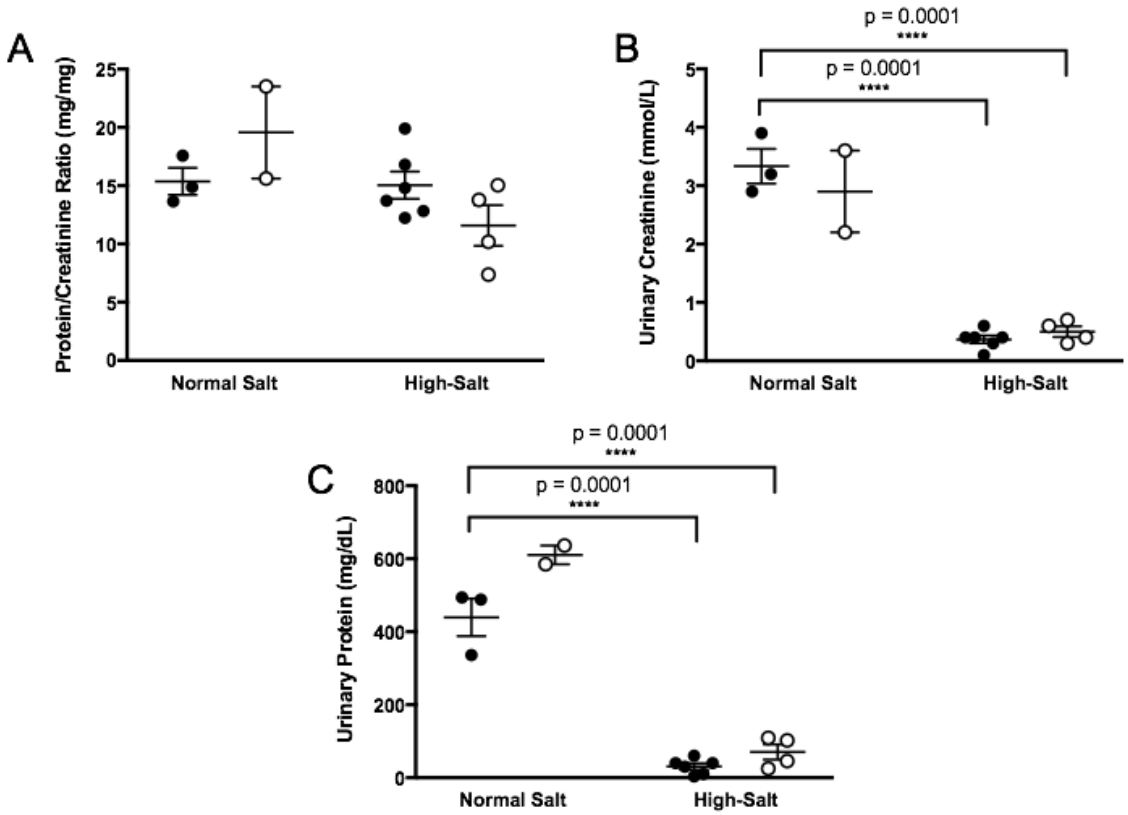

Figure 3.13 A high-salt diet decreases urinary protein and creatinine. Random spot urine was collected from WT and *Shroom3*$^{+/Gt}$ mice on a NS diet and HS diet for urinalysis to measure the levels of urinary protein/creatinine ratio (A), creatinine (B), and protein (C). A high-salt diet causes a significant reduction in the level of urinary protein and creatinine in both WT and *Shroom3*$^{+/Gt}$ mice compared to WT mice on a NS diet (****p=0.0001, one-way ANOVA with Dunnett's multiple comparisons test). Statistical comparisons to *Shroom3*$^{+/Gt}$ mice on a NS diet could not be conducted due to low n-value (n=2). One outlier was removed from the WT-NS group as the value was triple that of the others in the group. Data expressed as mean ± SD; n= 3 for WT-NS and n=4-6 for HS groups.

3.3.3 Loss of *Shroom3* promotes cardiac hypertrophy on a long-term high-salt diet

Long-term BPV sustained past a period of 4 weeks induces cardiac hypertrophy in rats that have undergone sinoaortic denervation, a surgical procedure that consists of sectioning the baroreceptors within the aortic nerve, thereby inducing cardiac and pulmonary remodeling; the procedure is used to model blood pressure variability (Guyenet, 2006). In the present study, a long-term high-salt diet was found to cause increased heart weight to body weight ratios in *Shroom3*$^{+/Gt}$ mice compared to WT mice on a long-term normal-salt diet (p=0.0111; Fig 3.14), suggesting that loss of *Shroom3* may promote cardiac remodeling resulting in cardiac hypertrophy.

3.3.4 Evaluation of renal injury

In order to determine whether prolonged exposure to increased dietary sodium could promote renal damage in *Shroom3*$^{+/Gt}$ mice, kidneys were again subject to histological analysis. Assessment of kidneys by H&E staining revealed no overt signs of kidney disease across experimental groups, similar to the findings of the short-term HS diet (Figure 3.14). H&E slides were blindly examined by the same pathologist (Dr. Aaron Haig, University Hospital, London, ON) who also did not see any gross signs of kidney injury. Staining with Masson's Trichrome for fibrotic injury, however, did suggest an increase in fibrosis in *Shroom3*$^{+/Gt}$ mice on a HS diet. Specifically, I observed an increase in collagen deposition in the tubular interstitium of *Shroom3*$^{+/Gt}$ mice on a HS diet (Figure 3.15). However, the absence of glomerular injury assessed by H&E staining might suggest that the increase in collagen deposition in the tubular interstitium may be in its early stages and has not yet pervaded the glomeruli. These results suggest that loss of *Shroom3* does not increase susceptibility to kidney damage during short-term exposure to a high-salt diet, but may potentially increase susceptibility to kidney damage, specifically fibrotic injury, during long-term exposure to a high-salt. However, additional experiments are needed in order to quantify the potential increase in tubulointerstitial fibrosis.

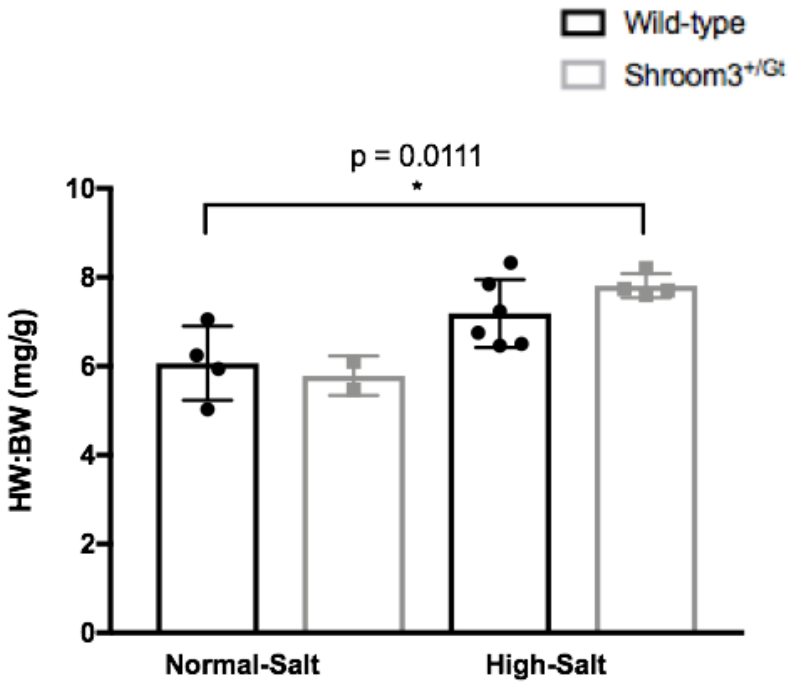

Figure 3.14 Loss of *Shroom3* increases heart weight to body weight ratio on a long-term high-salt diet. The ratio of heart weight to body weight in wild-type and *Shroom3*$^{+/Gt}$ mice fed either a normal-salt or high-salt diet over a long-term 14-week period. When placed on a long-term HS diet, *Shroom3*$^{+/}$Gt mice display a higher heart to body weight ratio, indicative of cardiac hypertrophy, compared to WT mice on a NS diet (*p=0.0111, one-way ANOVA with Tukey's post-hoc test). Statistical comparisons to *Shroom3*$^{+/Gt}$ mice on a NS diet could not be conducted due to low n-value (n=2). Data expressed as mean ± SEM; n= 4 for WT-NS and n=4-6 for HS groups.

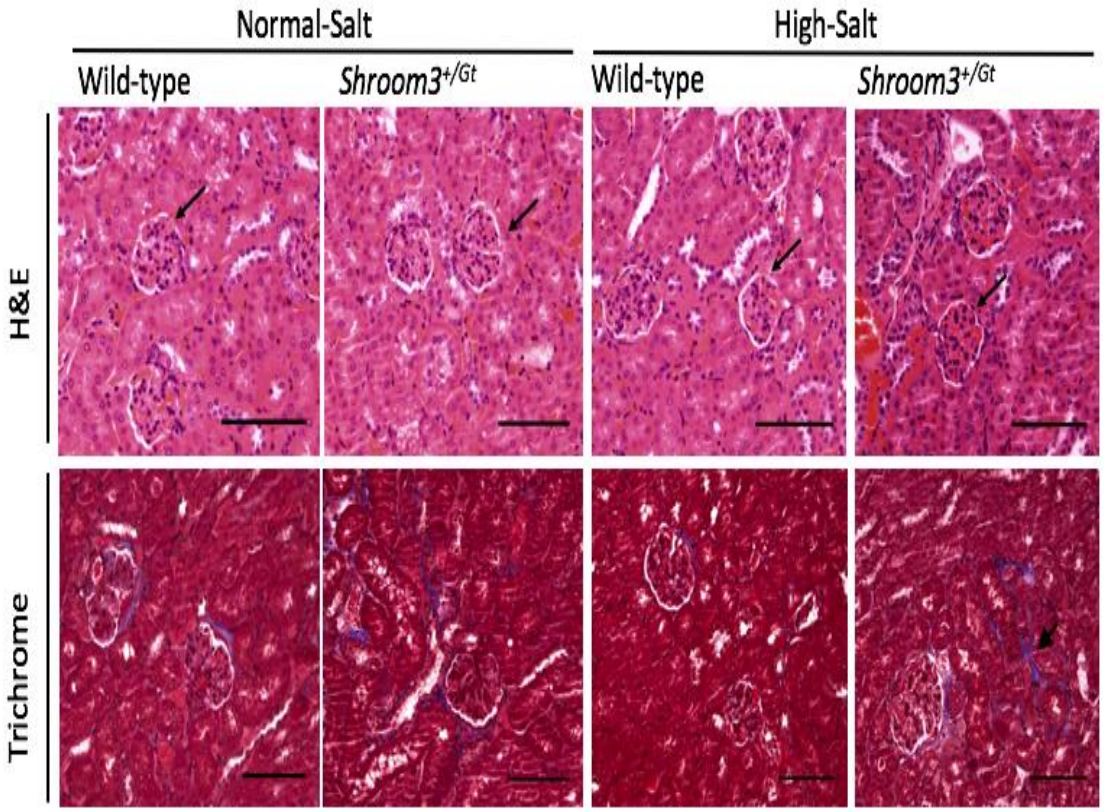

Figure 3.15 Histological assessment of kidneys from WT and *Shroom3*$^{+/Gt}$ mice on a long-term high-salt diet. Representative images of kidney sections stained with H&E (top panel) and Masson's Trichrome (bottom panel). Kidneys were extracted from mice after the cessation of the 14-week dietary period and examined for markers of kidney damage. Staining with H&E revealed no gross pathological markers of glomerular injury in *Shroom3*$^{+/}$Gt mice (black arrow). Staining with Masson's Trichrome revealed an increase in collagen deposition in *Shroom3*$^{+/}$Gt mice, with an increased deposition in the HS group. Arrowhead indicates the presence of fibrotic tissue in the tubular interstitium as seen by the area in blue. N=4 (WT-NS), n=2 (*Shroom3*$^{+/}$Gt-NS), n=6 (WT-HS), n=4 (*Shroom3*$^{+/}$Gt -HS). Black scale bars = 100 μm.

3.4 Functional assessment of human *SHROOM3* variants

The *in vitro* aspect of this thesis focussed on analyzing if there are functional deficits in the ability of known *SHROOM3* variants identified by the NHLBI to cause apical constriction. As described in *1.4.*1, previous studies have suggested that human *SHROOM3* variants within the population may have functional consequences. Out of the hundreds of *SHROOM3* variants identified by the NHLBI, several were predicted to be probably damaging based on PolyPhen-2 analysis. From this dataset of *SHROOM3* variants predicted to be probably damaging, our lab previously compiled a list of variants of interest based on the following criteria: they occur in the coding region of *SHROOM3* and they have been identified more than 5 times in the alleles sequenced to date (see Appendix D); four variants have substitutions in one of Shroom3's known domain locations. Whether these variants exhibit impaired function remains unknown, although two of them have already been associated with heterotaxy (Tariq et al., 2011). Thus, to assess the functional consequences of these variants, I used an established assay to test for the ability of Shroom3 to drive apical constriction in transfected MDCK epithelial cells. The variants were generated using a bicistronic vector that also expresses GFP, for 3 of the 4 variants that occur in a known domain location, and subsequently examined their ability to drive apical constriction was tested. Prior to transfection, all of the expression vectors were verified by sequencing to confirm that the expected mutation substitution occurred (see Appendix E).

Transfection of MDCK cells with each of the three *SHROOM3* variants resulted in markedly reduced apical constriction compared to cells transfected with WT *SHROOM3*, with apical surface areas comparable to those of control cells transfected with GFP alone (Figure 3.15A). To quantify the degree of apical constriction, the apical surface defined by ZO-1 was traced and measured for transfected cells as well as neighboring untransfected cells (see Appendix F). As expected, the apical surface area of cells transfected with WT *SHROOM3* was significantly decreased compared to the apical surface area of neighboring untransfected cells ($p<0.0001$; Figure 3.15C). The apical surface area of MDCK cells transfected with the *SHROOM3* variants G60V, T1012N, and G1864D was not significantly reduced compared to untransfected neighboring cells,

indicating that these variants have reduced ability to drive apical constriction. Interestingly, the apical surface area of MDCK cells transfected with the GFP control or the G1864D *SHROOM3* variant was found to be significantly larger than neighboring, untransfected cells, perhaps due to the nature of the transfection itself. Moreover, the apical surface area of cells expressing WT *SHROOM3* was significantly smaller than cells transfected with G60V (p=0.003), T1012N (p=0.0001), or 1864D (p=0.0001), indicating that the *SHROOM3* variants have abrogated apical constriction ability (Figure 3.16B). There was no significant difference in the apical surface area of cells transfected with a variant compared to those transfected with GFP alone (G60V p=0.0621, T1012N p=0.4941, G1864D p=0.9026). These results suggest that three of the *SHROOM3* variants identified by the NHLBI with substitutions in known domain locations and that are predicted to be damaging have impaired cellular function with respect to their ability to drive apical constriction.

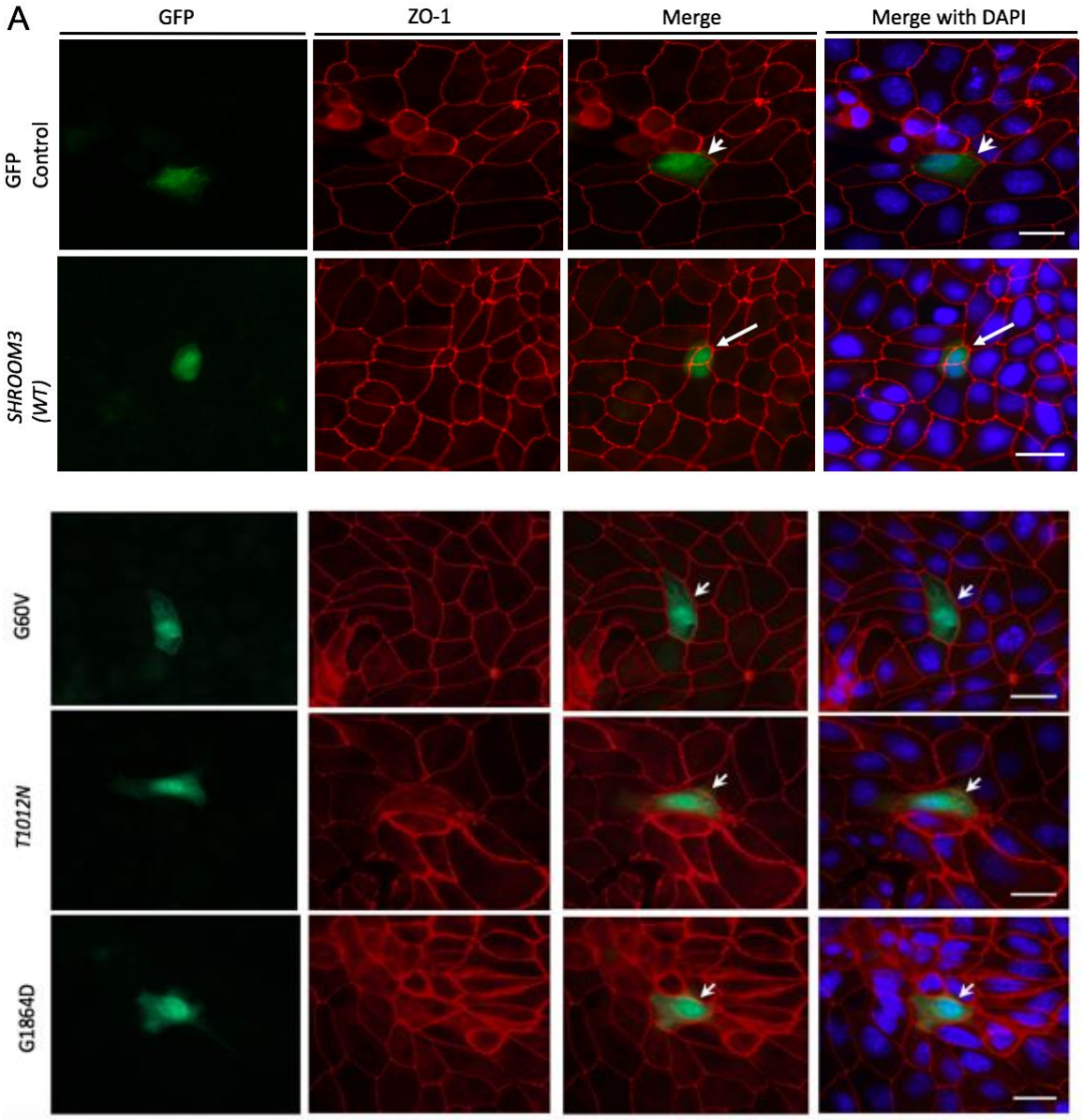
A
GFP
ZO-1
Merge
Merge with DAPI
GFP Control
SHROOM3 (WT)
G60V
T1012N
G1864D

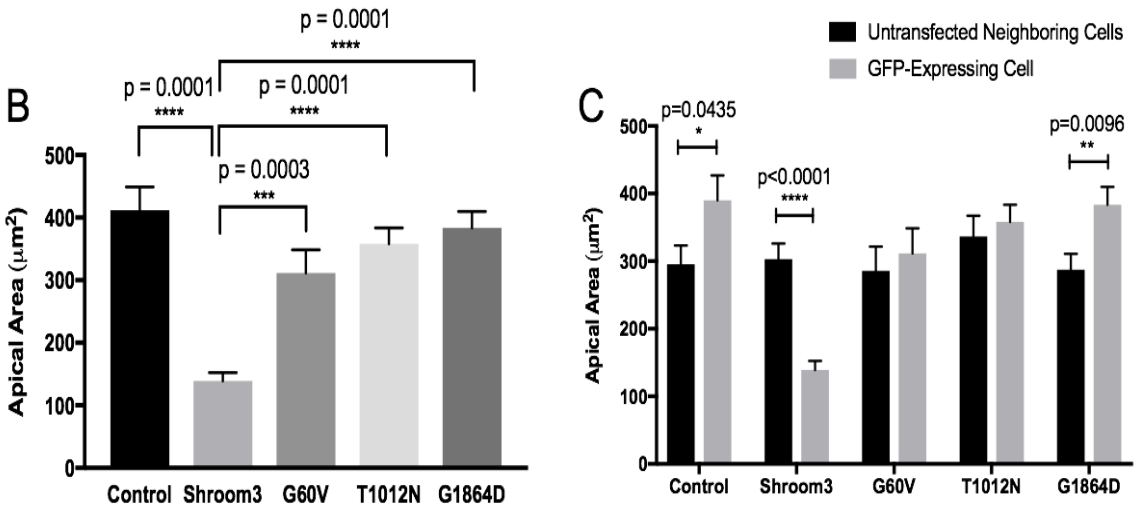

Figure 3.16 Human variants of *SHROOM3* have attenuated ability to drive apical constriction. Representative fluorescence images of ZO-1 (red) and GFP (green) labelled MDCK cells transfected with either an empty GFP plasmid (top panel), WT *SHROOM3* (second panel), or the indicated plasmids carrying one of the *SHROOM3* variants (bottom three panels) (A). Transfected cells were visualized by GFP (left panel), apical cell-cell boundaries were visualized by staining with ZO-1 antibody (middle panels), and nuclei of cells were marked with DAPI (right panel). MDCK cells transfected with a GFP plasmid alone display no decrease in cellular area (white arrowhead), while cells transfected with WT *SHROOM3* display a marked decrease in cellular area, indicating apical constriction (white arrow). Transfection of MDCK cells with the *SHROOM3* variants resulted in cells of similar size to those transfected with GFP alone and of greater size compared to those transfected with WT *SHROOM3*, indicating reduced apical constriction ability. To quantify apical constriction, the apical area of transfected cells outlined by ZO-1 was traced and measured using ImageJ. Differences in apical constriction ability between groups was analyzed by comparing the apical area of transfected cells (B) and comparing transfected cells with neighboring untransfected cells within groups (C). All three of the *SHROOM3* variants analyzed had significantly increased apical area compared to WT *SHROOM3* (****p=0.0001, one-way ANOVA with Tukey's post-hoc test) and were not found with decreased apical areas in comparison to untransfected neighboring cells (unpaired t-test). White scale bar = 50 µm, n=23-25 cells analyzed from at least three independent experiments.

Chapter 4

4 Discussion

4.1 Overview

The interplay between genetics and the environment is central to the development of complex human diseases. Recent studies, including previous work conducted in our lab, have demonstrated an important role for Shroom3 in both the developing and mature kidney, lending functional support for the GWAS that have strongly associated *SHROOM3* with CKD (Khalili et al., 2016; Yeo et al., 2015). At the same time, the emergence of evidence linking human variants of *SHROOM3* to disorders including heterotaxy and diseases of the nervous system have necessitated the need to further explore and characterize the functional changes associated with these potentially damaging variants (Ganief et al., 2017; Tariq et al., 2011). In this thesis, I sought to investigate the potential consequences of alterations in the expression and sequence of *SHROOM3* using an *in vivo* and *in vitro* model, respectively. Here, I demonstrate that loss of *Shroom3* may increase the salt sensitivity of blood pressure and that rare human variants of *SHROOM3* have abrogated cellular function.

4.2 Loss of *Shroom3* elevates blood pressure variability but not hypertension in the presence of a sodium insult

Our lab has previously shown that loss of *Shroom3* during development leads to glomerular defects in mice attributed to reduced glomerular number and podocyte foot process effacement that are manifested by adult onset proteinuria and glomerulosclerosis (Khalili et al., 2016). As described in Chapter 1, the kidney plays an essential role in the regulation of blood pressure and impaired renal sodium excretion leads to an increase in systemic blood pressure. Previous studies have shown that under high dietary salt conditions, knockdown or knockout of genes implicated in kidney function are associated with the development of hypertension and concomitant renal injury (Daumerie et al., 2010; Schlote et al., 2013; Ye et al., 2006). Conversely, in the present study, a high-salt diet was not found to cause hypertension in *Shroom3* deficient mice (Figure 3.6).

However, loss of *Shroom3* was associated with greater fluctuations in blood pressure under high-salt conditions (Figure 3.7). This was evidenced by both a greater change in systolic blood pressure throughout the dietary period when compared to baseline, with both positive and negative changes taken into the same consideration, as well as significantly elevated blood pressure variability in *Shroom3*$^{+/Gt}$ mice on a HS diet (Figure 3.8 & 3.9).

Both long-term and short-term blood pressure variability are quickly emerging as important risk factors for cardiovascular disease and all-cause mortality, independent of mean blood pressure (Dolan & O'Brien, 2010; Mancia, 2012; Parati et al., 2013; Rothwell et al., 2010; Stevens et al., 2016; Suchy-Dicey et al., 2013). Traditional approaches for quantifying short-term 24 hour BPV in mice have involved power spectral analysis of SBP using surgically implanted telemetry devices (Desjardins et al., 2008; Farah et al., 2004; Stauss et al., 1999). However, as this procedure was outside the scope of this thesis, the standard deviation of SBP was used as an index for BPV. The SD of SBP is an established index for BPV in humans. Here, I found that a HS diet generally caused a greater variability in SBP, and this variability was significantly exacerbated by loss of *Shroom3.* The increased BPV observed in WT mice on a HS diet is consistent with a previous study that showed a HS diet elevated BPV in normotensive, salt-resistant rats through the sodium-induced enhancement of sympathetic nerve activity, without increasing the mean BP (Simmonds et al., 2014). Importantly, the increased BPV seen in *Shroom3*$^{+/Gt}$ mice suggests that loss of *Shroom3* attenuates the ability of blood pressure to autoregulate when challenged with increased dietary sodium.

The observation that a high-salt diet does not cause hypertension in *Shroom3*$^{+/Gt}$ mice are complemented by our histological analyses, which revealed that *Shroom3*$^{+/Gt}$ mice on a HS diet do not exhibit any hallmarks of kidney damage, including glomerular and fibrotic injury, in comparison to WT controls on a NS diet (Figure 3.10). Sustained elevations in systemic blood pressure propagate kidney damage by increasing glomerular capillary pressure, which induces glomerular hypertrophy and consequent podocyte foot process effacement, eventually culminating into glomerulosclerosis (Endlich & Endlich, 2012; Kretzler et al., 1994). As podocyte morphology was not examined in this thesis, it cannot

be excluded that a HS diet did not induce podocyte injury in *Shroom3*$^{+/Gt}$ mice. However, the lack of overt glomerular injury observed in these mice would suggest that if the HS diet did induce such podocyte injury, it had not progressed to a stage capable of transmitting the injury at the level of the glomerulus.

The renin-angiotensin system (RAS) and the type I angiotensin receptor (AT1) have been established as key contributors in the development of essential hypertension, primarily through their actions in the kidney (Crowley et al., 2006). Aberrant activation of the RAS has been directly linked to hypertension and cardiovascular morbidity through the stimulation of angiotensin II (Ang II) activity, with KO of AT1 receptors in the kidney being sufficient to ameliorate Ang II-dependent hypertension (Crowley et al., 2006; Lonn et al., 1994). This provides the basis for the administration of angiotensin-converting-enzymes (ACEs) and angiotensin receptor blockers for the reduction of blood pressure in patients with hypertension and kidney disease (NHLBI, 2004). Importantly, a unifying common pathway for the onset of salt-sensitive hypertension seems to implicate a critical role for Ang II activity in the kidney, as high intrarenal Ang II levels contribute to increased sodium and water retention (Kobori et al., 2007). This is directly evidenced by the Dahl salt-sensitive (DS) rat model, in which a high-salt diet augments intrarenal angiotensinogen levels in DS rats and contributes to impaired renal sodium excretion and consequent systemic hypertension (Kobori et al., 2003). This also explains why numerous past studies that have used a high-salt model for hypertension have coupled the high-salt diet with simultaneous administration of Ang II in order to induce hypertension in non salt-sensitive animals (Chen et al., 2010; Crowley et al., 2011; Lee et al., 2012; Manhiani et al., 2015; Singh et al., 2009; Wang et al., 2015). In many of these studies, a high-salt diet alone was either not sufficient to induce hypertension in the absence of Ang II infusion or salt-dependent hypertension was exacerbated upon Ang II administration (Lee et al., 2006; Manhiani et al., 2015; Singh et al., 2009). Therefore, while a high-salt diet was not sufficient to induce hypertension in *Shroom3*$^{+/Gt}$, it may be the case that salt-sensitive hypertension in *Shroom3*$^{+/Gt}$ mice critically depends on activation of the RAS in the kidney. Thus, an evident focus of future studies should be on determining whether *Shroom3*$^{+/Gt}$ mice develop salt-sensitive hypertension upon Ang II infusion. Although an alternative possibility would appear to be that hypertension in *Shroom3*$^{+/Gt}$ mice is simply

not salt-sensitive, the increased blood pressure variability in *Shroom3*$^{+/Gt}$ mice brought on by a high-salt diet would suggest that their blood pressure response is in fact salt-sensitive.

In keeping with the importance of using a model that includes Ang II administration, a study on DSS rats found that treatment with a HS diet for four weeks led to significant hypertension, proteinuria, glomerulosclerosis, and tubulointerstitial fibrosis (Rafiq et al., 2014). Subsequent administration of hydralazine (HYD), which mimics the effects of dietary sodium restriction, was found to ameliorate hypertension but not renal histopathologies. However, treatment with HYD in combination with Angiotensin II typ 1 receptor blocker and a calcium channel blocker that is known to enhance the protective effects of ARBs was found to elicit strong renoprotective effects that regressed renal injuries induced by a HS diet (Rafiq et al., 2014). This suggests that fibrotic damage caused by salt-sensitive hypertension critically depends on the activity of Ang II as dietary salt restriction by itself was not sufficient to reverse renal injury. Thus, Ang-II infusion may not only be valuable for studying salt-sensitive hypertension, but also for assessing salt-sensitive kidney damage.

4.3 Potential long-term effects of *Shroom3* loss upon prolonged exposure to a high-salt diet

Age is another established risk factor for both the development of hypertension as well as CKD (National Kidney Foundation, 2002; NHLBI, 2004). In particular, CKD is a disease of the elderly rather than the young as kidney function progressively declines with age (Levey & Coresh, 2012). The previous finding in our lab that loss of *Shroom3* leads to glomerulosclerosis and proteinuria in adult mice was dependent on age. Specifically, these functional consequences were not observed in mice at 3 months of age, but rather at one year of age (Khalili et al., 2016). The absence of both hypertension and renal injury in the *Shroom3*$^{+/Gt}$ mice used in my study may be an outcome of their younger age, as they were between the ages of 5-7 months at the start of the experimental period. Additionally, previous studies that have used a high-salt diet model for hypertension maintained animals on the diet for extended periods upwards of four weeks (Bertorello et al., 2015; Laverman et al., 2003; R. E. Schmieder et al., 1988; Vasdev et al., 2006).

Extending the period of dietary salt-loading has been shown to exacerbate hypertension, proteinuria, and renal injury in DS rats (Rafiq et al., 2014). Additionally, in Sprague-Dawley rats, a long-term HS diet of 8 weeks was found to result in hypertension, proteinuria, and renal injury, while a short-term 4 week HS diet had no such consequences (Gu et al., 2008). While the effects of a long-term HS diet have been well-established in rat models, less is known about the effects of extended salt loading in mice (Van Vliet & Montani, 2008). In the present study, extending the salt loading period to 14 weeks did not induce hypertension in *Shroom3*$^{+/Gt}$ mice (Figure 3.11). However, a significant finding was that BPV was maintained throughout the prolonged dietary period (Figure 3.12).

A critical outcome of increased long-term BPV is increased end organ damage (Höcht, 2013). Assessment of heart and body weight of mice in my current study demonstrated that loss of *Shroom3* is associated with cardiac hypertrophy under long-term high-salt conditions (Figure 3.14). Blood pressure variability can be experimentally induced without sustained hypertension through sinoaortic denervation (SAD) (Miao et al., 2003). In sinoaortic denervated rats, a chronic increase in BPV results in myocardial damage (Su & Miao, 2001). At 16 weeks post-surgical denervation, cardiomyocyte swelling was observed and at 32 weeks post-surgical denervation, SAD rats were found with interstitial fibrosis in the myocardium (Su & Miao, 2001). SAD rats also have overt symptoms of kidney damage, with thickening of the Bowman's capsule being visible 8 weeks, interstitial fibrosis visible at 16 weeks, and severe glomerular lesions and glomerular collapse visible at 32 weeks post-surgical denervation (Su & Miao, 2001). Importantly, the organ damage observed in SAD rats was directly caused by a high BPV, independent of high BP; chronic SAD in rats causes a significant increase in BPV but no change in the 24-hour BP average. Therefore, BPV is a risk factor for organ damage independent of the presence of hypertension (Su & Miao, 2001). Moreover, in rat models, a high-salt diet (8%) induces cardiac hypertrophy through a blood pressure-independent mechanism (Ferreira et al., 2010; Radin et al., 2008). This suggests that the cardiac hypertrophy observed in *Shroom3*$^{+/Gt}$ mice on a long-term HS diet may be a myocardial outcome of their sustained elevation in long-term BPV.

A potential link between *Shroom3* and cardiac function is strengthened by previous work in our lab that has revealed that *Shroom3* is expressed throughout the myocardium during cardiogenesis and that loss of *Shroom3* results in cardiac defects in embryonic mice. Furthermore, another significant finding in the present study was the observation that DBP in *Shroom3*$^{+/Gt}$ mice was significantly reduced on a short-term HS diet. This decrease was not seen in WT mice on a HS diet or *Shroom3*$^{+/Gt}$ mice on a NS diet, indicating that the reduction in DBP in HS-*Shroom3*$^{+/Gt}$ mice was dependent on loss of *Shroom3* in the presence of increased dietary sodium intake (Figure 3.4). Recently, a large observational study conducted on the Atherosclerosis Risk In Communities cohort found that a low DBP was strongly associated with myocardial damage and coronary heart disease (McEvoy et al., 2016). Similarly, a separate study has also strongly associated isolated diastolic hypotension with incident heart failure in older adults (Guichard et al., 2011). Therefore, the changes in blood pressure observed in response to a HS diet in *Shroom3*$^{+/Gt}$ mice could be due to an underlying cardiac phenotype rather than one associated with the kidney.

Examination of the functional effects of *Shroom3* loss on the kidney under long-term high-salt conditions revealed that HS *Shroom3*$^{+/Gt}$ mice displayed significantly lower urinary protein and creatinine levels, corresponding to a decrease, although not significant, in the urinary protein to creatinine ratio, compared to WT mice on a NS diet and WT mice on a HS diet (Figure 3.13). A UPCR is used as an index for proteinuria for random spot urine samples. However, I wanted to separately examine the total urinary protein and creatinine levels because I noticed that a HS diet was causing increased water intake and more frequent urination in both WT and *Shroom3*$^{+/Gt}$ mice. Although these two variables were not directly measured, it is clear that they had an impact on urine composition. Low urinary creatinine levels are an indication of an abnormally large consumption of water, thus in the case of mice on a HS diet, a urinalysis may not be an accurate method for assessment of proteinuria. It can therefore not be excluded that *Shroom3*$^{+/Gt}$ mice on a HS diet do not exhibit proteinuria. However, given that proteinuria is an early clinical manifestation of high blood pressure, owing to the leakage of protein into urine due to foot process effacement caused by increased pressure load to

the renal microvasculature, and that *Shroom3*$^{+/Gt}$ mice were not found to be hypertensive, it is most likely the case that these mice were also not proteinuric.

Glomerular hyperfiltration is a phenomenon that occurs in both hypertensive nephropathy as well as diabetic nephropathy, and is proposed to be a pathogenic mechanism of renal injury common to both diseases. It is characterized by the compensatory rise in single-neprhon GFR in response to some form of renal insult. As discussed in Chapter 1, Brenner's hypothesis proposed that this renal insult could be in the form of reduced nephron endowment, inducing hyperfiltration in the remaining glomeruli and ultimately culminating into systemic hypertension and glomerulosclerosis. Importantly, glomerular hyperfiltration has been shown to precede the development of microalbuminuria and thus macroalbuminuria and proteinuria in both stage 1 hypertensive patients as well as type I diabetic patients (Magee et al., 2009; Palatini et al., 2006). Moreover, glomerular hyperfiltration in humans occurs in the earliest stages of hypertension, and is driven by the interactions between Ang II and the sympathetic nervous system in response to a stressor, which can then propagate into persistent hypertension (Schmieder et al., 1997).

Although in the present study I did not observe hypertension in *Shroom3*$^{+/Gt}$ mice placed on a long-term HS diet, it cannot be excluded that the *Shroom3*$^{+/Gt}$ mice were in the earliest stages of hypertension where elevations in blood pressure were not sustained long enough to be detected nor can it be excluded that *Shroom3*$^{+/Gt}$ mice may be more susceptible to hypertension in the presence of an additional stressor such as older age or augmented Ang II levels. Therefore, I propose that future experiments should focus on measuring eGFR, through assessment of serum creatinine levels, rather than proteinuria, in order to determine whether *Shroom3*$^{+/Gt}$ mice on a HS diet exhibit increased eGFR, which would be indicative of a hyperfiltration state. If an abnormally high eGFR is observed in *Shroom3*$^{+/Gt}$ mice on a HS diet, it would provide evidence that these mice may be in the early stages of hypertension. Although glomerular hyperfiltration is also a mechanism present in the early stages of diabetes, increased salt intake in early type I diabetes, unlike salt-dependent hypertension, actually leads to a decrease in eGFR, a phenomenon known as the "salt paradox" (Vallon, 2003). Thus, an abnormally high

eGFR in the presence of increased dietary sodium intake, would most likely point towards the direction of hypertensive rather than diabetic nephropathy.

Alternatively, it is possible that loss of *Shroom3* involves a combination of the pathogenic mechanisms associated with both diabetic nephropathy and hypertension. As mentioned in *1.2.6*, a 2012 GWAS conducted by Köttgen et al. revealed that the association between *SHROOM3* and lower eGFR also corresponded to lower albuminuria. This association was abnormal in comparison to the traditional inverse relationship between eGFR and proteinuria. The authors postulated that this atypical relationship may have two potential explanations: Shroom3 may either be exerting pleiotropic effects or is interacting with mechanisms that substantiate both a higher eGFR and a higher urinary albumin to creatinine ratio, as in the case of glomerular hyperfiltration states present in early diabetes and hypertension. Furthermore, a subsequent GWAS found a strong association between *SHROOM3* and eGFR in type 2 diabetes, and this association was dependent on the presence of albuminuria (Deshmukh et al., 2013). These findings suggest that the presence of a hyperfiltration state in *Shroom3*$^{+/Gt}$ mice on a HS diet is highly likely and further necessitates the need for future experiments to assess eGFR.

Similar to the findings from my short-term HS study, histological analyses revealed that a long-term HS diet of 14 weeks did not induce glomerular injury in *Shroom3* deficient mice (Figure 3.15). However, *Shroom3*$^{+/Gt}$ mice appear to display slightly increased collagen deposition in the interstititium, although my observation was not confirmed by a pathologist. CKD is defined as a progressive disease and overt histopathological as well as functional changes are often not observable in the early stages of CKD (Rysz et al., 2017). The use of biomarkers in the early detection of CKD has thus become an increasingly important area of focus in CKD diagnostic research (Khan & Pandey, 2014; Rysz et al., 2017). Future experiments should be aimed at determining whether *Shroom3*$^{+/Gt}$ mice on a HS diet displayed altered expression of genes implicated in the molecular mechanisms involved in kidney injury using established biomarkers. These biomarkers would be more sensitive to the early detection of CKD, present before CKD is manifested by histopathological and functional changes.

Taken together, my *in vivo* studies have elucidated the potential effects of *Shroom3* loss on blood pressure and the kidney under acute and chronic exposure to increased dietary sodium. Additionally, I suggest a novel approach to studying salt-dependent hypertension in *Shroom3*$^{+/Gt}$ mice that involves augmentation of the renin-angiotensin system as an additional stressor. While salt-sensitive hypertension has been extensively used in rat models, its use in mice is still a relatively emerging field. As alluded to throughout this Discussion, the most apparent limitation present in my *in vivo* work was the establishment of a hypertensive model using a high-salt diet. As C57BL/6 mice are normally not salt-sensitive, the addition of a secondary insult other than salt may be necessary to induce hypertension in these animals. Furthermore, future experiments examining blood pressure variability in *Shroom3*$^{+/Gt}$ mice should use the implantable blood pressure radiotelemetry system for BPV analysis that employs power spectral analysis rather than the tail-cuff system. Due to the tail-cuff system being non-invasive, it requires physical restraint of the animal, and stress-induced blood pressure changes are an inevitable limitation to this method. Although the radiotelemetry method is much more costly and invasive, it would eliminate the unavoidable physiological blood pressure response to stress. Radiotelemetry also allows for continuous 24-hour blood pressure monitoring of conscious animals in their natural environment, providing a more sensitive arterial pressure reading compared to the single-point periodic monitoring of blood pressure by the tail-cuff system (Zhao et al., 2011).

In addition, an important caveat with respect to the present study is that BPV was analyzed within the given experimental groups (or populations) rather than at the individual level. Further assessment would be needed to determine if the BPV of the population reflects the outcomes of increased individual BPV. Lastly, one study assessing the validity of the tail-cuff blood pressure system showed that the tail-cuff method may underestimate DBP, therefore the findings in my study that demonstrated loss of *Shroom3* may result in decreased DBP under high-salt conditions would have to be confirmed using other blood-pressure measurement systems (Feng et al., 2008).

4.4 Altered cellular function of human *SHROOM3* variants

Several human variants of *SHROOM3* that exist within the current population have been identified by the NHLBI and have been predicted to be probably damaging by PolyPhen-2 analysis. Two of these identified *SHROOM3* variants have already been found to be linked to heterotaxy in a separate study (Tariq et al., 2011). Here, I provide the first direct evidence that at least three of the *SHROOM3* variants identified by the NHLBI, two of which are the variants that been linked to heterotaxy in the aforementioned study, have abrogated cellular function. Using an established *in vitro* assay for Shroom3 function in MDCK epithelial cells, I demonstrated that cells transfected with any of the three *SHROOM3* variants have significantly reduced ability to undergo apical constriction, as evidenced by the increased apical area in cells transfected with a *SHROOM3* variant in comparison to cells transfected with wild-type *SHROOM3*.

While previous studies have linked human variants of *SHROOM3* to complex diseases, no studies to date have provided mechanistic evidence that these variants have functional consequences. Importantly, the observation that the two human *SHROOM3* variants associated with heterotaxy in humans have attenuated apical constriction activity provides the first functional link between these variants and the PolyPhen2 prediction that these variants are damaging. A clear aim for future studies would then be to characterize the molecular mechanisms underlying this loss of function observed in the *SHROOM3* variants. Given that the three *SHROOM3* variants here that have been shown to have compromised cellular function have mutations in one of Shroom3's known domain locations, it would be of priority to analyze the interactions between Shroom3 and ROCK1/2 as well as Shroom3 and actin. In particular, ROCK has been found to be required for proper left-right patterning in humans, and it is the absence of proper left-right patterning that causes the disease phenotype in heterotaxy patients (Fakhro et al., 2011; G. Wang et al., 2011). One of the *SHROOM3* variants associated with heterotaxy that was assessed in the present study, G1864D, contains the substitution in the ASD2 domain, which is the domain that directly binds to ROCK. This strongly suggests that the abrogated apical constriction function of this variant is likely due to a perturbation in Shroom3's interaction with ROCK.

4.5 Future Directions and Conclusions

As our current model for *Shroom3* loss involves a global knockdown of *Shroom3*, the inability to delineate between the confounding effects of *Shroom3* loss in the heart and the kidney presents another limitation to our *in vivo* studies. Currently, our lab has been working on generating a conditional knockout of *Shroom3* using a Cre-Lox recombination model, specific to the kidney. This conditional knockout model would circumvent the embryonic lethality associated with complete loss of *Shroom3* as it would still be expressed in the neural tube during development. Through the use of podocyte-specific promoters, or other kidney cell type promoters, conditional knockout of *Shroom3* would help further elucidate its kidney-specific role while eliminating the confounding effects of global *Shroom3* loss. Future studies using this model will be critical in establishing a causative relationship between the podocyte defects associated with loss of *Shroom3* and reduced nephron endowment, as well as differentiating between the pathogenic mechanisms of kidney disease and heart disease.

In summary, the findings presented in this thesis have provided insight into how loss of *Shroom3* or alterations in the sequence of *Shroom3* may confer risk for disease. I have conducted the first experiments aimed at determining whether loss of *Shroom3* increases susceptibility to hypertension, a leading cause and comorbidity of CKD, in the presence of a sodium insult. The increase in the consumption of processed foods observed in the diets of Western societies has made it even more important to determine whether some individuals may be predisposed to the ramifications of increased dietary sodium intake. While the present study showed that partial loss of *Shroom3* did not induce hypertension in mice in the presence of a high-salt diet, loss of *Shroom3* was found to be associated with greater variability in blood pressure in response to a high-salt diet. The implications of these findings are relevant to the pathophysiology of CKD especially when taking into consideration the importance of blood pressure control at all CKD stages. If loss of *Shroom3* augments salt-sensitive blood pressure variability, then individuals that possess compromised Shroom3 function may be at higher risk for end-organ damage under increased dietary sodium conditions. An important preemptive course of action in these individuals would then be reducing salt intake in combination with continuous blood

pressure monitoring. However, further work using more definitive inducers of hypertension in salt-resistant mice, including the established Ang II infusion model for hypertension, will be needed to ascertain the salt-sensitive blood pressure response caused by loss of *Shroom3*. Moreover, overcoming the limitations of the salt-resistant nature of C57BL/6 mice will be necessary in order to determine whether a deficiency in *Shroom3* predisposes individuals to salt-sensitive hypertension.

Through *in vitro* analysis, my work provides the first evidence of the functional consequences of human *SHROOM3* variants that have been predicted to be damaging by the NHLBI, and two of which have been previously associated with heterotaxy in humans. Exploring the underlying molecular mechanisms of these variants will be an important future experiment. Additionally, to determine whether these functional consequences directly translate into human disease traits, analysis will have to be conducted to characterize the effects of these *SHROOM3* variants using *in vivo* models.

References

Adler, P. N., Krasnow, R. E., & Liu, J. (1997). Tissue polarity points from cells that have higher Frizzled levels towards cells that have lower Frizzled levels. *Current Biology*, *7*(12), 940–949. https://doi.org/10.1016/S0960-9822(06)00413-1

Amano, M., Nakayama, M., & Kaibuchi, K. (2010). Rho-kinase/ROCK: A key regulator of the cytoskeleton and cell polarity. *Cytoskeleton*, *67*(9), 545–554. https://doi.org/10.1002/cm.20472

Anstrom, J. A. (1992). Microfilaments, cell shape changes, and the formation of primary mesenchyme in sea urchin embryos. *The Journal of Experimental Zoology*, *264*(3), 312–22. https://doi.org/10.1002/jez.1402640310

Antinori, A., Arendt, G., Becker, J. T., Brew, B. J., Byrd, D. A., Cherner, M., … Wojna, V. E. (2007). Updated research nosology for HIV-associated neurocognitive disorders. *Neurology*, *69*(18), 1789–99. https://doi.org/10.1212/01.WNL.0000287431.88658.8b

Arora, P., Vasa, P., Brenner, D., Iglar, K., McFarlane, P., Morrison, H., & Badawi, A. (2013). Prevalence estimates of chronic kidney disease in Canada: results of a nationally representative survey. *Canadian Medical Association.Journal*, *185*(9), E417--23. https://doi.org/10.1503/cmaj.120833

Asanuma, K., Kim, K., Oh, J., Giardino, L., Chabanis, S., Faul, C., … Mundel, P. (2005). Synaptopodin regulates the actin-bundling activity of alpha-actinin in an isoform-specific manner. *The Journal of Clinical Investigation*, *115*(5), 1188–98. https://doi.org/10.1172/JCI23371

Asanuma, K., Yanagida-Asanuma, E., Faul, C., Tomino, Y., Kim, K., & Mundel, P. (2006). Synaptopodin orchestrates actin organization and cell motility via regulation of RhoA signalling. *Nature Cell Biology*, *8*(5), 485–491. https://doi.org/10.1038/ncb1400

Atwal, J. K., Pinkston-Gosse, J., Syken, J., Stawicki, S., Wu, Y., Shatz, C., & Tessier-Lavigne, M. (2008). PirB is a Functional Receptor for Myelin Inhibitors of Axonal Regeneration. *Science*, *322*(5903), 967–970. https://doi.org/10.1126/science.1161151

Bakris, G. (2005). Proteinuria: a link to understanding changes in vascular compliance? *Hypertension (Dallas, Tex. : 1979)*, *46*(3), 473–4. https://doi.org/10.1161/01.HYP.0000178188.29446.48

Bao, H.-F., Thai, T. L., Yue, Q., Ma, H.-P., Eaton, A. F., Cai, H., … Eaton, D. C. (2014). ENaC activity is increased in isolated, split-open cortical collecting ducts from protein kinase C knockout mice. *AJP: Renal Physiology*, *306*(3), F309–F320. https://doi.org/10.1152/ajprenal.00519.2013

Benstein, J. A., Feiner, H. D., Parker, M., & Dworkin, L. D. (1990). Superiority of salt restriction over diuretics in reducing renal hypertrophy and injury in uninephrectomized SHR. *The American Journal of Physiology*, *258*(6 Pt 2), F1675-81. Retrieved from http://www.ncbi.nlm.nih.gov/pubmed/2193543

Bertorello, A. M., Pires, N., Igreja, B., Pinho, M. J., Vorkapic, E., Wågsäter, D., … Brion, L. (2015). Increased arterial blood pressure and vascular remodeling in mice lacking salt-inducible kinase 1 (SIK1). *Circulation Research*, *116*(4), 642–52. https://doi.org/10.1161/CIRCRESAHA.116.304529

Bertram, J. F., Douglas-Denton, R. N., Diouf, B., Hughson, M. D., & Hoy, W. E. (2011). Human nephron number: implications for health and disease. *Pediatric Nephrology*, *26*(9), 1529–1533. https://doi.org/10.1007/s00467-011-1843-8

Bezanilla, M., Gladfelter, A. S., Kovar, D. R., & Lee, W. L. (2015). Cytoskeletal dynamics: A view from the membrane. *Journal of Cell Biology*, *209*(3), 329–337. https://doi.org/10.1083/jcb.201502062

Bidani, A. K., & Griffin, K. A. (2004). Pathophysiology of hypertensive renal damage: Implications for therapy. *Hypertension*, *44*(5), 595–601. https://doi.org/10.1161/01.HYP.0000145180.38707.84

Böger, C. A., Gorski, M., Li, M., Hoffmann, M. M., Huang, C., Yang, Q., … Kao, W. H. (2011). Association of eGFR-related loci identified by GWAS with incident CKD and ESRD. *PLoS Genetics*, *7*(9), 3–10. https://doi.org/10.1371/journal.pgen.1002292

Bohlooly-Y, M., Carlson, L., Olsson, B., Gustafsson, H., Andersson, I. J. L., Törnell, J., & Bergström, G. (2001). Vascular Function and Blood Pressure in GH Transgenic Mice. *Endocrinology*, *142*(8), 3317–3323. https://doi.org/10.1210/endo.142.8.8296

Brenner, B. M., Garcia, D. L., & Anderson, S. (1988). Glomeruli and blood pressure. Less of one, more the other? *American Journal of Hypertension*, *1*(4 Pt 1), 335–47. Retrieved from http://www.ncbi.nlm.nih.gov/pubmed/3063284

Brenner, B. M., & Mackenzie, H. S. (1997). 12 . Nephron endowment and the pathogenesis of chronic renal failure, 93–94. http://www.ncbi.nlm.nih.gov/pubmed/3063284

Brewster, U. C., & Perazella, M. A. (2004). The renin-angiotensin-aldosterone system and the kidney: effects on kidney disease. *The American Journal of Medicine*, *116*(4), 263–272. http://www.doi.org/10.1016/j.amjmed.2003.09.034

Brinkkoetter, P. T., Ising, C., & Benzing, T. (2013). The role of the podocyte in albumin filtration. *Nature Reviews. Nephrology*, *9*(6), 328–336. https://doi.org/10.1038/nrneph.2013.78

Brochu, I., Labonté, J., Bkaily, G., & D'Orléans-Juste, P. (2002). Role of endothelin

receptors in the hypertensive state of kinin B(2) knockout mice subjected to a high-salt diet. *Clinical Science (London, England : 1979)*, *103 Suppl*(s2002), 380S–384S. https://doi.org/10.1042/CS103S380S

Brunskill, E. W., Georgas, K., Rumballe, B., Little, M. H., & Potter, S. S. (2011). Defining the molecular character of the developing and adult kidney podocyte. *PLoS ONE*, *6*(9), 1–12. https://doi.org/10.1371/journal.pone.0024640

Brzezinski, W. A. (1990). *Blood Pressure*. *Clinical methods: The history, physical, and laboratory examinations*. Butterworths. Retrieved from http://www.ncbi.nlm.nih.gov/pubmed/21250111

Bush, W. S., & Moore, J. H. (2012). Chapter 11: Genome-Wide Association Studies. *PLoS Computational Biology*, *8*(12). https://doi.org/10.1371/journal.pcbi.1002822

Carroll, R. G. (2007). Chapter 11: Renal System and Urinary Tract. *Elsevier's Integrated Physiology.* 117–137. https://doi.org/10.1016/B978-0-323-04318-2.50017-0

Center for Health Statistics, N. (2011). End-stage renal disease patients, by selected characteristics: US, selected years 1980-2010, *2010*, 2012. Retrieved from https://www.cdc.gov/nchs/data/hus/2011/051.pdf

Chae, J., Kim, M. J., Goo, J. H., Collier, S., Gubb, D., Charlton, J., … Park, W. J. (1999). The Drosophila tissue polarity gene starry night encodes a member of the protocadherin family. *Development (Cambridge, England)*, *126*(23), 5421–9. Retrieved from http://www.ncbi.nlm.nih.gov/pubmed/10556066

Chambers, J. C., Zhang, W., Lord, G. M., Harst, P. Van Der, & Debbie, A. (2010). Genetic Loci influencing kidney function and chronic kidney disease in man. *Nature Genetics*, *42*(5), 373–375. https://doi.org/10.1038/ng.566.Genetic

Chen, C. C. A., Pedraza, P. L., Hao, S., Stier, C. T., & Ferreri, N. R. (2010). TNFR1-deficient mice display altered blood pressure and renal responses to ANG II infusion. *AJP: Renal Physiology*, *299*(5), F1141–F1150. https://doi.org/10.1152/ajprenal.00344.2010

Chu, C. W., Gerstenzang, E., Ossipova, O., & Sokol, S. Y. (2013). Lulu regulates shroom-induced apical constriction during neural tube closure. *PLoS ONE*, *8*(11), 1–10. https://doi.org/10.1371/journal.pone.0081854

Chung, M.-I., Nascone-Yoder, N. M., Grover, S. a, Drysdale, T. a, & Wallingford, J. B. (2010). Direct activation of Shroom3 transcription by Pitx proteins drives epithelial morphogenesis in the developing gut. *Development (Cambridge, England)*, *137*(8), 1339–49. https://doi.org/10.1242/dev.044610

Conduit, P. T. (2016). Microtubule organization: A complex solution. *Journal of Cell Biology*, *213*(6), 609–612. https://doi.org/10.1083/jcb.201606008

Crowley, S. D., Gurley, S. B., Herrera, M. J., Ruiz, P., Griffiths, R., Kumar, A. P., … Coffman, T. M. (2006). Angiotensin II causes hypertension and cardiac hypertrophy through its receptors in the kidney. *Proceedings of the National Academy of Sciences of the United States of America*, *103*(47), 17985–90. https://doi.org/10.1073/pnas.0605545103

Crowley, S. D., Zhang, J., Herrera, M., Griffiths, R., Ruiz, P., & Coffman, T. M. (2011). Role of AT1 receptor-mediated salt retention in angiotensin II-dependent hypertension. *AJP: Renal Physiology*, *301*(5), F1124–F1130. https://doi.org/10.1152/ajprenal.00305.2011

D'Agati, V. D. (2008). Podocyte injury in focal segmental glomerulosclerosis: Lessons from animal models (a play in five acts). *Kidney International*, *73*(4), 399–406. https://doi.org/10.1038/sj.ki.5002655

D'Agati, V. D., Kaskel, F. J., & Falk, R. J. (2014). Focal Segmental Glomerulosclerosis. *New England Journal of Medicine*, *365*(26), 2398–2411. https://doi.org/CJN.05960616 [pii]10.2215/CJN.05960616

Dandapani, S. V., Sugimoto, H., Matthews, B. D., Kolb, R. J., Sinha, S., Gerszten, R. E., … Pollak, M. R. (2007). α-Actinin-4 Is Required for Normal Podocyte Adhesion. *Journal of Biological Chemistry*, *282*(1), 467–477. https://doi.org/10.1074/jbc.M605024200

Das, D., Zalewski, J. K., Mohan, S., Plageman, T. F., VanDemark, A. P., & Hildebrand, J. D. (2014). The interaction between Shroom3 and Rho-kinase is required for neural tube morphogenesis in mice. *Biology Open*, *3*(9), 850–860. https://doi.org/10.1242/bio.20147450

Daumerie, G., Bridges, L., Yancey, S., Davis, W., Huang, P., Loscalzo, J., & Pointer, M. A. (2010). The effect of salt on renal damage in eNOS-deficient mice. *Hypertension Research : Official Journal of the Japanese Society of Hypertension*, *33*(2), 170–6. https://doi.org/10.1038/hr.2009.197

Davenport, A., Drüeke, T. B., Nangaku, M., & Toby Coates, P. (2015). High-volume plasma exchange in patients with acute liver failure: an open randomized controlled trial. *Kidney International*, *88*(6), 1215–1216. https://doi.org/10.1038/ki.2015.338

Davidson, A. (2008). Mouse kidney development. *StemBook*, 1–30. https://doi.org/10.3824/stembook.1.34.1

Davidson, L. A., Ezin, A. M., & Keller, R. (2002). Embryonic wound healing by apical contraction and ingression in Xenopus laevis. *Cell Motility and the Cytoskeleton*, *53*(3), 163–176. https://doi.org/10.1002/cm.10070

Davis, N. M., Kurpios, N. A., Sun, X., Gros, J., Martin, J. F., & Tabin, C. J. (2008). The Chirality of Gut Rotation Derives from Left-Right Asymmetric Changes in the Architecture of the Dorsal Mesentery. *Developmental Cell*, *15*(1), 134–145.

https://doi.org/10.1016/j.devcel.2008.05.001

De Matos Simões, S., Mainieri, A., & Zallen, J. A. (2014). Rho GTPase and Shroom direct planar polarized actomyosin contractility during convergent extension. *Journal of Cell Biology*, *204*(4), 575–589. https://doi.org/10.1083/jcb.201307070

Deshmukh, H. a, Palmer, C. N. a, Morris, a D., & Colhoun, H. M. (2013). Investigation of known estimated glomerular filtration rate loci in patients with type 2 diabetes. *Diabetic Medicine : A Journal of the British Diabetic Association*, *30*(10), 1230–5. https://doi.org/10.1111/dme.12211

Desjardins, F., Lobysheva, I., Pelat, M., Gallez, B., Feron, O., Dessy, C., & Balligand, J.-L. (2008). Control of blood pressure variability in caveolin-1-deficient mice: role of nitric oxide identified in vivo through spectral analysis. *Cardiovascular Research*, *79*(3), 527–536. https://doi.org/10.1093/cvr/cvn080

Dickson, H. M., Wilbur, A., Reinke, A. A., Young, M. A., & Vojtek, A. B. (2015). Targeted inhibition of the Shroom3–Rho kinase protein–protein interaction circumvents Nogo66 to promote axon outgrowth. *BMC Neuroscience*, *16*(1), 34. https://doi.org/10.1186/s12868-015-0171-5

Dickson, H. M., Zurawski, J., Zhang, H., Turner, D. L., & Vojtek, A. B. (2010). POSH is an Intracellular Signal Transducer for the Axon Outgrowth Inhibitor Nogo66. *Journal of Neuroscience*, *30*(40), 13319–13325. https://doi.org/10.1523/JNEUROSCI.1324-10.2010

Didion, S. P. (2017). A novel genetic model to explore the Brenner hypothesis: Linking nephron endowment and number with hypertension. *Medical Hypotheses*, *106*(Supplement C), 6–9. https://doi.org/https://doi.org/10.1016/j.mehy.2017.06.020

Dietz, M. L., Bernaciak, T. M., Vendetti, F., Kielec, J. M., & Hildebrand, J. D. (2006). Differential actin-dependent localization modulates the evolutionarily conserved activity of Shroom family proteins. *Journal of Biological Chemistry*, *281*(29), 20542–20554. https://doi.org/10.1074/jbc.M512463200

Dolan, E., & O'Brien, E. (2010). Blood pressure variability: clarity for clinical practice. *Hypertension (Dallas, Tex. : 1979)*, *56*(2), 179–81. https://doi.org/10.1161/HYPERTENSIONAHA.110.154708

Dressler, G. R. (2006). The Cellular Basis of Kidney Development. *Annual Review of Cell and Developmental Biology*, *22*(1), 509–529. https://doi.org/10.1146/annurev.cellbio.22.010305.104340

Durvasula, R. V., Petermann, A. T., Hiromura, K., Blonski, M., Pippin, J., Mundel, P., … Shankland, S. J. (2004). Activation of a local tissue angiotensin system in podocytes by mechanical strain11See Editorial by Kriz, p. 333. *Kidney International*, *65*(1), 30–39. https://doi.org/10.1111/j.1523-1755.2004.00362.x

El-Achkar, T. M., Wu, X.-R., Rauchman, M., McCracken, R., Kiefer, S., & Dagher, P. C. (2008). Tamm-Horsfall protein protects the kidney from ischemic injury by decreasing inflammation and altering TLR4 expression. *American Journal of Physiology. Renal Physiology*, *295*(2), F534-44. https://doi.org/10.1152/ajprenal.00083.2008

Ellis, J. W., Chen, M. H., Foster, M. C., Liu, C. T., Larson, M. G., De boer, I., … O'Seaghdha, C. M. (2012). Validated SNPs for eGFR and their associations with albuminuria. *Human Molecular Genetics*, *21*(14), 3293–3298. https://doi.org/10.1093/hmg/dds138

Endlich, N., & Endlich, K. (2012). The Challenge and Response of Podocytes to Glomerular Hypertension. *Seminars in Nephrology*, *32*(4), 327–341. https://doi.org/10.1016/j.semnephrol.2012.06.004

Ernst, S., Liu, K., Agarwala, S., Moratscheck, N., Avci, M. E., Nogare, D. D., … Lecaudey, V. (2012). Shroom3 is required downstream of FGF signalling to mediate proneuromast assembly in zebrafish. *Development*, *139*(24), 4571–4581. https://doi.org/10.1242/dev.083253

Fakhro, K. A., Choi, M., Ware, S. M., Belmont, J. W., Towbin, J. A., Lifton, R. P., … Brueckner, M. (2011). Rare copy number variations in congenital heart disease patients identify unique genes in left-right patterning. *Proceedings of the National Academy of Sciences*, *108*(7), 2915–2920. https://doi.org/10.1073/pnas.1019645108

Farah, V. M. A., Joaquim, L. F., Bernatova, I., & Morris, M. (2004). Acute and chronic stress influence blood pressure variability in mice. *Physiology & Behavior*, *83*(1), 135–142. https://doi.org/10.1016/J.PHYSBEH.2004.08.004

Farber, H. W., & Loscalzo, J. (2004). Pulmonary Arterial Hypertension. *New England Journal of Medicine*, *351*(16), 1655–1665. https://doi.org/10.1056/NEJMra035488

Faul, C., Asanuma, K., Yanagida-Asanuma, E., Kim, K., & Mundel, P. (2007). Actin up: regulation of podocyte structure and function by components of the actin cytoskeleton. *Trends in Cell Biology*, *17*(9), 428–437. https://doi.org/10.1016/j.tcb.2007.06.006

Feiguin, F., Hannus, M., Mlodzik, M., & Eaton, S. (2001). The ankyrin repeat protein Diego mediates Frizzled-dependent planar polarization. *Developmental Cell*, *1*(1), 93–101. Retrieved from http://www.ncbi.nlm.nih.gov/pubmed/11703927

Feng, M., Whitesall, S., Zhang, Y., Beibel, M., D'Alecy, L., & DiPetrillo, K. (2008). Validation of volume-pressure recording tail-cuff blood pressure measurements. *American Journal of Hypertension*, *21*(12), 1288–1291. https://doi.org/10.1038/ajh.2008.301

Ferreira, D. N., Katayama, I. A., Oliveira, I. B., Rosa, K. T., Furukawa, L. N. S., Coelho, M. S., … Heimann, J. C. (2010). Salt-Induced Cardiac Hypertrophy and Interstitial

Fibrosis Are Due to a Blood Pressure-Independent Mechanism in Wistar Rats. *Journal of Nutrition*, *140*(10), 1742–1751. https://doi.org/10.3945/jn.109.117473

Fletcher, D. A., & Mullins, R. D. (2010). Cell mechanics and the cytoskeleton. *Nature*, *463*(7280), 485–492. https://doi.org/10.1038/nature08908

Foëx, P., & Sear, J. W. (2004). Hypertension: Pathophysiology and treatment. *Continuing Education in Anaesthesia, Critical Care and Pain*, *4*(3), 71–75. https://doi.org/10.1093/bjaceaccp/mkh020

Fogo, A. B. (2007). Mechanisms of progression of chronic kidney disease. *Pediatric Nephrology*, *22*(12), 2011–2022. https://doi.org/10.1007/s00467-007-0524-0

Fournier, A. E., GrandPre, T., & Strittmatter, S. M. (2001). Identification of a receptor mediating Nogo-66 inhibition of axonal regeneration. *Nature*, *409*(6818), 341–346. https://doi.org/10.1038/35053072

Friedel, R. H., & Soriano, P. (2010). Gene trap mutagenesis in the mouse. *Methods in Enzymology*, *477*, 243–69. https://doi.org/10.1016/S0076-6879(10)77013-0

Friedrich, G., & Soriano, P. (1991). Promotor traps in embryonic stem cells: a genetic screen to identify and mutate developmental genes in mice. *Genes & Development*, *5*, 1513–1523.

Ganief, T., Gqamana, P., Garnett, S., Hoare, J., Stein, D. J., Joska, J., … Blackburn, J. M. (2017). Quantitative proteomic analysis of HIV-1 Tat-induced dysregulation in SH-SY5Y neuroblastoma cells. *PROTEOMICS*, *17*(6), 1600236. https://doi.org/10.1002/pmic.201600236

Greenwald, J. E., Sakata, M., Michener, M. L., Sides, S. D., & Needleman, P. (1988). Is atriopeptin a physiological or pathophysiological substance? Studies in the autoimmune rat. *The Journal of Clinical Investigation*, *81*(4), 1036–41. https://doi.org/10.1172/JCI113414

Grosse, A. S., Pressprich, M. F., Curley, L. B., Hamilton, K. L., Margolis, B., Hildebrand, J. D., & Gumucio, D. L. (2011). Cell dynamics in fetal intestinal epithelium: implications for intestinal growth and morphogenesis. *Development*, *138*(20), 4423–4432. https://doi.org/10.1242/dev.065789

Gu, J.-W., Bailey, A. P., Tan, W., Shparago, M., & Young, E. (2008). Long-term High Salt Diet Causes Hypertension and Decreases Renal Expression of Vascular Endothelial Growth Factor in Sprague-Dawley Rats. *Journal of the American Society of Hypertension : JASH*, *2*(4), 275–85. https://doi.org/10.1016/j.jash.2008.03.001

Gubb, D., & García-Bellido, A. (1982). A genetic analysis of the determination of cuticular polarity during development in Drosophila melanogaster. *Journal of Embryology and Experimental Morphology*, *68*, 37–57. Retrieved from

http://www.ncbi.nlm.nih.gov/pubmed/6809878

Guichard, J. L., Desai, R. V., Ahmed, M. I., Mujib, M., Fonarow, G. C., Feller, M. A., … Ahmed, A. (2011). Isolated diastolic hypotension and incident heart failure in older adults. *Hypertension*, *58*(5), 895–901. https://doi.org/10.1161/HYPERTENSIONAHA.111.178178

Gurusinghe, S., Tambay, A., & Sethna, C. B. (2017). Developmental Origins and Nephron Endowment in Hypertension. *Frontiers in Pediatrics*, *5*(June), 1–8. https://doi.org/10.3389/fped.2017.00151

Habas, R., Kato, Y., & He, X. (2001). Wnt/Frizzled activation of Rho regulates vertebrate gastrulation and requires a novel formin homology protein Daam1. *Cell*, *107*(7), 843–854. https://doi.org/10.1016/S0092-8674(01)00614-6

Hagens, O., Ballabio, A., Kalscheuer, V., Kraehenbuhl, J.-P., Schiaffino, M. V., Smith, P., … Wallingford, J. B. (2006). A new standard nomenclature for proteins related to Apx and Shroom. *BMC Cell Biology*, *7*, 18. https://doi.org/10.1186/1471-2121-7-18

Haigo, S. L., Hildebrand, J. D., Harland, R. M., & Wallingford, J. B. (2003). Shroom Induces Apical Constriction and Is Required for Hingepoint Formation during Neural Tube Closure. *Current Biology*, *13*(24), 2125–2137. https://doi.org/10.1016/j.cub.2003.11.054

Haraldsson, B., Nystrom, J., & Deen, W. M. (2008). Properties of the Glomerular Barrier and Mechanisms of Proteinuria. *Physiological Reviews*, *88*(2), 451–487. https://doi.org/10.1152/physrev.00055.2006

He, F. J., & MacGregor, G. A. (2010). Reducing Population Salt Intake Worldwide: From Evidence to Implementation. *Progress in Cardiovascular Diseases*, *52*(5), 363–382. https://doi.org/10.1016/J.PCAD.2009.12.006

Heisenberg, C. P., & Bellaïche, Y. (2013). XForces in tissue morphogenesis and patterning. *Cell*, *153*(5). https://doi.org/10.1016/j.cell.2013.05.008

Hernandez, A. L., Kitz, A., Wu, C., Lowther, D. E., Rodriguez, D. M., Vudattu, N., … Hafler, D. A. (2015). Sodium chloride inhibits the suppressive function of FOXP3+ regulatory T cells. *The Journal of Clinical Investigation*, *125*(11), 4212–4222. https://doi.org/10.1172/JCI81151

Hewitson, T. D. (2012). Fibrosis in the kidney: is a problem shared a problem halved? *Fibrogenesis & Tissue Repair*, *5*(Suppl 1 Proceedings of Fibroproliferative disorders: from biochemical analysis to targeted therapiesPetro E Petrides and David Brenner), S14. https://doi.org/10.1186/1755-1536-5-S1-S14

Hildebrand, J. D. (2005). Shroom regulates epithelial cell shape via the apical positioning of an actomyosin network. *Journal of Cell Science*, *118*(22), 5191–5203.

https://doi.org/10.1242/jcs.02626

Hildebrand, J. D., & Soriano, P. (1999). Shroom, a PDZ domain–containing actin-binding protein, is required for neural tube morphogenesis in mice. *Cell*, *99*(5), 485–497. https://doi.org/10.1016/S0092-8674(00)81537-8

Hill, N. R., Fatoba, S. T., Oke, J. L., Hirst, J. A., Callaghan, A. O., Lasserson, D. S., & Hobbs, F. D. R. (2016). Global Prevalence of Chronic Kidney Disease – A Systematic Review and Meta-Analysis, 1–18. https://doi.org/10.5061/dryad.3s7rd.Funding

Höcht, C. (2013). Blood Pressure Variability: Prognostic Value and Therapeutic Implications. *ISRN Hypertension*, *2013*, 1–16. https://doi.org/10.5402/2013/398485

Hoy, W. E., Hughson, M. D., Bertram, J. F., Douglas-Denton, R., & Amann, K. (2005). Nephron number, hypertension, renal disease, and renal failure. *Journal of the American Society of Nephrology : JASN*, *16*(9), 2557–64. https://doi.org/10.1681/ASN.2005020172

Huang, Z., Zhang, L., Chen, Y., Zhang, H., Yu, C., Zhou, F., … Shi, W. (2016). RhoA deficiency disrupts podocyte cytoskeleton and induces podocyte apoptosis by inhibiting YAP/dendrin signal. *BMC Nephrology*, *17*(1), 66. https://doi.org/10.1186/s12882-016-0287-6

Humbert, M., Morrell, N. W., Archer, S. L., Stenmark, K. R., MacLean, M. R., Lang, I. M., … Rabinovitch, M. (2004). Cellular and molecular pathobiology of pulmonary arterial hypertension. *Journal of the American College of Cardiology*, *43*(12), S13–S24. https://doi.org/10.1016/j.jacc.2004.02.029

Ichikawa, I., Ma, J., Motojima, M., & Matsusaka, T. (2005). Podocyte damage damages podocytes : autonomous vicious cycle that drives local spread of glomerular sclerosis, 205–210.

Iida, S., Baumbach, G. L., Lavoie, J. L., Faraci, F. M., Sigmund, C. D., & Heistad, D. D. (2005). Spontaneous stroke in a genetic model of hypertension in mice. *Stroke*, *36*(6), 1253–8. https://doi.org/10.1161/01.str.0000167694.58419.a2

Jha, V., Garcia-Garcia, G., Iseki, K., Li, Z., Naicker, S., Plattner, B., … Yang, C. W. (2013). Chronic kidney disease: Global dimension and perspectives. *The Lancet*, *382*(9888), 260–272. https://doi.org/10.1016/S0140-6736(13)60687-X

Jones, N., Blasutig, I. M., Eremina, V., Ruston, J. M., Bladt, F., Li, H., … Pawson, T. (2006). Nck adaptor proteins link nephrin to the actin cytoskeleton of kidney podocytes. *Nature*, *440*(7085), 818–823. https://doi.org/10.1038/nature04662

Joska, J., Hoare, J., Stein, D., & Flisher, A. (2011). The neurobiology of HIV dementia: implications for practice in South Africa. *African Journal of Psychiatry*, *14*(1). https://doi.org/10.4314/ajpsy.v14i1.65463

Judd, E., & Calhoun, D. A. (2015). Management of Hypertension in CKD: Beyond the Guidelines. *Advances in Chronic Kidney Disease*, *22*(2), 116–122. https://doi.org/10.1053/j.ackd.2014.12.001

Kannel, W. B. (2000). Elevated systolic blood pressure as a cardiovascular risk factor. *The American Journal of Cardiology*, *85*(2), 251–255. https://doi.org/10.1016/S0002-9149(99)00635-9

Kaplan, J. M., Kim, S. H., North, K. N., Rennke, H., Correia, L. A., Tong, H., … Pollak, M. R. (2000). Mutations in ACTN4 , encoding α -actinin-4 , cause familial focal segmental glomerulosclerosis, *24*(march), 251–256.

Kasner, E., Hunter, C. A., Ph, D., Kariko, K., & Ph, D. (2013). NIH Public Access, *70*(4), 646–656. https://doi.org/10.1002/ana.22528.Toll-like

Kearney, P. M., Whelton, M., Reynolds, K., Muntner, P., Whelton, P. K., & He, J. (2005). Global burden of hypertension: analysis of worldwide data. *The Lancet*, *365*(9455), 217–223. https://doi.org/10.1016/S0140-6736(05)17741-1

Khalili, H., Sull, A., Sarin, S., Boivin, F. J., Halabi, R., Svajger, B., … Bridgewater, D. (2016). Developmental Origins for Kidney Disease Due to Shroom3 Deficiency. *Journal of the American Society of Nephrology*, *27*(10), 2965–2973. https://doi.org/10.1681/ASN.2015060621

Khan, Z., & Pandey, M. (2014). Role of kidney biomarkers of chronic kidney disease: An update. *Saudi Journal of Biological Sciences*, *21*(4), 294–299. https://doi.org/10.1016/J.SJBS.2014.07.003

Kikuya, M., Ohkubo, T., Metoki, H., Asayama, K., Hara, A., Obara, T., … Imai, Y. (2008). Day-by-day variability of blood pressure and heart rate at home as a novel predictor of prognosis: The Ohasama study. *Hypertension*, *52*(6), 1045–1050. https://doi.org/10.1161/HYPERTENSIONAHA.107.104620

Kim, S.-J. (2011). Heterotaxy syndrome. *Korean Circulation Journal*, *41*(5), 227–32. https://doi.org/10.4070/kcj.2011.41.5.227

Kistler, A. D., Altintas, M. M., & Reiser, J. (2012). Podocyte GTPases regulate kidney filter dynamics. *Kidney International*, *81*(11), 1053–5. https://doi.org/10.1038/ki.2012.12

Kobori, H., Nangaku, M., Navar, L. G., & Nishiyama, A. (2007). The intrarenal renin-angiotensin system: from physiology to the pathobiology of hypertension and kidney disease. *Pharmacological Reviews*, *59*(3), 251–87. https://doi.org/10.1124/pr.59.3.3

Kobori, H., Nishiyama, A., Abe, Y., & Navar, L. G. (2003). Enhancement of intrarenal angiotensinogen in Dahl salt-sensitive rats on high salt diet. *Hypertension*, *41*(3 I), 592–597. https://doi.org/10.1161/01.HYP.0000056768.03657.B4

Komiya, Y., & Habas, R. (2008). Wnt signal transduction pathways, *4*(2), 68–75.

Kondo, T., & Hayashi, S. (2015). Mechanisms of cell height changes that mediate epithelial invagination. *Development Growth and Differentiation*, *57*(4), 313–323. https://doi.org/10.1111/dgd.12224

Kos, C. H., Le, T. C., Sinha, S., Henderson, J. M., Kim, S. H., Sugimoto, H., … Pollak, M. R. (2003). Mice deficient in alpha-actinin-4 have severe glomerular disease. *The Journal of Clinical Investigation*, *111*(11), 1683–90. https://doi.org/10.1172/JCI17988

Kottgen, A., Glazer, N. L., Dehghan, A., Hwang, S. J., Katz, R., Li, M., … Fox, C. S. (2009). Multiple loci associated with indices of renal function and chronic kidney disease. *Nat.Genet.*, *41*(6), 712–717. https://doi.org/10.1038/ng.377

Köttgen, A., Pattaro, C., Böger, C. A., Fuchsberger, C., Olden, M., Glazer, N. L., … Fox, C. S. (2010). New loci associated with kidney function and chronic kidney disease. *Nature Genetics*, *42*(5), 376–384. https://doi.org/10.1038/ng.568

Kretzler, M., Koeppen-Hagemann, I., & Kriz, W. (1994). Podocyte damage is a critical step in the development of glomerulosclerosis in the uninephrectomised-desoxycorticosterone hypertensive rat. *Virchows Archiv : An International Journal of Pathology*, *425*(2), 181–93. Retrieved from http://www.ncbi.nlm.nih.gov/pubmed/7952502

Kriz, W., Shirato, I., Nagata, M., LeHir, M., & Lemley, K. V. (2013). The podocyte's response to stress: the enigma of foot process effacement. *AJP: Renal Physiology*, *304*(4), F333–F347. https://doi.org/10.1152/ajprenal.00478.2012

Kurts, C., Panzer, U., Anders, H.-J., & Rees, A. J. (2013). The immune system and kidney disease: basic concepts and clinical implications. *Nature Reviews Immunology*, *13*(10), 738–753. https://doi.org/10.1038/nri3523

Lamb, E. J., MacKenzie, F., & Stevens, P. E. (2009). How should proteinuria be detected and measured? *Annals of Clinical Biochemistry*, *46*(3), 205–217. https://doi.org/10.1258/acb.2009.009007

Lang, R. A., Herman, K., Reynolds, A. B., Hildebrand, J. D., & Plageman, T. F. (2014). p120-catenin-dependent junctional recruitment of Shroom3 is required for apical constriction during lens pit morphogenesis. *Development (Cambridge, England)*, *141*(16), 3177–87. https://doi.org/10.1242/dev.107433

Laverman, G. D., van Goor, H., Henning, R. H., de Jong, P. E., de Zeeuw, D., & Navis, G. (2003). Renoprotective effects of VPI versus ACEI in normotensive nephrotic rats on different sodium intakes. *Kidney International*, *63*(1), 64–71. https://doi.org/10.1046/J.1523-1755.2003.00708.X

Lecaudey, V., Cakan-Akdogan, G., Norton, W. H. J., & Gilmour, D. (2008). Dynamic

Fgf signaling couples morphogenesis and migration in the zebrafish lateral line primordium. *Development (Cambridge, England)*, *135*(16), 2695–705. https://doi.org/10.1242/dev.025981

Lee, C., Le, M. P., & Wallingford, J. B. (2009). The Shroom family proteins play broad roles in the morphogenesis of thickened epithelial sheets. *Developmental Dynamics*, *238*(6), 1480–1491. https://doi.org/10.1002/dvdy.21942

Lee, C., Scherr, H. M., & Wallingford, J. B. (2007). Shroom family proteins regulate -tubulin distribution and microtubule architecture during epithelial cell shape change. *Development*, *134*(7), 1431–1441. https://doi.org/10.1242/dev.02828

Lee, D. L., Bell, T. D., Bhupatkar, J., Solis, G., & Welch, W. J. (2012). Adenosine A1-receptor knockout mice have a decreased blood pressure response to low-dose ANG II infusion. *AJP: Regulatory, Integrative and Comparative Physiology*, *303*(6), R683–R688. https://doi.org/10.1152/ajpregu.00116.2012

Lee, D. L., Sturgis, L. C., Labazi, H., Osborne, J. B., Fleming, C., Pollock, J. S., … Brands, M. W. (2006). Angiotensin II hypertension is attenuated in interleukin-6 knockout mice. *American Journal of Physiology. Heart and Circulatory Physiology*, *290*(3), H935-40. https://doi.org/10.1152/ajpheart.00708.2005

Lee, J. D., Silva-Gagliardi, N. F., Tepass, U., McGlade, C. J., & Anderson, K. V. (2007). The FERM protein Epb4.1l5 is required for organization of the neural plate and for the epithelial-mesenchymal transition at the primitive streak of the mouse embryo. *Development*, *134*(11), 2007–2016. https://doi.org/10.1242/dev.000885

Lemay, P., Guyot, M.-C., Tremblay, É., Dionne-Laporte, A., Spiegelman, D., Henrion, É., … Kibar, Z. (2015). Loss-of-function de novo mutations play an important role in severe human neural tube defects. *Journal of Medical Genetics*, *52*(7), 493–7. https://doi.org/10.1136/jmedgenet-2015-103027

Leonetti, G., Cuspidi, C., Facchini, M., & Stramba-Badiale, M. (2000). Is systolic pressure a better target for antihypertensive treatment than diastolic pressure? *Journal of Hypertension. Supplement : Official Journal of the International Society of Hypertension*, *18*(3), S13-20. Retrieved from http://www.ncbi.nlm.nih.gov/pubmed/10952083

Levey, A. S., & Coresh, J. (2012). Chronic kidney disease. *The Lancet*, *379*(9811), 165–180. https://doi.org/10.1016/S0140-6736(11)60178-5

Levey, A. S., Coresh, J., Balk, E., Kausz, A. T., Levin, A., Steffes, M. W., … Eknoya, G. (2003). Clinical Guidelines National Kidney Foundation Practice Guidelines for Chronic Kidney. *Annals of Internal Medicine*, *139*, 137–147. https://doi.org/200307150-00013 [pii]

Levey, A. S., & Inker, L. A. (2016). GFR as the “gold Standard”: Estimated, Measured, and True. *American Journal of Kidney Diseases*, *67*(1), 9–12.

https://doi.org/10.1053/j.ajkd.2015.09.014

Lhotta, K. (2010). Uromodulin and chronic kidney disease. *Kidney & Blood Pressure Research*, *33*(5), 393–8. https://doi.org/10.1159/000320681

Little, M. H., & McMahon, A. P. (2012). Mammalian kidney development: Principles, progress, and projections. *Cold Spring Harbor Perspectives in Biology*, *4*(5), 3. https://doi.org/10.1101/cshperspect.a008300

Loebel, D. A. F., Plageman, T. F., Tang, T. L., Jones, V. J., Muccioli, M., & Tam, P. P. L. (2016). Thyroid bud morphogenesis requires CDC42- and SHROOM3-dependent apical constriction. *Biology Open*, *5*(2), 130–139. https://doi.org/10.1242/bio.014415

Lonn, E. M., Yusuf, S., Jha, P., Montague, T. J., Teo, K. K., Benedict, C. R., & Pitt, B. (1994). Emerging role of angiotensin-converting enzyme inhibitors in cardiac and vascular protection. *Circulation*, *90*(4), 2056–69. Retrieved from http://www.ncbi.nlm.nih.gov/pubmed/7923694

López-Novoa, J. M., Rodríguez-Peña, A. B., Ortiz, A., Martínez-Salgado, C., & López Hernández, F. J. (2011). Etiopathology of chronic tubular, glomerular and renovascular nephropathies: Clinical implications. *Journal of Translational Medicine*, *9*(1), 13. https://doi.org/10.1186/1479-5876-9-13

Lote, C. J. (2013). *Principles of renal physiology*. *Principles of Renal Physiology*. https://doi.org/10.1007/978-1-4614-3785-7

Luft, F. C. (2000). Hypertensive nephrosclerosis-a cause of end-stage renal disease? *Nephrology Dialysis Transplantation*, *15*(10), 1515–1517. https://doi.org/10.1093/ndt/15.10.1515

Magee, G. M., Bilous, R. W., Cardwell, C. R., Hunter, S. J., Kee, F., & Fogarty, D. G. (2009). Is hyperfiltration associated with the future risk of developing diabetic nephropathy? A meta-analysis. *Diabetologia*, *52*(4), 691–697. https://doi.org/10.1007/s00125-009-1268-0

Manalich, R., Reyes, L., Herrera, M., Melendi, C., & Fundora, I. (2000). Relationship between weight at birth and the number and size of renal glomeruli in humans: A histomorphometric study. *Kidney International*, *58*(2), 770–773. https://doi.org/10.1046/j.1523-1755.2000.00225.x

Mancia, G. (n.d.). Short-and Long-Term Blood Pressure Variability Present and Future. https://doi.org/10.1161/HYPERTENSIONAHA.112.194340

Mancia, G. (2012). Short- and long-term blood pressure variability: Present and future. *Hypertension*, *60*(2), 512–517. https://doi.org/10.1161/HYPERTENSIONAHA.112.194340

Manhiani, M. M., Seth, D. M., Banes-Berceli, A. K. L., Satou, R., Navar, L. G., & Brands, M. W. (2015). The role of IL-6 in the physiologic versus hypertensive blood pressure actions of angiotensin II. *Physiological Reports*, *3*(10), e12595. https://doi.org/10.14814/phy2.12595

Manolio, T. A. (2010). Genomewide Association Studies and Assessment of the Risk of Disease. *http://dx.doi.org/10.1056/NEJMra0905980*. https://doi.org/doi:10.1056/NEJMra0905980

Marlow, F., Topczewski, J., Sepich, D., & Solnica-Krezel, L. (2002). Zebrafish Rho kinase 2 acts downstream of Wnt11 to mediate cell polarity and effective convergence and extension movements. *Current Biology*, *12*(11), 876–884. https://doi.org/10.1016/S0960-9822(02)00864-3

Martin, A. C., & Goldstein, B. (2014). Apical constriction: themes and variations on a cellular mechanism driving morphogenesis. *Development*, *141*(10), 1987–1998. https://doi.org/10.1242/dev.102228

Mathis, K. W., Venegas-Pont, M., Masterson, C. W., Wasson, K. L., & Ryan, M. J. (2011). Blood pressure in a hypertensive mouse model of SLE is not salt-sensitive. *AJP: Regulatory, Integrative and Comparative Physiology*, *301*(5), R1281–R1285. https://doi.org/10.1152/ajpregu.00386.2011

Matsusaka, T., Sandgren, E., Shintani, A., Kon, V., & Pastan, I. (2011). Podocyte Injury Damages Other Podocytes, 1275–1285. https://doi.org/10.1681/ASN.2010090963

McEvoy, J. W., Chen, Y., Rawlings, A., Hoogeveen, R. C., Ballantyne, C. M., Blumenthal, R. S., … Selvin, E. (2016). Diastolic Blood Pressure, Subclinical Myocardial Damage, and Cardiac Events: Implications for Blood Pressure Control. *Journal of the American College of Cardiology*, *68*(16), 1713–1722. https://doi.org/10.1016/J.JACC.2016.07.754

McGreevy, E. M., Vijayraghavan, D., Davidson, L. A., & Hildebrand, J. D. (2015). Shroom3 functions downstream of planar cell polarity to regulate myosin II distribution and cellular organization during neural tube closure. *Biology Open*, *4*(2), 186–196. https://doi.org/10.1242/bio.20149589

Menon, M. C., Chuang, P. Y., & He, C. J. (2012). The glomerular filtration barrier: Components and crosstalk. *International Journal of Nephrology*, *2012*. https://doi.org/10.1155/2012/749010

Menon, M. C., Chuang, P. Y., Li, Z., Wei, C., Zhang, W., Luan, Y., … Murphy, B. (2015). Intronic locus determines SHROOM3 expression and potentiates renal allograft fibrosis. *Journal of Clinical Investigation*, *125*(1), 208–221. https://doi.org/10.1172/JCI76902

Meyer, T. E., Verwoert, G. C., Hwang, S. J., Glazer, N. L., Smith, A. V., van Rooij, F. J. A., … Köttgen, A. (2010). Genome-wide association studies of serum magnesium,

potassium, and sodium concentrations identify six loci influencing serum magnesium levels. *PLoS Genetics*, *6*(8). https://doi.org/10.1371/journal.pgen.1001045

Miao, C., Yuan, W.-J., & Su, D.-F. (2003). Comparative study of sinoaortic denervated rats and spontaneously hypertensive rats. *American Journal of Hypertension*, *16*(7), 585–591. https://doi.org/10.1016/S0895-7061(03)00866-5

Moe, S. M., Drueke, T. B., & Group, for the K. W. (2017). KDIGO clinical practice guideline for the diagnosis, evaluation, prevention and treatment of chronic kidney disease mineral and bone disorder (CKD-MBD). *Kidney Int*, *76*(Suppl 113), S1–S128. https://doi.org/10.1038/ki.2009.188

Mohan, S., Das, D., Bauer, R. J., Heroux, A., Zalewski, J. K., Heber, S., … VanDemark, A. P. (2013). Structure of a highly conserved domain of rock1 required for shroom-mediated regulation of cell morphology. *PLoS ONE*, *8*(12). https://doi.org/10.1371/journal.pone.0081075

Mohan, S., Rizaldy, R., Das, D., Bauer, R. J., Heroux, A., Trakselis, M. A., … VanDemark, A. P. (2012). Structure of Shroom domain 2 reveals a three-segmented coiled-coil required for dimerization, Rock binding, and apical constriction. *Molecular Biology of the Cell*, *23*(11), 2131–2142. https://doi.org/10.1091/mbc.E11-11-0937

Müller, F., & O'Rahilly, R. (1991). Development of anencephaly and its variants. *American Journal of Anatomy*, *190*(3), 193–218. https://doi.org/10.1002/aja.1001900302

Nagase, M., Shibata, S., Yoshida, S., Nagase, T., Gotoda, T., & Fujita, T. (2006). Podocyte Injury Underlies the Glomerulopathy of Dahl Salt-Hypertensive Rats and Is Reversed by Aldosterone Blocker. *Hypertension*, *47*(6), 1084–1093. https://doi.org/10.1161/01.HYP.0000222003.28517.99

Nagata, M. (2016). Podocyte injury and its consequences. *Kidney International*, *89*(6), 1221–1230. https://doi.org/10.1016/j.kint.2016.01.012

Nahas, a M. El, & Bello, A. K. (2010). Chronic kidney disease: the global challenge. *Lancet*, *365*(9456), 331–40. https://doi.org/10.1016/S0140-6736(05)17789-7

Nakagawa, K., Holla, V. R., Wei, Y., Wang, W.-H., Gatica, A., Wei, S., … Capdevila, J. H. (2006). Salt-sensitive hypertension is associated with dysfunctional Cyp4a10 gene and kidney epithelial sodium channel. *The Journal of Clinical Investigation*, *116*(6), 1696–702. https://doi.org/10.1172/JCI27546

National Kidney Foundation. (2002). *K/DOQI Clinical Practice Guidelines for Chronic Kidney Disease: Evaluation, Clasification and Stratification*. *Am J Kidney Dis.* (Vol. 39). https://doi.org/10.1634/theoncologist.2011-S2-45

Nechiporuk, A., & Raible, D. W. (2008). FGF-Dependent Mechanosensory Organ Patterning in Zebrafish. *Science*, *320*(5884), 1774–1777. https://doi.org/10.1126/science.1156547

NHLBI. (n.d.). Seventh Report of the Joint National Committee on Prevention, Detection, Evaluation, and Treatment of High Blood Pressure (JNC7). Retrieved from https://www.nhlbi.nih.gov/files/docs/guidelines/jnc7full.pdf

Nishimura, T., Honda, H., & Takeichi, M. (2012). Planar Cell Polarity Links Axes of Spatial Dynamics in Neural-Tube Closure. *Cell*, *149*(5), 1084–1097. https://doi.org/10.1016/j.cell.2012.04.021

Nishimura, T., & Takeichi, M. (2008). Shroom3-mediated recruitment of Rho kinases to the apical cell junctions regulates epithelial and neuroepithelial planar remodeling. *Development*, *135*(8), 1493–1502. https://doi.org/10.1242/dev.019646

Nogales, E. (2001). S Tructural I Nsights Into. *Annual Reviews Biochem*, *69*, 277–302. https://doi.org/10.1146/annurev.biochem.74.061903.155440

Nogueira, A., Pires, M. J., & Oliveira, P. A. (2017). Pathophysiological mechanisms of renal fibrosis: A review of animal models and therapeutic strategies. *In Vivo*, *31*(1), 1–22. https://doi.org/10.21873/invivo.11019

Obih, P., & Oyekan, A. O. (2008). Regulation of blood pressure, natriuresis and renal thiazide/amiloride sensitivity in PPARα null mice. *Blood Pressure*, *17*(1), 55–63. https://doi.org/10.1080/08037050701789278

Ofem, O., Nna, V., Oka, V., Archibong, A. N., & Bassey, S. C. (2014). Vitamin C and E Supplementation Reverses Alterations in Haematological Indices Induced by High Salt Loading in Rats. *Journal of Pharmaceutical and Biomedical Sciences*, *4*(9), 763–768. Retrieved from http://www.cabdirect.org/abstracts/20143021789.html

Oliver, P. M., Fox, J. E., Kim, R., Rockman, H. A., Kim, H.-S., Reddick, R. L., … Maeda, N. (1997). Hypertension, cardiac hypertrophy, and sudden death in mice lacking natriuretic peptide receptor A (gene targetingechocardiographycardiac dilatationinterstitial fibrosisaortic dissection). *Medical Sciences*, *94*, 14730–14735. Retrieved from http://www.pnas.org/content/94/26/14730.full.pdf

Oparil, S., Zaman, M. A., & Calhoun, D. A. (2003). Pathogenesis of Hypertension. *Annals of Internal Medicine*, *139*(9), 761–776. https://doi.org/10.1016/B978-1-4557-4617-0.00065-0

Palatini, P., Mormino, P., Dorigatti, F., Santonastaso, M., Mos, L., De Toni, R., … Pessina, A. C. (2006). Glomerular hyperfiltration predicts the development of microalbuminuria in stage 1 hypertension: The HARVEST. *Kidney International*, *70*(3), 578–584. https://doi.org/10.1038/SJ.KI.5001603

Parati, G., Ochoa, J. E., Lombardi, C., & Bilo, G. (2013). Assessment and management

of blood-pressure variability. *Nature Reviews Cardiology*, *10*(3), 143–155. https://doi.org/10.1038/nrcardio.2013.1

Pattaro, C., De Grandi, A., Vitart, V., Hayward, C., Franke, A., Aulchenko, Y. S., … Pramstaller, P. P. (2010). A meta-analysis of genome-wide data from five European isolates reveals an association of COL22A1, SYT1, and GABRR2 with serum creatinine level. *BMC Medical Genetics*, *11*(1), 41. https://doi.org/10.1186/1471-2350-11-41

Pavenstadt, H., Kriz, W., & Kretzler, M. (2003). Cell Biology of the Glomerular Podocyte. *Physiological Reviews*, *83*(1), 253–307. https://doi.org/10.1152/physrev.00020.2002

Pfistershammer, K., Klauser, C., Leitner, J., Stockl, J., Majdic, O., Weichhart, T., … Steinberger, P. (2007). Identification of the scavenger receptors SREC-I, Cla-1 (SR-BI), and SR-AI as cellular receptors for Tamm-Horsfall protein. *Journal of Leukocyte Biology*, *83*(1), 131–138. https://doi.org/10.1189/jlb.0407231

Pitkin, R. M. (2007). Folate and neural tube defects. *The American Journal of Clinical Nutrition*, *85*(1), 285S–288S. Retrieved from http://www.ncbi.nlm.nih.gov/pubmed/17209211

Plageman, T. F., Chauhan, B. K., Yang, C., Jaudon, F., Shang, X., Zheng, Y., … Lang, R. A. (2011). A Trio-RhoA-Shroom3 pathway is required for apical constriction and epithelial invagination. *Development*, *138*(23), 5177–5188. https://doi.org/10.1242/dev.067868

Plageman, T. F., Chung, M.-I., Lou, M., Smith, A. N., Hildebrand, J. D., Wallingford, J. B., & Lang, R. A. (2010). Pax6-dependent Shroom3 expression regulates apical constriction during lens placode invagination. *Development*, *137*(3), 405–415. https://doi.org/10.1242/dev.045369

Plageman, T. F., Zacharias, A. L., Gage, P. J., & Lang, R. A. (2011). Shroom3 and a Pitx2-N-cadherin pathway function cooperatively to generate asymmetric cell shape changes during gut morphogenesis. *Developmental Biology*, *357*(1), 227–234. https://doi.org/10.1016/j.ydbio.2011.06.027

Plageman, T. F., Zacharias, A. L., Gage, P. J., & Lang, R. A. (2011). Shroom3 and a Pitx2-N-cadherin pathway function cooperatively to generate asymmetric cell shape changes during gut morphogenesis. https://doi.org/10.1016/j.ydbio.2011.06.027

Qiao, J. (n.d.). FGF-7 modulates kidney size. Retrieved from http://dev.biologists.org/content/develop/126/3/547.full.pdf

Radin, M. J., Holycross, B. J., Hoepf, T. M., & McCune, S. A. (2008). Salt-Induced Cardiac Hypertrophy Is Independent of Blood Pressure and Endothelin in Obese, Heart Failure-Prone SHHF Rats. *Clinical and Experimental Hypertension*, *30*(7), 541–552. https://doi.org/10.1080/10641960802251917

Rafiq, K., Nishiyama, A., Konishi, Y., Morikawa, T., Kitabayashi, C., Kohno, M., … Imanishi, M. (2014). Regression of Glomerular and Tubulointerstitial Injuries by Dietary Salt Reduction with Combination Therapy of Angiotensin II Receptor Blocker and Calcium Channel Blocker in Dahl Salt-Sensitive Rats. *PLoS ONE*, *9*(9), e107853. https://doi.org/10.1371/journal.pone.0107853

Ravera, M. (2006). Importance of Blood Pressure Control in Chronic Kidney Disease. *Journal of the American Society of Nephrology*, *17*(4_suppl_2), S98–S103. https://doi.org/10.1681/ASN.2005121319

Reiser, J., & Altintas, M. M. (2016). Podocytes. *F1000Research*, *5*, 1–19. https://doi.org/10.12688/f1000research.7255.1

Rosenberg, A. Z., & Kopp, J. B. (2017). Focal segmental glomerulosclerosis. *Clinical Journal of the American Society of Nephrology*, *12*(3), 502–517. https://doi.org/10.2215/CJN.05960616

Rossman, K. L., Der, C. J., & Sondek, J. (2005). GEF means go: turning on RHO GTPases with guanine nucleotide-exchange factors. *Nature Reviews Molecular Cell Biology*, *6*(2), 167–180. https://doi.org/10.1038/nrm1587

Rothwell, P. M., Howard, S. C., Dolan, E., O'Brien, E., Dobson, J. E., Dahlöf, B., … Poulter, N. R. (2010). Prognostic significance of visit-to-visit variability, maximum systolic blood pressure, and episodic hypertension. *Lancet (London, England)*, *375*(9718), 895–905. https://doi.org/10.1016/S0140-6736(10)60308-X

Rubin, L. J. (2006). Pulmonary Arterial Hypertension. *Proceedings of the American Thoracic Society*, *3*(1), 111–115. https://doi.org/10.1513/pats.200510-112JH

Ruta, L.-A. M., Dickinson, H., Thomas, M. C., Denton, K. M., Anderson, W. P., & Kett, M. M. (2010). High-salt diet reveals the hypertensive and renal effects of reduced nephron endowment. *American Journal of Physiology. Renal Physiology*, *298*(6), F1384-92. https://doi.org/10.1152/ajprenal.00049.2010

Rysz, J., Gluba-Brzózka, A., Franczyk, B., Jabłonowski, Z., & Ciałkowska-Rysz, A. (2017). Novel Biomarkers in the Diagnosis of Chronic Kidney Disease and the Prediction of Its Outcome. *International Journal of Molecular Sciences*, *18*(8). https://doi.org/10.3390/ijms18081702

Sarnak, M. J., Levey, A. S., Schoolwerth, A. C., Coresh, J., Culleton, B., Hamm, L. L., … Wilson, P. W. (2003). Kidney Disease as a Risk Factor for Development of Cardiovascular Disease: A Statement From the American Heart Association Councils on Kidney in Cardiovascular Disease, High Blood Pressure Research, Clinical Cardiology, and Epidemiology and Prevention. *Circulation*, *108*(17), 2154–2169. https://doi.org/10.1161/01.CIR.0000095676.90936.80

Sawyer, J. M., Harrell, J. R., Shemer, G., Sullivan-Brown, J., Roh-Johnson, M., & Goldstein, B. (2010). Apical constriction: A cell shape change that can drive

morphogenesis. *Developmental Biology*, *341*(1), 5–19. https://doi.org/10.1016/j.ydbio.2009.09.009

Schlote, J., Schröder, A., Dahlmann, A., Karpe, B., Cordasic, N., Daniel, C., … Benz, K. (2013). Cardiovascular and Renal Effects of High Salt Diet in GDNF+/- Mice with Low Nephron Number. *Kidney and Blood Pressure Research*, *37*(4–5), 379–391. https://doi.org/10.1159/000355716

Schmieder, R. E., Messerli, F. H., Garavaglia, G. E., Nunez, B. D., Dilley, R. J., Cooper, M. E., & Johnston, C. I. (1988). Dietary salt intake. A determinant of cardiac involvement in essential hypertension. *Circulation*, *78*(4), 951–6. https://doi.org/10.1161/01.cir.98.23.2621

Schmieder, R. E., Veelken, R., Schobel, H., Dominiak, P., Mann, J. F., & Luft, F. C. (1997). Glomerular hyperfiltration during sympathetic nervous system activation in early essential hypertension. *J Am Soc Nephrol*, *8*(6), 893–900. Retrieved from http://www.ncbi.nlm.nih.gov/pubmed/9189855

Schmieder, S., Nagai, M., Orlando, R. A., Takeda, T., & Farquhar, M. G. (2004). Podocalyxin Activates RhoA and Induces Actin Reorganization through NHERF1 and Ezrin in MDCK Cells. *Journal of the American Society of Nephrology*, *15*(9), 2289–2298. https://doi.org/10.1097/01.ASN.0000135968.49899.E8

Schwartz, G. J., & Furth, S. L. (2007). Glomerular filtration rate measurement and estimation in chronic kidney disease. *Pediatric Nephrology*, *22*(11), 1839–1848. https://doi.org/10.1007/s00467-006-0358-1

Sevilla-Pérez, J., Königshoff, M., Kwapiszewska, G., Amarie, O. V., Seeger, W., Weissmann, N., … Eickelberg, O. (2008). Shroom expression is attenuated in pulmonary arterial hypertension. *European Respiratory Journal*, *32*(4), 871–880. https://doi.org/10.1183/09031936.00045507

Short, K. M., & Smyth, I. M. (2016). The contribution of branching morphogenesis to kidney development and disease. *Nature Reviews Nephrology*, *12*(12), 754–767. https://doi.org/10.1038/nrneph.2016.157

Shutova, M., Yang, C., Vasiliev, J. M., & Svitkina, T. (2012). Functions of nonmuscle myosin ii in assembly of the cellular contractile system. *PLoS ONE*, *7*(7). https://doi.org/10.1371/journal.pone.0040814

Simmonds, S. S., Lay, J., & Stocker, S. D. (2014). Dietary salt intake exaggerates sympathetic reflexes and increases blood pressure variability in normotensive rats. *Hypertension (Dallas, Tex. : 1979)*, *64*(3), 583–9. https://doi.org/10.1161/HYPERTENSIONAHA.114.03250

Singh, P., Deng, A., Blantz, R. C., & Thomson, S. C. (2009). Unexpected effect of angiotensin AT1 receptor blockade on tubuloglomerular feedback in early subtotal nephrectomy. *AJP: Renal Physiology*, *296*(5), F1158–F1165.

https://doi.org/10.1152/ajprenal.90722.2008

Sit, S.-T., & Manser, E. (2011). Rho GTPases and their role in organizing the actin cytoskeleton. *Journal of Cell Science*, *124*(5), 679–683. https://doi.org/10.1242/jcs.064964

Smyth, L. J., Duffy, S., Maxwell, A. P., & McKnight, A. J. (2014). Genetic and epigenetic factors influencing chronic kidney disease. *AJP: Renal Physiology*, *307*(7), F757–F776. https://doi.org/10.1152/ajprenal.00306.2014

Stanford, W. L., Cohn, J. B., Cordes, S. P., & Lunenfeld, S. (2001). Gene-Trap Mutagenesis : Past , Present and Beyond, *2*(October), 756–768.

Stauss, H. M., Gödecke, A., Mrowka, R., Schrader, J., & Persson, P. B. (1999). Enhanced blood pressure variability in eNOS knockout mice. *Hypertension (Dallas, Tex. : 1979)*, *33*(6), 1359–63. Retrieved from http://www.ncbi.nlm.nih.gov/pubmed/10373216

Stenmark, K. R., Fagan, K. A., & Frid, M. G. (2006). Hypoxia-Induced Pulmonary Vascular Remodeling: Cellular and Molecular Mechanisms. *Circulation Research*, *99*(7), 675–691. https://doi.org/10.1161/01.RES.0000243584.45145.3f

Stevens, S. L., Wood, S., Koshiaris, C., Law, K., Glasziou, P., Stevens, R. J., & McManus, R. J. (2016). Blood pressure variability and cardiovascular disease: systematic review and meta-analysis. *BMJ (Clinical Research Ed.)*, *354*, i4098. https://doi.org/10.1136/BMJ.I4098

Su, D.-F., & Miao, C.-Y. (2001). Blood Pressure Variability And Organ Damage. *Clinical and Experimental Pharmacology and Physiology*, *28*(9), 709–715. https://doi.org/10.1046/j.1440-1681.2001.03508.x

Suchy-Dicey, A. M., Wallace, E. R., Mitchell, S. V. E., Aguilar, M., Gottesman, R. F., Rice, K., … Jr. (2013). Blood pressure variability and the risk of all-cause mortality, incident myocardial infarction, and incident stroke in the cardiovascular health study. *American Journal of Hypertension*, *26*(10), 1210–7. https://doi.org/10.1093/ajh/hpt092

Suzuki, M., Morita, H., & Ueno, N. (2012). Molecular mechanisms of cell shape changes that contribute to vertebrate neural tube closure. *Development, Growth & Differentiation*, *54*(3), 266–276. https://doi.org/10.1111/j.1440-169X.2012.01346.x

Takasato, M., & Little, M. H. (2015). The origin of the mammalian kidney: implications for recreating the kidney in vitro. *Development*, *142*(11), 1937–1947. https://doi.org/10.1242/dev.104802

Tanner, G. a. (2009). Kidney Function. *In Medical Physiology: Princi- Ples for Clinical Medicine*, 391–418.

Tariq, M., Belmont, J. W., Lalani, S., Smolarek, T., & Ware, S. M. (2011). SHROOM3 is a novel candidate for heterotaxy identified by whole exome sequencing. *Genome Biology*, *12*(9), R91. https://doi.org/10.1186/gb-2011-12-9-r91

Taylor, J., Abramova, N., Charlton, J., & Adler, P. N. (1998). Van Gogh: a new Drosophila tissue polarity gene. *Genetics*, *150*(1), 199–210. Retrieved from http://www.ncbi.nlm.nih.gov/pubmed/9725839

Taylor, J., Chung, K.-H., Figueroa, C., Zurawski, J., Dickson, H. M., Brace, E. J., … Vojtek, A. B. (2008). The scaffold protein POSH regulates axon outgrowth. *Molecular Biology of the Cell*, *19*(12), 5181–92. https://doi.org/10.1091/mbc.E08-02-0231

Tedla, F. M., Brar, A., Browne, R., & Brown, C. (2011). Hypertension in Chronic Kidney Disease: Navigating the Evidence. *International Journal of Hypertension*, *2011*, 1–9. https://doi.org/10.4061/2011/132405

Theisen, H., Purcell, J., Bennett, M., Kansagara, D., Syed, A., & Marsh, J. L. (1994). dishevelled is required during wingless signaling to establish both cell polarity and cell identity. *Development (Cambridge, England)*, *120*(2), 347–60. Retrieved from http://www.ncbi.nlm.nih.gov/pubmed/8149913

Tian, X., & Ishibe, S. (2016). Targeting the podocyte cytoskeleton: from pathogenesis to therapy in proteinuric kidney disease. *Nephrology, Dialysis, Transplantation : Official Publication of the European Dialysis and Transplant Association - European Renal Association*, *31*(10), 1577–83. https://doi.org/10.1093/ndt/gfw021

Togawa, A., Miyoshi, J., Ishizaki, H., Tanaka, M., Takakura, A., Nishioka, H., … Takai, Y. (1999). Progressive impairment of kidneys and reproductive organs in mice lacking Rho GDIα. *Oncogene*, *18*(39), 5373–5380. https://doi.org/10.1038/sj.onc.1202921

Townsend, R. R., & Taler, S. J. (2015). Management of hypertension in chronic kidney disease. *Nature Reviews Nephrology*, *11*(9), 555–563. https://doi.org/10.1038/nrneph.2015.114

Toyama, Y., Peralta, X. G., Wells, A. R., Kiehart, D. P., & Edwards, G. S. (2008). Apoptotic Force and Tissue Dynamics During Drosophila Embryogenesis. *Science*, *321*(5896), 1683–1686. https://doi.org/10.1126/science.1157052

Tozawa, M., Iseki, K., Iseki, C., Kinjo, K., Ikemiya, Y., & Takishita, S. (2003). Blood pressure predicts risk of developing end-stage renal disease in men and women. *Hypertension*, *41*(6), 1341–1345. https://doi.org/10.1161/01.HYP.0000069699.92349.8C

Tryggvason, K. (2005). How Does the Kidney Filter Plasma? *Physiology*, *20*(2), 96–101. https://doi.org/10.1152/physiol.00045.2004

Usui, T., Shima, Y., Shimada, Y., Hirano, S., Burgess, R. W., Schwarz, T. L., … Uemura, T. (1999). Flamingo, a seven-pass transmembrane cadherin, regulates planar cell polarity under the control of Frizzled. *Cell*, *98*(5), 585–95. Retrieved from http://www.ncbi.nlm.nih.gov/pubmed/10490098

Vallon, V. (2003). Glomerular Hyperfiltration and the Salt Paradox in Early Type 1 Diabetes Mellitus: A Tubulo-Centric View. *Journal of the American Society of Nephrology*, *14*(2), 530–537. https://doi.org/10.1097/01.ASN.0000051700.07403.27

Van Vliet, B. N., & Montani, J.-P. (2008). The time course of salt-induced hypertension and why it matters. *International Journal of Obesity*, *32*(S6), S35–S47. https://doi.org/10.1038/ijo.2008.205

Vasdev, S., Gill, V., Parai, S., & Gadag, V. (2006). Low ethanol intake prevents salt-induced hypertension in WKY rats. *Molecular and Cellular Biochemistry*, *287*(1–2), 53–60. https://doi.org/10.1007/s11010-005-9058-6

Veltman, J. A., & Brunner, H. G. (2012). De novo mutations in human genetic disease. *Nature Reviews Genetics*, *13*(8), 565–575. https://doi.org/10.1038/nrg3241

Verma, R., Kovari, I., Soofi, A., Nihalani, D., Patrie, K., & Holzman, L. B. (2006). Nephrin ectodomain engagement results in Src kinase activation, nephrin phosphorylation, Nck recruitment, and actin polymerization. *Journal of Clinical Investigation*, *116*(5), 1346–1359. https://doi.org/10.1172/JCI27414

Vinson, C. R., Conover, S., & Adler, P. N. (1989). A Drosophila tissue polarity locus encodes a protein containing seven potential transmembrane domains. *Nature*, *338*(6212), 263–264. https://doi.org/10.1038/338263a0

Vyletal, P., Bleyer, A. J., & Kmoch, S. (2010a). Uromodulin biology and pathophysiology--an update. *Kidney & Blood Pressure Research*, *33*(6), 456–75. https://doi.org/10.1159/000321013

Vyletal, P., Bleyer, J., & Kmoch, S. (2010b). Uromodulin Biology and Pathophysiology – An Update, 456–475. https://doi.org/10.1159/000321013

Wallingford, J. B., Fraser, S. E., & Harland, R. M. (2002). Convergent extension: The molecular control of polarized cell movement during embryonic development. *Developmental Cell*, *2*(6), 695–706. https://doi.org/10.1016/S1534-5807(02)00197-1

Wallingford, J. B., Niswander, L. A., Shaw, G. M., & Finnell, R. H. (2013). The continuing challenge of understanding, preventing, and treating neural tube defects. *Science (New York, N.Y.)*, *339*(6123), 1222002. https://doi.org/10.1126/science.1222002

Wang, G., Cadwallader, A. B., Jang, D. S., Tsang, M., Yost, H. J., & Amack, J. D. (2011). The Rho kinase Rock2b establishes anteroposterior asymmetry of the ciliated Kupffer's vesicle in zebrafish. *Development*, *138*(1), 45–54.

https://doi.org/10.1242/dev.052985

Wang, Y., Chen, L., Li, M., Cha, H., Iwamoto, T., & Zhang, J. (2015). Conditional knockout of smooth muscle sodium calcium exchanger type-1 lowers blood pressure and attenuates Angiotensin II-salt hypertension. *Physiological Reports*, *3*(1), e12273. https://doi.org/10.14814/phy2.12273

Watanabe, H., Katoh, T., Eiro, M., Iwamoto, M., Ushikubi, F., Narumiya, S., & Watanabe, T. (2005). Effects of salt loading on blood pressure in mice lacking the prostanoid receptor gene. *Circulation Journal*, *69*(1), 124–126. https://doi.org/10.1253/circj.69.124

Webster, A. C., Nagler, E. V., Morton, R. L., & Masson, P. (2017). Chronic Kidney Disease. *The Lancet*, *389*(10075), 1238–1252. https://doi.org/10.1016/S0140-6736(16)32064-5

Weir, M.R., & Dzau, V. J. (1999). Renin-angiotensin-aldosterone system: a specific target for hypertension management. *American Journal of Hypertension*, *12*(9), 205S – 213S. https://doi.org/10.1016/S0895-7061(99)00103-X

Wharram, B. L., Goyal, M., Wiggins, J. E., Sanden, S. K., Hussain, S., Filipiak, W. E., … Wiggins, R. C. (n.d.). Podocyte Depletion Causes Glomerulosclerosis : Diphtheria Toxin – Induced Podocyte Depletion in Rats Expressing Human Diphtheria Toxin Receptor Transgene, (21), 2941–2952. https://doi.org/10.1681/ASN.2005010055

Wiese, C., & Zheng, Y. (2006). Microtubule nucleation: -tubulin and beyond. *Journal of Cell Science*, *119*(20), 4143–4153. https://doi.org/10.1242/jcs.03226

Wiggins, R.-C. (2007). The spectrum of podocytopathies: A unifying view of glomerular diseases. *Kidney International*, *71*(12), 1205–1214. https://doi.org/10.1038/sj.ki.5002222

Wilkinson, I. B., & Cockcroft, J. R. (2000). Mind the gap: pulse pressure, cardiovascular risk, and isolated systolic hypertension. *American Journal of Hypertension*, *13*(12), 1315–1317. https://doi.org/10.1016/S0895-7061(00)01269-3

Williams, M., Burdsal, C., Periasamy, A., Lewandoski, M., & Sutherland, A. (2012). Mouse primitive streak forms in situ by initiation of epithelial to mesenchymal transition without migration of a cell population. *Developmental Dynamics*, *241*(2), 270–283. https://doi.org/10.1002/dvdy.23711

Winter, C. G., Wang, B., Ballew, A., Royou, A., Karess, R., Axelrod, J. D., & Luo, L. (2001). Drosophila Rho-associated kinase (Drok) links Frizzled-mediated planar cell polarity signaling to the actin cytoskeleton. *Cell*, *105*(1), 81–91. https://doi.org/10.1016/S0092-8674(01)00298-7

Wolff, T., & Rubin, G. M. (1998). Strabismus, a novel gene that regulates tissue polarity

and cell fate decisions in Drosophila. *Development (Cambridge, England)*, *125*(6), 1149–59. Retrieved from http://www.ncbi.nlm.nih.gov/pubmed/9463361

World Health Organization. (2011). WHO | Raised blood pressure. *World Health Organization*, 39–40. Retrieved from http://www.who.int/gho/ncd/risk_factors/blood_pressure_prevalence_text/en/

Wright, J., & Hutchison, A. (2009). Vascular Health and Risk Management Cardiovascular disease in patients with chronic kidney disease. *Vascular Health and Risk Management*, *5*, 713–722. https://doi.org/10.2147/VHRM.S6206

Wuttke, M., & Köttgen, A. (2016). Insights into kidney diseases from genome-wide association studies. *Nature Reviews. Nephrology*, *12*(9), 549–62. https://doi.org/10.1038/nrneph.2016.107

Xu, Z., Kukekov, N. V, & Greene, L. A. (2003). POSH acts as a scaffold for a multiprotein complex that mediates JNK activation in apoptosis. *The EMBO Journal*, *22*(2), 252–61. https://doi.org/10.1093/emboj/cdg021

Ye, W., Zhang, H., Hillas, E., Kohan, D. E., Miller, R. L., Nelson, R. D., … Yang, T. (2006). Expression and function of COX isoforms in renal medulla: evidence for regulation of salt sensitivity and blood pressure. *American Journal of Physiology. Renal Physiology*, *290*(2), F542-9. https://doi.org/10.1152/ajprenal.00232.2005

Yeo, N. C., O'Meara, C. C., Bonomo, J. A., Veth, K. N., Tomar, R., Flister, M. J., … Jacob, H. J. (2015). Shroom3 contributes to the maintenance of the glomerular filtration barrier integrity. *Genome Research*, *25*(1), 57–65. https://doi.org/10.1101/gr.182881.114

Yu, Q., Larson, D. F., Slayback, D., Lundeen, T. F., Baxter, J. H., & Watson, R. R. (2004). Characterization of high-salt and high-fat diets on cardiac and vascular function in mice. *Cardiovascular Toxicology*, *4*(1), 37–46. Retrieved from http://www.ncbi.nlm.nih.gov/pubmed/15034204

Zalewski, J. K., Mo, J. H., Heber, S., Heroux, A., Gardner, R. G., Hildebrand, J. D., & VanDemark, A. P. (2016). Structure of the Shroom-Rho Kinase Complex Reveals a Binding Interface with Monomeric Shroom That Regulates Cell Morphology and Stimulates Kinase Activity. *The Journal of Biological Chemistry*, *291*(49), 25364–25374. https://doi.org/10.1074/jbc.M116.738559

Zallen, J. A. (2007). Planar Polarity and Tissue Morphogenesis. *Cell*, *129*(6), 1051–1063. https://doi.org/10.1016/j.cell.2007.05.050

Zelmer, J. L. (2007). The economic burden of end-stage renal disease in Canada. *Kidney International*, *72*(9), 1122–1129. https://doi.org/10.1038/sj.ki.5002459

Zhao, X., Ho, D., Gao, S., Hong, C., Vatner, D. E., & Vatner, S. F. (2011). Arterial Pressure Monitoring in Mice. *Current Protocols in Mouse Biology*, *1*, 105–122.

https://doi.org/10.1002/9780470942390.mo100149

Zhu, H., Barmada, M. M., & Bleyer, A. J. (2002). Mutations of the, 882–893.

Zhu, L., Jiang, R., Aoudjit, L., Jones, N., & Takano, T. (2011). Activation of RhoA in Podocytes Induces Focal Segmental Glomerulosclerosis. *Journal of the American Society of Nephrology*, *22*(9), 1621–1630. https://doi.org/10.1681/ASN.2010111146

Appendices

Appendix A: Supplemental information for blood pressure measurements and list of mice omitted from statistical analysis

The nature of the tail-cuff system requires that the mouse is conscious and inevitably, there were days where blood pressure measurements could not be obtained or had to be omitted. In the former case, such instances included when a mouse exhibited resistance towards being placed in the holder or displayed frequent movement or signs of stress when blood pressure was being measured. Although measurements were re-taken the next day with no issues in the majority of instances, there were rare cases where the mouse also displayed signs of distress the following day, and thus, no blood pressure measurement could be obtained for that mouse during that week. Additionally, after blood pressure data was collected on any given day, the mean and standard deviation of 30 cycles for each individual mouse was calculated. If the standard deviation was greater than 30 for any mouse on a given day, the blood pressure data from that day was not included in analysis, as recommended by standard protocol.

The statistical analysis for my physiological time-course data included a two-way ANOVA analysis with a Tukey's post-hoc test for significant differences between experimental groups and a repeated-measures one-way ANOVA with a Dunnett's multiple comparison test for significant differences within groups in comparison to baseline values. For repeated measures one-way ANOVA, analysis cannot be conducted with missing values, and as stated above, there were instances where data could not be obtained on two sequential days in a given week. Three individuals in total were omitted from repeated-measures one-way ANOVA analysis due to missing values: a WT NS mouse that did not provide readings for weeks 2 and 4, a WT HS mouse that did not provide a reading for week 4, and a *Shroom3*$^{+/Gt}$ HS mouse that was euthanized after week 1 upon veterinary request due to overt symptoms of severe, spontaneous neurological damage. However, because the two-way ANOVA analysis between groups is not repeated-measures, the three mice were included in analysis.

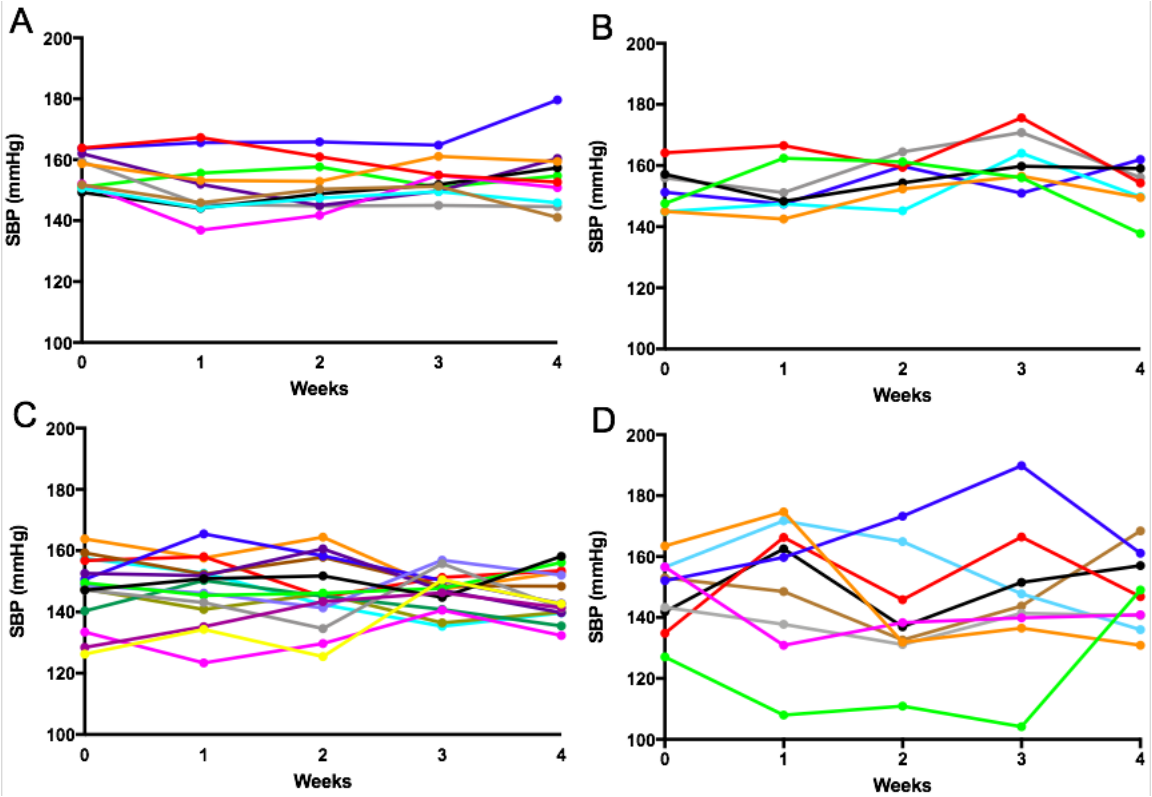

Appendix B: Representative variability in SBP response of *Shroom3*$^{+/Gt}$ mice on a high-salt diet. Time-course of SBP plotted for each individual mouse for WT mice on a NS diet (A), *Shroom3*$^{+/Gt}$ mice on a NS diet (B), WT mice on a HS diet (C), and *Shroom3*$^{+/Gt}$ mice on a HS diet (D) over the four-week treatment period. Upon initiation of the HS diet, *Shroom3*$^{+/Gt}$ mice exhibited large variation in their blood pressure response, prompting the analysis of absolute change in SBP as well as blood pressure variability. Due to some mice exhibiting a large decrease in SBP while others exhibited a large increase, the mean SBP of the group was not significantly different from that of WT mice on a HS diet. Of note, the WT mouse on a NS diet mentioned in *3.1.1* that gained a large amount of weight in the last two weeks of the experimental period and exhibited extremely high blood-pressure levels, is indicated in blue in (A). Due to missing values, the individual mice described in Appendix A were also omitted from these figures. N=10 for WT NS, n=7 for *Shroom3*$^{+/Gt}$ NS, n=15 for WT HS, n=9 for *Shroom3*$^{+/Gt}$ HS.

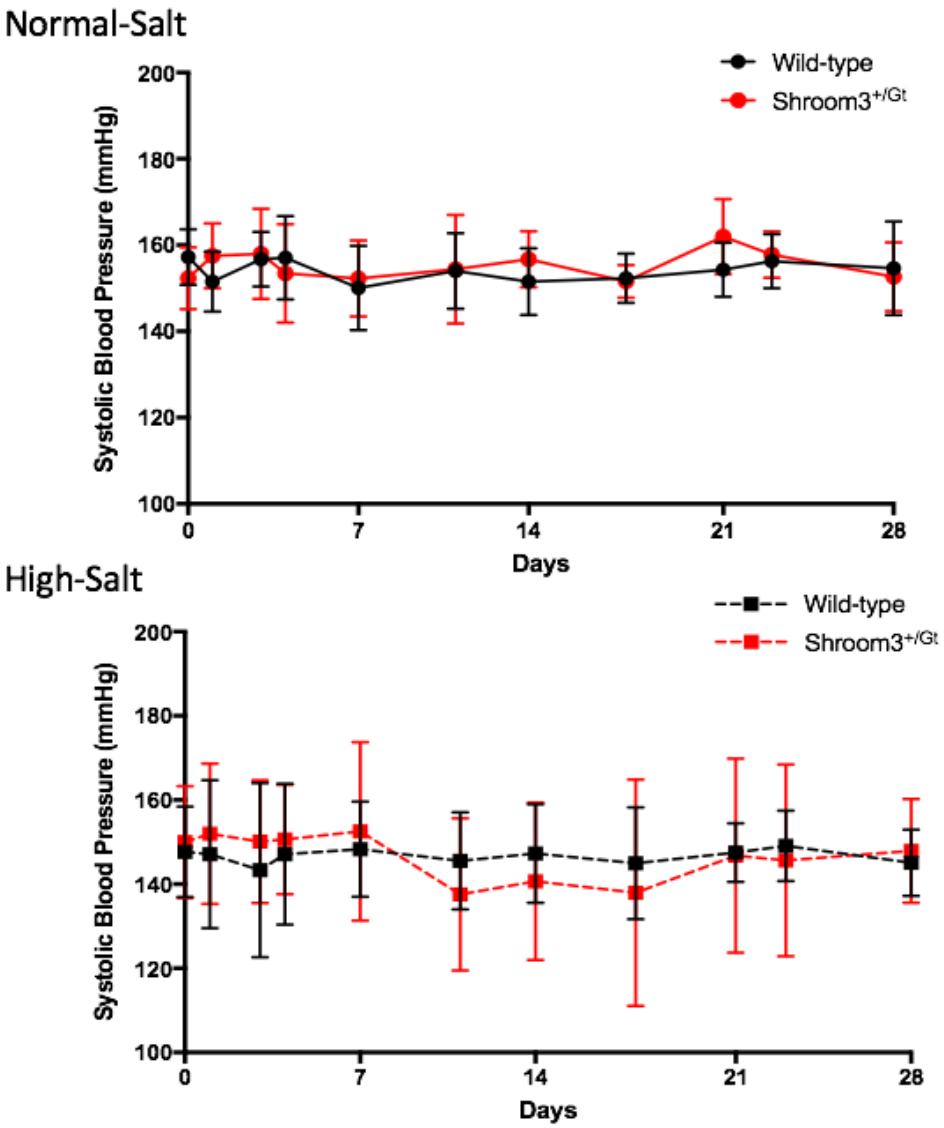

Appendix C: SBP measurements used for BPV analysis. Time-course of SBP taken at various days throughout the four-week dietary period. In total, 11 measurements were taken for each mouse and the individual SD of the 11 SBP measurements was used as an index for BPV. N=7-11 for NS groups, n=9-16 for HS groups.

Amino Acid Position	Variant Allele	Allele Frequency	Amino Acid Change	Polyphen Prediction	Domain Location
60/1997	T/G	T=34/G=12972	Val,Gly	Probably Damaging	PDZ*
147/1997	A/T	A=1891/T=11115	His,Leu	Probably Damaging	?
619/1997	T/C	T=27/C=12979	Tyr,His	Probably Damaging	?
325/1997	G/T	G=799/T=7801	Ala,Ser	Possibly Damaging	?
352/1997	A/G	A=15/G=12991	Gln,Arg	Probably Damaging	?
367/1997	G/T	G=20/T=12986	Arg,Ser	Probably Damaging	?
469/1997	G/C	G=7225/C=5781	Ala,Pro	Probably Damaging	?
512/1997	A/G	A=9/G=12997	Thr,Ala	Probably Damaging	?
564/1997	C/A	C=145/A=8455	Ala,Glu	Probably Damaging	?
601/1997	T/C	T=8/C=12998	Tyr,His	Probably Damaging	?
793/1997	C/A	C=40/A=12966	Pro,,Gln	Probably Damaging	?
1012/1997	A/C	A=67/C=12581	Asn,Thr	Probably Damaging	Asd1*
1054/1997	T/G	T=924/G=12076	Leu,Val	Probably Damaging	Asd1
1507/1997	A/G	A=15/G=12991	Lys,Glu	Probably Damaging	?
1864/1997	A/G	A=7/G=12999	Asp,Gly	Probably Damaging	Asd2*

Appendix D: List of identified human *SHROOM3* variants of interest. Based on the criteria described, these variants were previously selected as variants of interest by our lab. The present study has analyzed the three variants marked by an asterisk (*).

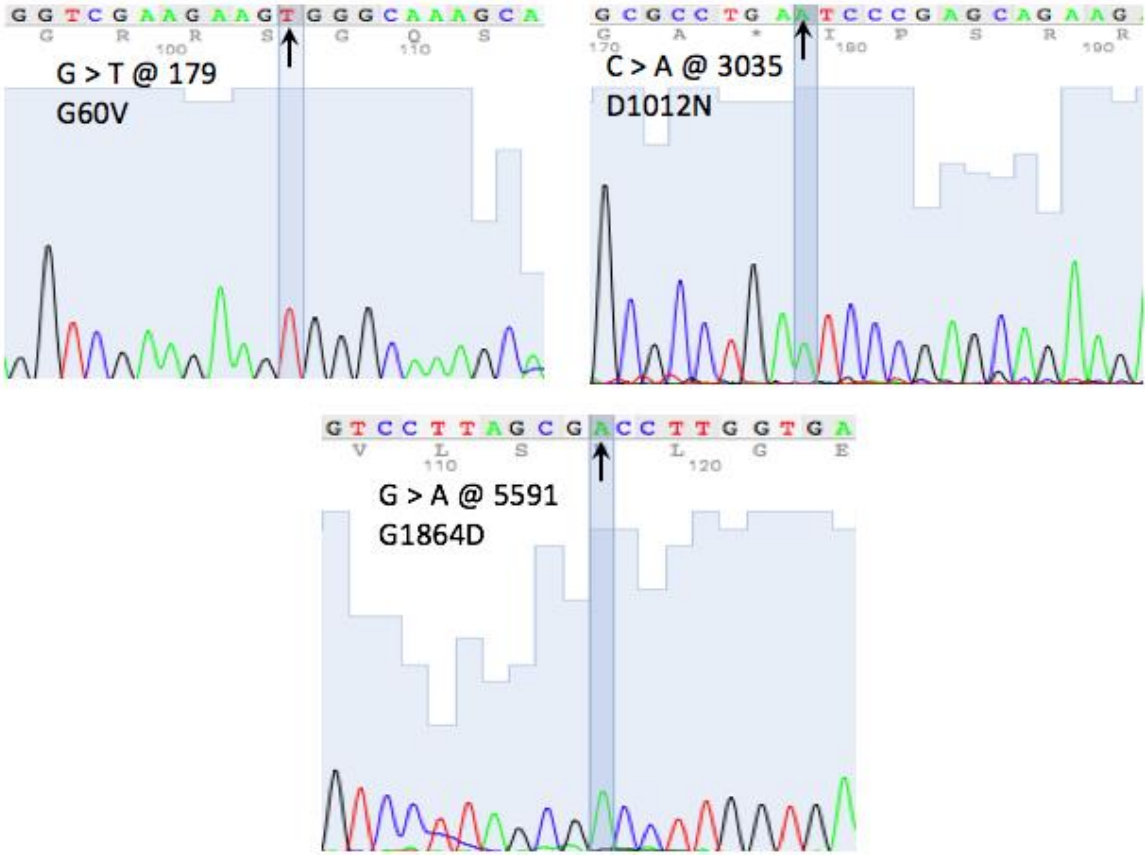

Appendix E: Representative electropherograms of variants confirmed by DNA sequencing. Sequencing results indicating successful mutagenesis of variants. Black arrows indicate the location of the substitution.

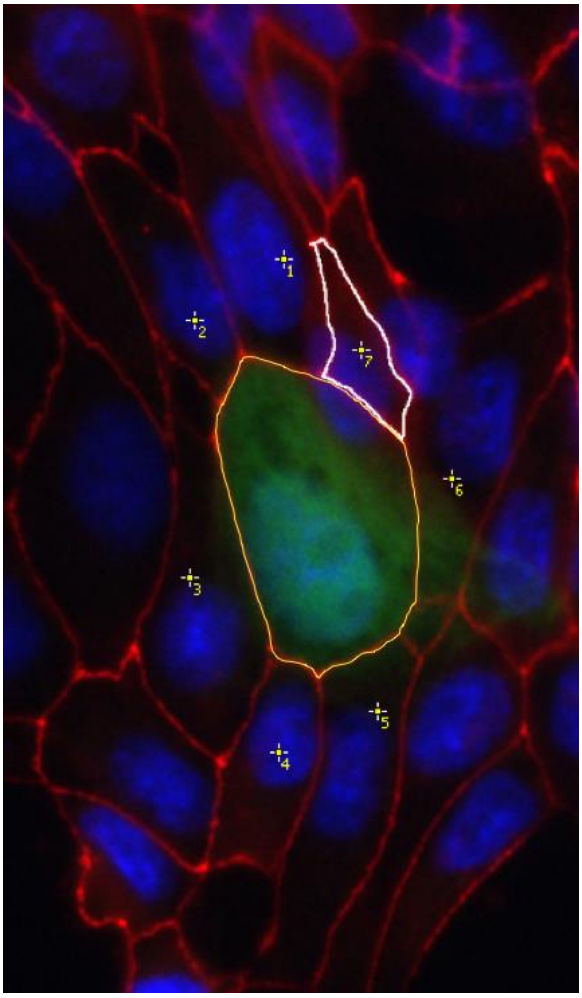

Appendix F Representative analysis of apical constriction determined by ZO-1 staining. Cells were labeled with an antibody against ZO-1 (anti-ZO-1, red) and nuclei were labeled with DAPI (blue). Transfected cells were visualized by GFP (green). To determine apical area of the transfected cell, the apical cell boundary outlined by ZO-1 was traced (indicated in yellow). To determine apical area of neighboring cells, the apical cell boundary outlined by ZO-1 was traced for non-GFP expressing cells (indicated in white). Only cells that were directly in contact with the cell boundary of the transfected GFP-expressing cell were considered “neighboring” cells (indicated in numbers). The GFP control vector is shown here.

Curriculum Vitae

Name:	Doyun Ko
Post-secondary Education and Degrees:	The University of Western Ontario London, Ontario, Canada 2011 – 2015 Bachelor of Science, Honors Specialization in Biology The University of Western Ontario London, Ontario, Canada 2015 – 2018 Master of Science, Biology
Honours and Awards:	Western Graduate Research Scholarship 2015 – 2017 Dean's Honour List 2014, 2015 Anne Sale Porte Scholarship 2014
Related Work Experience	Teaching Assistant Department of Biology *Biology for Sciences (BIO 1001), Analysis & Interpretation of Biological Data (BIO 2244), Scientific Methods in Biology (BIO 2290)* The University of Western Ontario 2015 – 2017

Poster Presentations:

Ko D, Drysdale TA, Gros R. Functional changes associated with *SHROOM3* deficiency and mutation: An *in vivo* and *in vitro* analysis. 13th Annual Paediatric Research Day. London Health Sciences Center, London, Ontario, Canada. May 10th, 2017.

Ko D, Drysdale TA. Functional changes associated with *SHROOM3* deficiency and mutation: An *in vivo* and *in vitro* analysis. 9th Annual Developmental Biology Research Day. Western University, London, Ontario, Canada. June 1st, 2017.